

**Analytic Design Software for Single-Sided Linear Induction Motor**

**PhD Thesis  
in  
Electrical and Electronic Engineering  
University of Gaziantep**

**Supervisor  
Asst. Prof. Dr. Vedat Mehmet KARSLI**

**by  
Ali Suat GERÇEK  
JULY 2009**

## **ABSTRACT**

### **ANALYTIC DESIGN SOFTWARE FOR SINGLE-SIDED LINEAR INDUCTION MOTOR**

GERÇEK, A. Suat

PhD in Electrical&Electronic Engineering

Supervisor: Asst. Prof. Dr. Vedat M. KARSLI

July 2009,122 pages

Linear induction motors have an increased use for linear movement due to direct adaptation to linear movement, less friction, less maintenance, high reliability and ease of implementation. Although the analytic investigation of this type of motors has gained attention and has been the subject of various studies in the literature, research efforts are still continuing in this field. Particularly, needs on more accurate design and analyzes of a motor is a strong requirement. Therefore, this study aims to develop a novel design software for linear induction motors. The originality of the developed software is not only being linear induction motor design software, but also modeling of secondary iron impedance using Least Square method for linear approximation. Thus, this new approach improves the accuracy of the performance calculations. Although the proposed method is computationally intensive, it is still preferable to existing methods because of its higher precision obtained at around 40 Hz.

The analyzed values of the design parameters which obtained with the proposed software are compared with the experimental data of the Canadian Guided Ground Transportation motor and observed to be in good agreement with them. The experimental thrust observations suggest that the software with the novel approach is highly promising.

**Keywords:** Method of layer, single-sided linear induction motor, computer-aided design, secondary impedance.

## ÖZET

### TEK-TARAFLI DOĞRUSAL ENDÜKSİYON MOTORUNUN ANALİTİK TASARIM YAZILIMI

GERÇEK, A. Suat

Doktora Tezi, Elektrik - Elektronik Mühendisliği

Tez yöneticisi: Yrd. Doç. Dr. Vedat M. KARSLI

Temmuz 2009,122 sayfa

Doğrusal endüksiyon motorları, doğrudan doğrusal hareket sağlaması, az sürtünme, az kayıp, yüksek güvenilirlik ve kolay imalatı nedeniyle doğrusal hareket sağlama da artan bir kullanıma haizdir. Her ne kadar bu tip motorların literatürde analitik incelemesine odaklanılsa da ve bir çok çalışma yapılsa da, bu alandaki araştırma çabaları devam etmektedir. Özellikle, motorun daha doğru tasarım ve analizinde ki ihtiyaçlar çok önemli bir gereksinimdir. Bu nedenle, bu çalışma doğrusal endüksiyon motoru için yeni bir tasarım yazılımı geliştirmeyi amaçlamaktadır. Geliştirilen yazılımın orijinalliği, sadece doğrusal endüksiyon motoru için bir tasarım yazılımı olması değil aynı zamanda da sekonder demir empedansının belirlenmesinde lineer bir yakınsamayla çok küçük kareler yöntemi kullanmasıdır. Böylece, bu yeni yaklaşım performans hesaplamalarında ki doğruluğu arttırmıştır. Her ne kadar, önerilen yöntem, işlemsel yoğunluğa sahip olsa da, 40 Hz deki yüksek duyarlılığından dolayı mevcut çalışmalara tercih edilir. Önerilen yazılımla elde edilen tasarım parametrelerinin analiz değerleri Kanada Enstitüsü Kılavuzlu Kara Taşımacılık motorunun deneysel sonuçları ile kıyaslanmış ve bu sonuçlarla iyi bir uyum içinde olduğu gözlemlenmiştir. İtme kuvveti için yapılan deneysel gözlemler, yeni metoda göre geliştirilen yazılımın oldukça ümit verici olduğunu göstermektedir.

**Keywords:** Katman metodu, Tek taraflı doğrusal endüksiyon motoru, Bilgisayar yardımıyla tasarım , Sekonder empedansı

## **ACKNOWLEDGMENTS**

I express sincere appreciation to my supervisor Asst. Prof. Dr. Vedat M. KARSLI and Prof. Dr. Osman GÜRDAL for his guidance and great help and to my family.

I would like to thank Mustafa KARABULUT, Assoc. Prof. Dr. Ergun ERÇELEBİ and Asst. Prof. Dr. Nihat ATMACA for their support.

Finally, I wish to express my heartfelt gratitude to my beloved family. First of all, I owe everything to my parents, who raised me of respect certain universal moral values. I also thank to my wife and my son, my daughter for all their love and support.

## CONTENT

ABSTRACT .....	ii
ÖZET.....	iii
ACKNOWLEDGEMENTS .....	iiv
CONTENT .....	v
LIST OF FIGURES .....	viii
LIST OF TABLES .....	xi
LIST OF SYMBOL.....	xii

## CHAPTER 1

1.1 Introduction .....	1
1.2 The Layout of Thesis .....	3

## CHAPTER 2 LITERATURE REVIEW

2.1 Introduction .....	4
2.2 Analytic Techniques.....	4
2.3 Numerical Techniques .....	10
2.4 Summary .....	13

## CHAPTER 3

### ANALYTICAL MODELLING OF SINGLE-SIDED LINEAR INDUCTION MOTOR

3.1 Introduction.....	15
3.2 Operation Principle of Single-sided Linear Induction Motor.....	16
3.3 Electromagnetic Field Model of Linear Induction Motor.....	17
3.4 Analytical Methods of Linear Induction Motor.....	20
3.4.1 Quasi-one-dimensional Model of Single-sided Linear Induction Motor .....	20
3.4.2 One-dimensional Electromagnetic Field Equation in the Air-gap.....	22
3.4.3 Method of the Layers.....	24
3.5 Analytical Modeling of Single-sided Linear Induction Motor by Using Method of Layer.....	26
3.5.1 Two-dimensional (2D) electromagnetic field distribution of SLIM with double layer scoundary.....	30

3.6 Summary.....	35
------------------	----

## **CHAPTER 4 EQUIVALENT CIRCUIT TECHNIQUE**

4.1 Introduction.....	36
4.2 Longitudinal end effect and saturation factor.....	37
4.3 Wave penetration depth concept .....	38
4.4 Calculation of saturation level .....	39
4.5 Simulating the CIGGT LIM .....	41
4.6 Obtaining the Equivalent Circuit Parameters of SLIM from Electromagnetic Equations .....	43
4.6.1 A new approach to obtaining the secondary impedance of SLIM in ECT .....	46
4.7 Conclusions and Remarks .....	52

## **CHAPTER 5 COMPUTER AIDED ANALYTICAL DESIGN OF SLIM**

5.1 Introduction.....	56
5.2 Electric machine design with the aided of computer.....	58
5.3 Design methodology of SLIM.....	58
5.3.1 Dimensioning of SLIM.....	59
5.3.2 Procedural calculation of the dimensioning.....	61
5.3.3 Optimization of the dimensioning.....	61
5.3.3.1 The Influence of some design parameters on performance of SLIM.....	64
5.3.3.2 Design Optimization in the SLIM by using Enumeration method.....	73
5.4 Design of SLIM with the aided of computer.....	75
5.4.1 Independent of slip function.....	75
5.4.2 Boundary function.....	77
5.4.3 Maxwell function.....	77
5.4.4 End effect function.....	79
5.4.5 Equivalentcircuit function.....	81
5.4.6 Initialcurrent function.....	81
5.5 The software infrastructure of LIMCAD.....	81

5.5.1 The user-interface of LIMCAD.....	82
5.5.1.1 The new project interfaces of LIMCAD.....	84
5.5.2 A design application using developed software.....	87
5.6 Summary.....	87
 <b>CHAPTER 6 SUMMARY AND CONCLUSION</b>	
6.1 Conclusion.....	93
6.2 Recommendation for Future Work.....	95
<b>REFERENCES</b> .....	96
<b>APPENDICES</b> .....	103
A.1 Presentation of the test bench of CIGGT of ‘Quens’s University’.....	103
A.2 Carter coefficient.....	105
A.3 Saturation factor.....	105
A.4 Equivalent conductivity of the conducting plate.....	106
A.5 Longitudinal end effect factor.....	108
A.6 Simulation Programme (M-File Programming).....	113
<b>CIRICULUM VITAE</b> .....	122

## LIST OF FIGURES

Fig. 3.1 Structure of a single-sided linear induction motor with double layer secondary.....	17
Fig. 3.2 SLIM model used in quasi-one-dimensional theory.....	21
Fig. 3.3 Basic model of method of layer for SLIM.....	25
Fig. 3.4 Model of Single-sided Linear Induction Motor with double layer secondary.....	27
Fig. 4.1 Back iron half space layer modeling.....	39
Fig. 4.2 Linear speed vs. penetration depth at different constant input frequency....	42
Fig. 4.3 Variation of the equivalent permeability vs. linear speed at different input frequencies.....	43
Fig. 4.4 Per-phase equivalent circuit of SLIM.....	48
Fig. 4.5 Secondary impedance vs. linear speed of CIGGT SLIM.....	52
Fig. 4.6 Simulation results for performance of the CIGGT SLIM Experimental points: + 40 Hz, x 28 Hz, o 18 Hz, * 11 Hz, Δ 5 Hz.....	53
Fig. 4.7 Simulation results for performance of the CIGGT SLIM at different air gaps. Experimental points: + 20mm, o 17.5mm, x 15mm, □ 12.5mm.....	54
Fig. 4.8 Simulation results for performance of the CIGGT SLIM at different constant current. Experimental points: + 100A, o 150A, □ 200A, Δ 250A.....	55
Fig. 5.1 Classical procedure of Electric machine design.....	69
Fig. 5.2 More effective design procedure of Electric machine design.....	60
Fig. 5.3 Simple block diagram of the SLIM system.....	61
Fig. 5.4 The structure of the SLIM with double layer and its geometrical parameters for constraints.....	63
Fig. 5.5 Variations of <i>Thrust</i> vs. <i>V<sub>r</sub></i> (linear speed) curves at different thickness of back iron ( <i>d<sub>ir</sub></i> ). .....	65
Fig. 5.6 Variations of <i>Power factor</i> vs. <i>V<sub>r</sub></i> (linear speed) curves at different thickness of back iron ( <i>d<sub>ir</sub></i> ). .....	66



Fig. 5.7 Variations of <i>Power factor product efficiency</i> vs. <i>Vr</i> (linear speed) curves at different thickness of back iron ( $d_{ir}$ ).....	66
Fig. 5.8 Variations of <i>Efficiency</i> vs. <i>Vr</i> (linear speed) curves at different thickness of back iron ( $d_{ir}$ ).....	67
Fig. 5.9 Variations of <i>Thrust</i> vs. <i>Vr</i> (linear speed) curves at different thickness of conducting plate ( $d_{al}$ ).....	68
Fig. 5.10 Variations of <i>Efficiency</i> vs. <i>Vr</i> (linear speed) curves at different thickness of conducting plate ( $d_{al}$ ).....	68
Fig. 5.11 Variations of <i>Efficiency product power factor</i> vs. <i>Vr</i> (linear speed) curves at different thickness of conducting plate ( $d_{al}$ ).....	69
Fig. 5.12 Variations of <i>power factor</i> vs. <i>Vr</i> (linear speed) curves at different thickness of conducting plate ( $d_{al}$ ).....	70
Fig. 5.13 <i>Thrust</i> vs. <i>Vr</i> (linear speed) curves at different air gap ( $g$ ).....	71
Fig. 5.14 Variations of <i>Efficiency</i> vs. <i>Vr</i> (linear speed) curves at different air gap ( $g$ ).....	72
Fig. 5.15 Variations of <i>power factor</i> vs. <i>Vr</i> (linear speed) curves at different air gap ( $g$ ).....	72
Fig. 5.16 Variations of <i>Efficiency product power factor</i> vs. <i>Vr</i> (linear speed) curves at different air gap ( $g$ ).....	73
Fig. 5.17 Flowchart of design algorithm of SLIM at the Constant Voltage excitation.....	76
Fig. 5.18 Flowchart of design algorithm of SLIM at the Constant current excitation.....	80
Fig. 5.19 Submenus of “Menu”.....	83
Fig. 5.20 Submenus of “Material”.....	83
Fig. 5.21 Submenus of “Run”.....	83
Fig. 5.22 Submenus of “Post Process”.....	84
Fig. 5.23 Semi-open slot structure.....	85
Fig. 5.24 Open slot structure.....	85
Fig. 5.25 User interface of General header .....	85
Fig. 5.26 User interface of Stator header .....	86
Fig. 5.27 User interface of Winding header.....	86
Fig. 5.28 User interface of Reaction Rail header .....	87
Fig. 5.29 Design output in program format .....	88

Fig. 5.30 Thrust vs. linear speed.....	89
Fig. 5.31 Efficiency vs. linear speed.....	89
Fig. 5.32 Power factor vs. linear speed.....	90
Fig. 5.33 Output power vs. linear speed.....	90
Fig. 5.34 Normal forces vs. linear speed.....	91
Fig. 5.35 Input power vs. linear speed.....	91

## LIST OF TABLES

Table 5.1 Performance values at discrete values of thickness of the back iron.....	65
Table 5.2 Performance values at discrete values of the conducting plate thickness.....	69
Table 5.3 Performance values at discrete values of the air gap.....	71
Table 5.4 Some structural constraints (u.b. =upper bound, l.b=lower bound) .....	74
Table A.1 Design data of single-sided, three-phase LIMs for propulsion of Vehicles.....	104
Table A.2 Design output in MS Excel format.....	111

## LIST OF SYMBOLS

$\mu_{re}$	Equivalent permeability of secondary iron
$\mu_{rs}$	Surface permeability of secondary iron
$sw$	Slot width
$W$	Secondary iron width
$L_p$	Primary length
$to_v$	Thickness of the overhang
$ho_v$	Height of the overhang
$W_p$	Primary width
$H_{mx}$	Tangential magnetic field intensity
$H_{my}$	Normal magnetic field intensity
$B_{my}$	Normal magnetic induction
$B_{mx}$	Tangential magnetic induction
$hp$	Height of the primary core
$dir$	Back iron thickness
$dal$	Aluminum thickness
$g$	Mechanical clearance
$g'$	Effective air gap
$k_\mu$	Saturation factor
$kc$	Carter coefficient
$k_{RN}$	Russel and Northwossy factor
$ktr$	Edge effect factor
$F_x$	Thrust
$F_y$	Normal force
$\tau_d$	Slot pitch
$h_e$	Slot height
$l_d$	Tooth width
$\sigma_{Al}$	Conductivity of aluminum
$\sigma_{Fe}$	Conductivity of iron
$V_r$	Linear speed

$V_s$	Synchronous speed
$s$	Slip
$K_{v1,2}$	Propagation constants
$\alpha_{1,2}$	Attenuation factor
$\tau_e$	End effect pole pitch
$T_e$	Attenuation Factor
$V_e$	End wave velocity
$V_o$	Boundary Speed
$k_e$	End Effect Factor
$d_R$	Equivalent thickness
$\delta$	Phase angle between end wave and principle wave

## CHAPTER 1

### 1.1 Introduction

Linear induction motors (LIM) have recently gained great popularity for use in transportation and industrial applications nowadays. It is because they consume low energy, cause low pollution and in addition to their advantages such as less friction and maintenance compared with traditional transportation vehicles and their simple implementation [1]. Due to such reasons, they are highly preferred for linear movement requirements in industry. Research studies [2-4] in the literature attempted to develop mathematical models to analyze and design such type of motors. Although their models were adequate for some particular cases, changing conditions and technology require the researchers to improve such models or develop new ones. As a result, research effort over the LIM is still an essential subject since required precise results in such motors has not been obtained yet.

In order to improve the accuracy and the performance of the LIM, an understanding of its physical structure and properties should be put into the research. One important point to deeply comprehend the internals of the LIM is the electromagnetic phenomena that occur due to its physical properties and structure. An adequate treatment of such phenomena is a vital point in calculation and estimation of performance of the LIM. The study [1] shows that the proposed mathematical models in the literature could not reach the desired accuracy due to the lack of adequate consideration of such phenomena.

The phenomena that primarily effect the performance calculations of the LIM can be listed as; the longitudinal end effect which is a consequence of the limited length of the LIM, the transverse edge effect which is a result of the lack of a specific path for the induced current, the slot effect, the saturation and hysteresis effect which happens due to the existence of the secondary iron. Electromagnetic analysis should be done in order to investigate these phenomena. The method of layer technique is a

frequently utilized technique in the literature for electromagnetic analysis, and this study also makes use of it as well. The electromagnetic equations obtained as a result of this technique are not only useful for the performance calculation of LIM, but also required for the acquirement of parameters that is used at the design and analysis of the LIM. Utilizing the equivalent circuit as a part of electromagnetic analysis is observed to be appropriate since direct application of electromagnetic equations for the purpose of design is known to be limited [3]. Hence, this study uses the equivalent circuit approach for the mentioned purposes.

Although, there are several studies in the literature which considers the equivalent circuit technique together with aforementioned important phenomena to make an accurate analysis, it is seen that the studies about some of the mentioned phenomena such as the saturation and hysteresis effects are still inadequate. Main reason of this is the errors in the parameter values, which are hard or impossible to measure, such as secondary impedance. In this study, a statistical method is used to estimate such a widely misevaluated phenomenon. Least Squares method as a linear approximation tool is employed in order to correctly estimate the secondary impedance. The outcomes of the proposed method are then compared with the results of Canadian Institute of Guided Ground Transportation LIM. As far as the results of this evaluation are concerned, the consideration of the important phenomena is observed to be adequate. Also, when the proposed method is compared with similar studies from the literature, it is seen to be superior to them, as well especially at 40 Hz.

On the other hand, advanced design of a LIM requires a computer software not only to accurately determine the performance of a LIM of given design parameters, but also will provide an interactive interface in the design of a LIM for a given set of specifications [2]. For this purpose, the proposed method of this study is implemented in a combination of software tools such as MATLAB and VC# .NET . More technically, the core components of the produced design software are implemented by using MATLAB since it is an appropriate software environment for scientific purposes. Although MATLAB provides powerful scientific tools, it is not capable of producing user-friendly software program, particularly for end-users. Thus, Visual C#.NET is utilized to build a user-friendly interface program for the

core components of the design software. The developed software is introduced in the chapter 5.

## **1.2 The Layout of Thesis**

General literature reviews for analytic methods used in analytical modeling of linear induction motor are summarized in the chapter 2.

A detailed analytical modeling of the linear induction motor based on the method of layer in two-dimension (2D) taking into account of longitudinal end, transverse edge, saturation, slot, hysteresis effects and non-linear magnetic permeability occurring during the steady state operation of SLIM is presented in the chapter 3.

The equivalent circuit technique (ECT) in calculation of the performance of single-sided linear induction motor (SLIM) is presented. Also novel approach for the estimation of secondary iron impedance of the SLIM is offered. Developed computer code for analysis of SLIM is validated by using experimental results and simulation data already exist in literature in the chapter 4.

A design methodology of SLIM based on the analytic tool are given and implementation tool of a computer-aided design of SLIM is presented in the chapter 5.

In the chapter 6 final conclusion and recommendations for future works are summarized.



## **CHAPTER 2**

### **LITERATURE REVIEW**

#### **2.1 Introduction**

There are a lot of studies on the analysis of linear induction motors in the literature, but very few papers focus directly on the design of a single-sided linear induction motor (SLIM). An analysis and design of a linear induction motor are based mainly on two different methods: analytic and numeric techniques. Linear induction motors have different characteristics from rotary induction motors due to having a beginning and an end in the direction of movement. These features cause some phenomena which effect on the performance of the single-sided linear induction motors. The longitudinal end and transverse edge effects are the phenomena which affect the performance of the linear induction motors. In order to get the high accuracy for the performance, these effects must be taken into account. In the literature, different methods have been proposed in order to take into account these effects in calculations of the performances of the linear induction motor. And the influence on the performances of the different linear induction motor configurations has been investigated. There has been also studying to reduce these effects on the performance of the linear induction motor. Literature review has been classified as numeric techniques and analytic techniques.

#### **2.2 Analytic Techniques**

Yamamura, [5] studied the theoretical aspect of linear induction motors, especially the influence the longitudinal end effect on the performance of linear induction motor. The linear induction motors were also investigated [6], especially single – sided linear induction motors is well discussed in their studies. Finally, the most recently book has been published and this book covers all aspect of the subject,

including constructional features, applications, electromagnetic effect and design [7].

An experiment was carried out for high speed linear induction motor with a saturable iron secondary by use of a rotary type test facility. This experimental study was compared to the calculations by a new theory derived equations considering the end effect and the magnetic saturation [8].

A number of assumptions which are frequently made in the analysis of linear induction motor were examined. Thrust and attractive force measurements which made on a 2-m diameter test wheel fitted with iron-backed aluminum sheet secondary and arc type primary, were compared with results from three-dimensional field analysis [9].

A quasi three- dimensional mathematical model was developed for the design of linear induction motors constant current and constant voltage excitation. In this study, the described analytical approach leads to mathematical model which is also a practical design tool for designer [10].

A summary of experimental research project to evaluate a single-sided linear induction motor (SLIM) as an integrated suspension/propulsion system (ISPS) for guided ground transportation vehicle was presented [11]. Also experimental results for rotating wheel tests of a full size section of a SLIM was presented.

A single-sided linear induction motor with solid iron secondary was studied [12]. A computer model described for the purpose of prediction of the reaction forces.

Calculation of magnetic flux density, currents, forces and power losses was performed for two layers of a secondary using Fourier's series method [13]. Conducting plate thickness and currents in the secondary back iron were taken into account in an idealized LIM model.

The Fourier series method was used to solve differential equations in linear induction motor (LIM) is based on a computational model in which the real primary

is replaced by a series of fictitious primaries distributed along the direction of motion. The distance between adjacent primaries ought to be big enough to avoid the influence of the primary field on the following one. A method was proposed to determine of this distance [14].

The performance of the single-sided finite length linear induction motor was analyzed with the special emphasis on the influence of hysteresis effects in the rotor yoke. The working parameters were significant especially in the low slip region. The dimensionless characteristics were obtained as a function of slip via Maxwell's equations in the air-gap and rotor yoke [15].

The influence of the secondary solid ferromagnetic plate thickness on the performance of the single-sided linear induction motors was analyzed for two different reaction-rails which are a simple solid strip and an aluminum cap over a solid steel core. An equivalent circuit of the single-sided linear induction motor, with speed and frequency dependent parameters, was used. The magnetizing and secondary impedances were evaluated from the solution of the two –dimensional field distribution in the machine. The analyses were validated by test results and were used to evaluate the effects of varying steel thickness under constant voltage and constant current excitation [16].

A single-sided linear induction motor with a double layer reaction-rail has been studied. This reaction-rail configuration consists of a conducting plate over a solid steel core. The width of the conducting plate is different than the width of the secondary steel core and the thickness of the conductive overhand is different from that over the steel core. A method for computing the SLIM with a double layer reaction-rail has been developed under constant current excitation. This method takes into account the reaction of the secondary eddy current on the air-gap field, transverse edge effect, longitudinal end effects, skin effect, saturation, nonlinear magnetic permeability and hysteresis in the solid steel core of reaction-rail. Equivalent circuit parameters have been derived from the two-dimensional (2D) electromagnetic field distribution. The developed expressions in this study can be used for small and large LIM's and also be used for constant voltage excitation [2].

The influence of conductive cap thickness on the performance of a single-sided linear induction motor with reaction-rail formed from a conductive cap over a solid or laminated steel core was analyzed. The results have been shown that the thickness of the conductive cap affects performance through the changes in the effective secondary impedance. The analysis was applied to examine the effects of changing the cap thickness of four single-sided linear induction motors [17].

A study was made on the design of the single-sided linear induction motors for urban transit. The performance characteristics were calculated using a space harmonic analysis. The outline of the practical design of the single-sided linear induction motor was presented and various ways to determine the design parameters were pointed out [18].

A hybrid method was used for analysis of the single-sided linear induction motor. This analysis method consists of field theory approach and a multilayer approach. The double layer secondary reaction-rail has nonlinear permeability due to the consisting of the solid steel core. In this method, the secondary iron permeability was adjusted to match tangential magnetizing field in conjunction with each layer using proposed iterative method [19].

The calculation method of the linear induction motor performance based on the Fourier series technique and takes into account the current asymmetry caused by the end effects was presented [20].

The phase unbalance conditions due to the asymmetry of the primary winding and the end effect in single sided linear induction motor was evaluated by two methods. One of these is analytical method based on the equivalent circuit model and another is finite element method [21].

An analytical method was presented for calculating the thrust of single-sided linear induction motor, including the effects of both phase unbalance and higher time harmonics. An analysis for computing the thrust of a LIM including the time harmonics and phase unbalance effects was validated with the test results from a

large-scale six-pole LIM. It was shown that these analyses can be applied to machine designed for transportation drives [22].

A method of the stray losses calculations in single-sided linear induction motors was described. The stray losses produced by the higher space harmonics of the primary winding and the primary slots were discussed and example calculations for a small and a large-scale linear induction motor were carried out [23].

An analytical layer model was developed in which the primary core was modeled by two different layers representing the yoke and teeth slot regions. A two-dimensional electromagnetic analysis was formulated for a multilayer linear induction motor model [24].

An improved analytic method and performance equations was derived for the estimation of the performance characteristics and the design of the linear induction motor. To simplify the estimation of the performance of the single-sided linear induction motor, an approximation was presented [25].

A new factor was established to thrust of a linear induction motor which named "Relation factor". This factor does not require such electric circuit. In this study, one more analysis tool for linear induction motor was presented [26].

An analytical technique based on the equivalent circuit was developed to use the performance prediction of single-sided linear induction motors. In order to account the longitudinal end effect analytically new approach was developed in this study. A new method for calculation of the equivalent resistance of the hypothetical layer with the thickness  $d_R'$  was proposed. In this method, the equivalent resistance is evaluated for the integrated secondary with two parallel aluminum and iron layers. New  $d_R'$  equation, which was derived according to the above idea, was compared to the other two equation of the  $d_R'$  and good correlation with the experimental results was obtained [1].

The determination of the equivalent circuit parameters, a new non-iterative method was derived. Prior to this, relative permeability of the back iron was calculated by a

non-iterative method. If the input current, input frequency and dimensional characteristics of the linear induction motor are available, the equivalent circuit parameter values can be obtained in each slip via a simple substitution [27].

A new analytic method based on the air-gap flux density equation was developed to calculate the performance of the single-sided linear induction motor taking into transverse edge, end, and skin effect account [28].

The design, the realization and the control of a linear induction motor devoted. In this order, a first modeling approach exploiting an analytical analysis technique articulated on the layers method was developed. To validate the previous results, a second modeling approach, exploiting numerical techniques was elaborated around a discretization by finite element [29].

The influence of the design parameters on linear induction motor end effect was investigated by using analytical method. A factor depending on the number of magnetic poles, secondary resistivity and frequency was developed. These design parameters influence the end effect of the linear induction motors. According to this parameter, the variation of this factor for linear induction motor end effect analysis was investigated [30].

Design optimization of a low speed single-sided linear induction motor for improved efficiency and power factor was studied. A multiobjective optimization method was used to improve both efficiency and power factor simultaneously. To calculate the efficiency and power factor was carried out by using analytic method. So that, the effects of the various motor specifications on the efficiency and power factor could be investigated [31].

An analysis of the single-sided linear induction motor with a solid-steel reaction plate was presented by solving for the two dimensional field distribution in the air-gap and in the secondary [50]. For motoring and for plugging operation under constant-current conditions was computed and compared with the experimental results from a large-scale test linear machine. It was observed that the experimental and simulations results were in good agreement.

### 2.3 Numerical Techniques

The FEM of the eddy current problem subject to the convective diffusion equation was applied to the numerical analysis of the low-speed and high speed LIM's [32].

The linear induction machine thrust and normal force was calculated using the Finite Element Method (FEM). The Lorentz formula and Maxwell stress tensor method were used to calculate the thrust. Some improvements in the accuracy Maxwell stress tensor calculations could be achieved by increasing mesh density in the air gap [33].

The electromagnetic field in linear induction motors are subjected to the convective diffusion equation is difficult to solve analytically. The numerical method such as Finite element method was applied to them. In this study, an Upwind Galerkin Finite element method was proposed for electromagnetic field problem in moving media [34].

A performance analysis of low speed linear induction motor with a solid steel secondary was carried out by the finite element method combined with the impedance boundary conditions at the surface of the secondary steel. It was used a numerical tool [35].

A new method in which an analysis calculation in the moving rail gives a convolution equation on the interface with the motionless region was proposed by [36]. This convolution was used as boundary condition in the motionless region where the computations use the finite element method (FEM).

A single-sided linear induction motor with a short primary and complicated secondary structure, which consists of solid-plate conductor section and a winding one, was analyzed [37]. To do this, electromagnetic field analysis by 3-D FEM was combined with electric circuit analysis and motion equation.

To investigate the drug plate linear induction motor (DP-LIM), the Fourier transform model was used considering saturation and skin affecting the back iron.

The Fourier transform model was obtained from the FEM analysis. The aim of this study is to analyze DP-SLIM from viewpoint of its suitability for different applications [38].

A new time-stepping, three-dimensional (3-D) numerical analysis method based on the magnetic equivalent circuit was proposed [39]. In this method, the analyzing linear induction was performed faster computation time and less memory than the conventional methods.

The model suggested by Duncan for simulation of linear induction motors was modified by means of the Finite Element Method (FEM) [4]. The modified model includes such effects as longitudinal end effect, transverse edge effect and saturation of the back iron. And this model computes the level of the saturation by both simple calculation and an iterative method firstly then it computes the equivalent circuit parameters using FEM. There is a change in magnetizing branch due to the end effect between this model and classical equivalent circuit. The magnetizing branch impedances were determined the results by the standard test. So, it was estimated that this model is not appropriate for the design.

A boundary structure for improving performances of single-sided linear induction motors was studied [40]. The transient phenomena which cause undesirable influences on the machinery at the basic boundary structures were discussed by adopting a three-dimensional finite element method.

The primary and secondary leakage inductance parameters was estimated by parameter estimation methods for linear induction motor that utilizes pulse width-modulator. This method was yield mutual inductance by numerically solving a third order polynomial [41].

A single-sided linear induction motor was modeled and simulated using finite element analysis based on MagNet 6.13. Torque and flux linkage characteristics of the machine were analyzed with respect to variation in the air gap, material variation, variation in secondary plate thickness [42].



The end effect in linear induction motors was investigated by using the Finite Element Method. This study focused on two developed model for investigation. The normal component of flux density distribution in the air gap was investigated by means of the end effect at different conditions [43].

The dynamic characteristics of a single-sided linear induction motor (SLIM) having the joints in the secondary conductor and the back iron were analyzed and discussed. In this analysis, the time-stepping finite element method and the moving mesh techniques were used for simulation. As a result of this simulation, the junction between the secondary conductors created a discontinuity of the eddy current and fluctuations of the thrust and the normal force [51].

A single-sided linear induction was analyzed by using two dimensional time-stepping finite elements. The analysis model has been taken into account transverse edge effect and primary moving. The Maxwell stress tensor was used to calculate the thrust and normal force at different speed. The simulation results were found to be good agreement to the thrust characteristics [52].

An accurate d-q axis equivalent circuit model of linear induction motor for drive system simulations was built based on nonlinear transient finite element analysis to obtain the asymmetric d-q equivalent constants for static end effect and distorted air gap distribution by velocity for dynamic end effect. The effectiveness of the proposed d-q equivalent circuit model has been tested through implementation of vector control examples taking into consideration the static and dynamic end effect [53].

The characteristic analysis of single-sided linear induction motors (SLIM's) with a short primary in accordance with the secondary reaction flat structure was described. The equivalent parameters according to the secondary conductor shape were calculated and estimated using 2-D FEM. Additional, on the basis of the comparison of the static and transient characteristics results simulated by the FEM program, it has been determined that secondary conductor structure affects the secondary impedance of the equivalent circuit of the SLIM [54].

The interpolating linear moving boundary method (ILMBM) in FEM to calculate transient electromagnetic field of SLIM was developed and the longitudinal end effect was analyzed taking into consideration eddy currents in secondary plate. The results of this analysis have been indicated that as the excitation frequency and primary speed raise, the longitudinal end effects will increase. And also, the efficiency of ILMBM has been confirmed in accordance with the computed result [55].

The influence of the longitudinal end effects to performance of linear induction motor was considered through equivalent electro-motive force (EMF). The transverse edge effects were painstaking with the aim to the conductivity of secondary and ferromagnetic secondary by different modified coefficient. Thrust and normal force was computed by a model of a single-sided linear induction motor under different air-gap and current frequency. These results have been applied to the single-sided linear induction motor to predict its performances. The calculated values of thrust and normal force were very close to the measured values [56].

The single-sided linear induction motor with a solid-steel reaction plate was analyzed by solving the two-dimensional field distribution in the air gap and in the secondary. Mutual and secondary impedance were derived taking into account the longitudinal end effect, transverse edge, the thickness of the secondary plate and skin effect. Simulation results created by this proposed method have been a good agreement with the traditional results under constant current conditions [57].

## **2.4 Summary**

It is clear from the literature review that a large amount of work has been carried out in the analysis of SLIM using different numerical and analytical techniques. Compared to rotary induction motors; linear induction motors have special electromagnetic phenomena: electromagnetic longitudinal end effect and transverse edge effect. These effects influence the performance of the linear induction motors. Recent works were focused on the investigation of these effects on the performance of the linear induction motors using analytic and numeric techniques. The main goal

of these studies anticipated to get the best performance results of the SLIM. In addition to that, in the literature there exist also other studies for compensating the longitudinal end effect which has the major affect on the performance of the SLIM.

Limited work has been done in the design of SLIM considering all effects. As a result of literature survey, it is obvious that increasing the accuracy of performance calculations requires adequate treatment of electromagnetic phenomena in order to enhance the existing models in the literature. Through these improvements it would be possible to realize high accuracy SLIM analysis and design.

## CHAPTER 3

### ANALYTICAL MODELLING OF SINGLE-SIDED LINEAR INDUCTION MOTOR

#### 3.1 Introduction

The studies of an analytic modeling of various type of linear induction motor are still subjected to research. Actually, there is very rich literature related to this type of modeling that includes an experiment and uncompleted research [1] and [30].

In the literature, the steady-state performance characteristics of linear induction motor have been determined using one-, two- and three- dimensional electromagnetic field analysis including the longitudinal end effects, transverse edge effect and reaction of eddy current in the secondary [6]. From the computational point of view, the calculation of two-dimensional field in a longitudinal section of a SLIM is preferable to a full three-dimensional analysis and is entirely adequate for performance evaluation [2]. In design consideration of SLIM, a direct application of the field equations is restrictive and using the equivalent circuit is convenient in such a case [3]. So that, analytic tool based on the design of the single-sided linear induction motor is appropriate for the analysis and design using the equivalent circuit approach.

The design of the linear induction motor can be achieved using analytic techniques and numerical techniques. In order to carry out the design of the linear induction motor, an analytical or numerical modeling of the various phenomena during the operation of the motor is essential. A preferable model should not require an excessive processing time and includes a minimum of simplifying assumptions. The appropriate analytic model of the single-sided linear induction motor should be chosen with respect to this aim for developing computer aided design software. There are several analytic methods to model the single-sided linear induction motor proposed in the literature [2],[3],[6].

The method of layer is the analytic method which is widely used for analysis of SLIM in the literature [50]. It seems to be used to model of SLIM for two-dimensional analysis of SLIM. The equivalent circuit parameters for SLIM are derived from the two-dimensional field analysis using the method of layer. So, the performance calculation can be carried out by using equivalent circuit parameters of SLIM.

In this chapter, the structure and principle operation of SLIM is presented. Then, the method of layer is also presented in detailed, in order to model the steady state performance characteristics of SLIM analytically.

### **3.2 Operation Principle of Single-sided Linear Induction Motor**

The various types of the linear motors correspond to the various rotary motor because the linear motor is only developed from the rotary motor. It generally uses the primary and secondary terms to indicate inductive and induced, instead of stator and rotor respectively. In addition, functions of the single-sided linear induction motor are the same principle as the rotary asynchronous motor.

The figure (3.1) represents structure of a single-sided linear induction motor, where the displacement of the armature (or the inductor) is carried out according to the longitudinal axis ( $x$ ) at a mechanical speed ( $Vr$ ) [18].

The primary field windings are located in the primary slots and are transverse by currents also circulating in the transverse direction ( $z$ ). Those create a principal induction directed along the normal axis ( $y$ ). If this winding, which is properly distributed, is fed by principally three-phase source of pulsation  $\omega$ , principal magnetic induction and the magneto motive force are propagated along the longitudinal axis ( $x$ ) in the form of a wave moving at the linear speed [18].

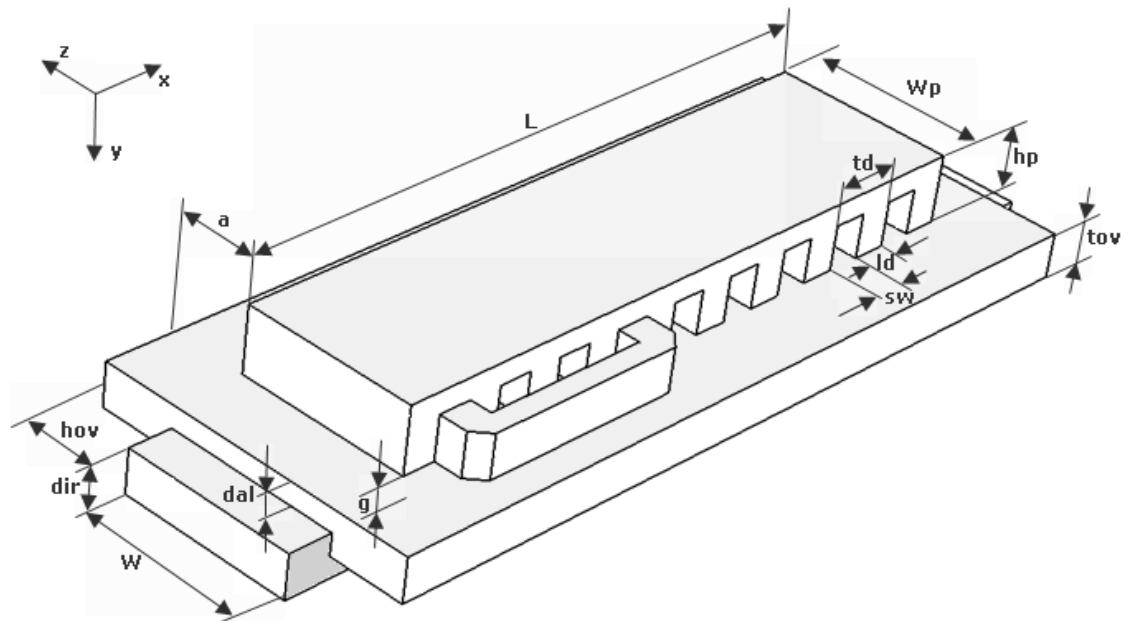


**Figure 3.1** Structure of a single-sided linear induction motor with double layer secondary

The magnetic flux across the air-gap generates the electromotive forces and the currents in the secondary conducting plate. The magnetic flux created by these currents slips compared to the inductor and with the armature, but it remains motionless compared to principal flow. The interaction from these two flows creates a linear push. The armature (or the inductor) is thus concerned with the continuation (in reverse direction) slipping field. Then, the elementary operation principle is similar to that of a machine with circling induction, which is based on an asynchronous magnetic coupling [7].

The secondary structure of SLIM is generally not the same compared to the secondary of the rotary induction motor. Indeed, this structure is generally composed of a ferromagnetic layer of steel and a conducting layer which is the seat of induced currents. The right and left width of the conducting layer in transverse direction part is to close circuits for the induced current [5].

### 3.3 Electromagnetic Field Model of Linear Induction Motor

Analytical or numerical methods start from a formulation of electromagnetic fields resulting from the Maxwell's equations. Those govern all those electromagnetic

phenomena within single-sided linear induction motor. Electromagnetic fields analysis problem within the single-sided linear induction motor arises in a fundamental way in terms of the Maxwell's equations [19]. They are as follow;

$$\overrightarrow{Rot} \overrightarrow{H} = \overrightarrow{J}_c \quad (3.1)$$

$$\overrightarrow{Rot} \overrightarrow{E} = -\frac{\partial \overrightarrow{B}}{\partial t} \quad (3.2)$$

$$\overrightarrow{J}_c = \sigma \overrightarrow{E} \quad (3.3)$$

$$\overrightarrow{B} = \mu \overrightarrow{H} \quad (3.4)$$

$$Div \overrightarrow{B} = 0 \quad (3.5)$$

In order to define electric scalar potential and magnetic potential vectors using the above equations are expressed as:

$$\overrightarrow{B} = \overrightarrow{Rot} \overrightarrow{A} \quad (3.6)$$

$$\overrightarrow{E} + \frac{\partial \overrightarrow{A}}{\partial t} = -Grad \phi \quad (3.7)$$

In the existing moving media, the conducting current density ( $\overrightarrow{J}_c$ ) is written in the following form;

$$\overrightarrow{J}_c = \overrightarrow{J}_{ex} - \sigma \frac{\partial \overrightarrow{A}}{\partial t} - \sigma Grad \phi + \sigma (\overrightarrow{V} \times \overrightarrow{B}) \quad (3.8)$$

Induced currents by a possible relative mechanical movement between conducting part and the magnetic field lines are defined in the reference study frame. The preceding equations can be combined to lead to the following total equation [44].

$$\overrightarrow{Rot} \left( \frac{1}{\mu} \overrightarrow{Rot} \overrightarrow{A} \right) = \overrightarrow{J}_{ex} - \sigma \left( \frac{\partial \overrightarrow{A}}{\partial t} + Grad \phi - \overrightarrow{V} \wedge \overrightarrow{Rot} \overrightarrow{A} \right) \quad (3.9)$$

This equation makes it possible to analyze the electromagnetic fields in an electromagnetic device fed during the operation in a general way and in the linear

induction motor in particular. Indeed, let us note that the magnetic potential vector is not single; the equation (3.7) shows that this one derives from rotational. Infinity of solutions arises and they differ from/to each other of a gradient. The gauge of Coulomb is often used to guarantee the unicity of the solution.

$$\text{Div}\vec{A} = 0 \quad (3.10)$$

The term (*Grad* $\phi$ ) in the induced currents, this assumption can be neglected because of the symmetry of the distribution of these currents in the apparatuses with induction in a general way [45].

Harmonic model is used in order to make it possible to be freed from the time constraint by supposing that the source currents are purely sinusoidal and the electromagnetic fields vary also in a sinusoidal way [44].

$$\frac{\partial \vec{A}}{\partial t} = js\omega \vec{A} \quad (3.11)$$

$$\vec{J}_{ex} = J_{ex} \exp(j(\omega t + \varphi)) \quad (3.12)$$

where  $s$  is the relative slip speed compared to slipping field, then equation (3.9) becomes [46].

$$\overrightarrow{\text{Rot}}\left(\frac{1}{\mu} \overrightarrow{\text{Rot}}\vec{A}\right) = \vec{J}_{ex} - \sigma(js\omega \vec{A} - \vec{V} \wedge \overrightarrow{\text{Rot}}\vec{A}) \quad (3.13)$$

Generally, an electromagnetic device comprises several materials which have some nonlinear characteristics. In addition, the electromagnetic phenomena strongly vary within the structure. Equation (3.13) can be used for the one-, two and three-dimensional electromagnetic field analysis of the single-sided linear induction motor. An analysis of the complete structure in three dimensions (3D) proves expensive in terms of computing time. In addition, one-dimensional (1D) analysis is not very representative. The use of the two-dimensional (2D) models is particularly simple and effective and its choice is realistic.



### **3.4 Analytical Methods of Linear Induction Motor**

Analytical modeling of single-sided linear induction motor is developed by using analytic method. In order to model the linear induction motor, these analytic methods are applied to this model with the appropriate assumptions according to dimensional analysis. These assumptions are intended to simplify the complex analysis in the model. 1D, 2D and 3D electromagnetic field analysis within the linear induction motors. The quasi-one dimensional model of SLIM has been given for an example of modeling. The method of the layers, which is one of the analytic methods to model of the single-sided linear induction motor with double layer secondary, can be used in order to model with 2D electromagnetic field analysis which seems to be adapted to the establishment of an analytic tool dedicated to the computer-aided design.

#### **3.4.1 Quasi-one-dimensional Model of Single-sided Linear Induction Motor**

The one-dimensional model, which takes only the variations in the x coordinate into consideration, is sufficient for many purposes [5]. In this model, the transverse edge effect, skin effect and secondary saturation are taken into account by means of appropriate coefficient (such as equivalent secondary conductivity and air gap). This model also used in two-dimensional electromagnetic field analysis for SLIM. Figure 3.2 [24] shows the SLIM model used for analysis in two-dimensions. It has four distinct regions: 1) Primary, 2) Air-gap, 3) Reaction rail, 4) Back-iron.

According to this model of SLIM, certain assumptions are made for one-dimensional (1-D), two-dimensional (2-D) electromagnetic analysis. For two-dimensional analysis of SLIM, certain assumptions are made [3]. They are as follows

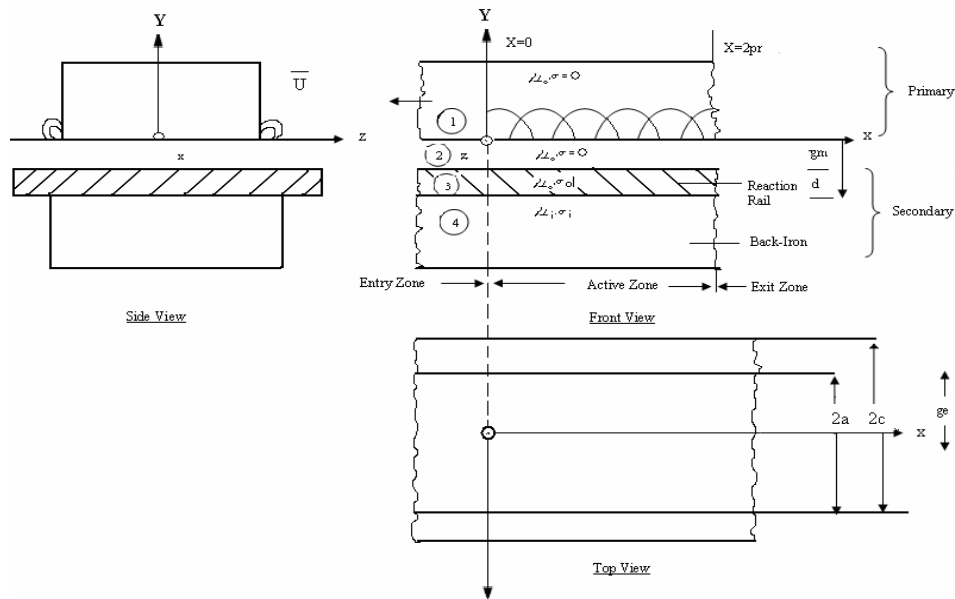


**Figure 3.2** SLIM model used in quasi-one-dimensional theory

- 1) All layers extend to infinity in the  $x$  direction. However, in calculating the thrust and the reactive power, the field behind the motor exit is ignored.
- 2) The frame of reference is attached to the primary. The primary winding is confined to an “active zone.”
- 3) Time and space variations are sinusoidal.
- 4) Excitation windings are located in the primary slot. The excitation is presented by an equivalent current sheet of negligible thickness which produces the same magneto motive force as primary winding
- 5) Edge effect, skin effect, back-iron saturation, air gap leakage, slot effect are taken into account by suitable correction factor.
- 6) Currents are only  $z$ -directed.
- 7) Variations in  $z$  direction are ignored.

Assumptions (6) and (7) facilitate analysis in two-dimensions. According to rest of these assumptions, simplification is carried out. So, electromagnetic field equations are obtained from the Ampere’s law by using the reference frame which includes three different media.

### 3.4.2 One-dimensional Electromagnetic Field Equation in the Air-gap

The longitudinal end effect is the phenomena which occur due to the limiting length of the motor in longitudinal section. In order to get the high precision results for the performance of SLIM, this effect must be taken into account. By using considerable simplifications and one-dimensional electromagnetic field model, the distribution of induction in the air-gap and the conducting layer of the armature are determined to characterize the end effects in SLIM.

In the end effect analysis of SLIM, the distribution of induction in the air gap is investigated by designer. By given appropriate simplifications for one-dimension, the distribution of induction is obtained by largely simplifying the three-dimensional equation (3.9) resulting from the Maxwell's equations.

For the machine represented in Figure (3.1), equation (3.13) can be simplified by assumptions that [47]:

- 1) Only the  $H_y$  component exists in the air-gap and the conducting part of the secondary;
- 2) The permeability of the ferromagnetic steel of the primary and the secondary is infinite;
- 3) Only the currents component induced along axis ( $z$ ) exists in the active part of the conducting layer of the secondary of the motor;
- 4) The currents induced along axis ( $x$ ) circulate in the part of the conducting layer located on both sides active part;
- 5) In steady operation, if the source of food is sinusoidal, the derivative compared to time  $\partial/\partial t$ , is replaced by  $jsw$ ;
- 6) And the primary currents feeding are represented by thin current density by:

$$j_{ex} = \text{Re} \left\{ J_{ex} \exp \left[ j \left( \omega t - \frac{\pi x}{\tau} \right) \right] \right\} \quad (3.13)$$

Under these conditions, equation (3.13) becomes [53]:

$$\frac{\partial^2 B_y}{\partial x^2} - j \frac{\mu_0 \sigma \omega s}{g} B_y = \frac{\mu_0}{g} \frac{\partial j_{ex}}{\partial x} \quad (3.14)$$

In steady-state operation, the solution of this equation is given by:

$$B_y = \text{Re} \left[ \begin{aligned} & B_s \exp \left\{ j \left( \omega t - \frac{\pi x}{\tau} \right) \right\} + B_1 \exp \left( \frac{-x}{\alpha_1} \right) \exp \left\{ j \left( \omega t - \frac{\pi x}{\tau_e} \right) \right\} + \\ & B_2 \exp \left( \frac{-x}{\alpha_2} \right) \exp \left\{ j \left( \omega t + \frac{\pi x}{\tau_e} \right) \right\} \end{aligned} \right] \quad (3.15)$$

where  $\alpha_1$ ,  $\alpha_2$  and  $\tau_e$  are related to linear speed, conductivity of the secondary conducting plate and thickness of the air gap. The constants  $B_s$ ,  $B_1$  and  $B_2$  can be deduced starting from the boundary conditions. The first term of equation (3.15) is a principal field slipping which is propagated in the opposite direction of movement of the primary and corresponds to the spinning field pattern in the air-gap of a rotary induction motor. The second term is magnetic induction due to the entry end effect of SLIM. This wave is propagated along axis (x) in the direction of the main field propagation. Lastly, the third term represents magnetic induction due to the exit end effect; this wave is propagated along axis (x) in the opposite direction of fundamental displacement field. These two waves are space harmonics of principal induction in the air-gap of SLIM. They cause the attenuation of the performances of SLIM compared to the rotary induction motor.

In general,  $\alpha_1$  is larger than  $\alpha_2$  and the wave due to the entry generates a broader effect on performances of the linear induction motor compare to the exit wave [7]. Moreover, for high speeds applications,  $\alpha_1$  becomes large and the two dominating waves that are propagated together over the entire length of the primary. The entry

end wave can be reached at the beginning of the exit end of primary. But the exit end wave never reaches the entry end of the linear induction motor. The performances of the SLIM are seriously affected for high speeds. In addition to that, these effects are also pronounced also for small slips.

### **3.4.3 Method of the Layers**

Generally, the linear induction motor has a rather large air-gap compared to its rotary induction motor due to the problems of guidance of movement. This is why; the assumption of the uniform magnetic field intensity ( $H$ ) through the air gap is not very realistic. Moreover, the secondary of this type of motor are made up of an aluminum plate and a ferromagnetic layer of steel, in general. Consequently, in order to obtain precise results the distribution of the induced currents in the secondary must be taken into account [7].

An approach of analysis known as method of layers was developed [48]. It consists in dividing the SLIM into layers as shown in the figure 3.3, then to calculate the distribution of magnetic induction.

On two-dimensional (2D) assumption, the fields are supposed invariants in the transverse direction ( $z$ ) and the currents induced in the secondary circulate according to the same direction. Nevertheless, in a linear induction motor including a conducting layer in the secondary, the induced currents have a component according to the longitudinal direction which corresponds to the direction of movement ( $x$ ). The effect of these currents is taken into account by adjusting the resistivity of the conducting parts of the armature by correct factors. Moreover, the slot effect can be taken into account by increasing the air-gap by the Carter coefficient and primary part is presented by an infinitely thin current sheet, deposited on surface between the primary education and the air-gap.

The inherent disadvantage of the method of the layers is that the transversal and longitudinal dimension effect of the primary applying to the electromagnetic field analysis of a linear induction motor is the difficulty.

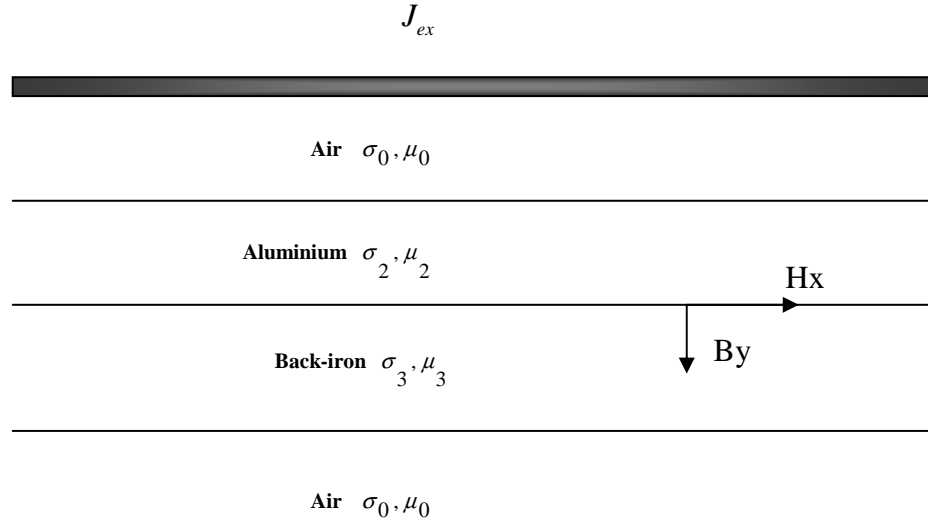


**Figure 3.3** Basic model of method of layer for SLIM

Figure 3.3 shows the provision of the layers in a single-sided linear induction motor supplied with a sinusoidal power source such as:

$$j_{ex} = \text{Re}\{J_{ex} \exp[j(\omega t - kx)]\} \quad (3.16)$$

The values of  $B_y$  and  $H_x$  of figure 3.3 are those of the interface between the layers, which must check the conditions of passage between two mediums. For the each layer and by supposing that the fields are sinusoidal and have a frequency  $\omega_n$ , equation (3.14) can reduce to the following equation:

$$\frac{\partial^2 B_y}{\partial y^2} = \gamma_n^2 B_y \quad (3.17)$$

Where:

$$\gamma_n = (k^2 + j\mu_n \sigma_n \omega_n)^{1/2} \quad (3.18)$$

Such as  $k = \frac{2\pi}{\lambda}$ ,  $\mu_n$  is the permeability of the nth layer,  $\omega_n = s_n \omega$  and  $s_n$  is the slip of the nth layer.

In equation (3.17),  $B_y$  is the complex module of normal magnetic induction  $b_y$ , such as

$$b_y = \text{Re}\{B_y \exp[j(\omega t - kx)]\} \quad (3.19)$$

The solution of equation (3.17) is like that:

$$B_y = A_1 \cosh \gamma_n y + B_1 \sinh \gamma_n y \quad (3.20)$$

Where  $A_l$  and  $B_l$  depend on the boundary conditions and the conditions of passage between the various layers.

At the borders between the layers,  $B_y$  is continuous and  $H_x$  is also safe in the presence of the surface currents. In this case,  $H_x$  undergoes a discontinuity equal to the density of these surface currents [7]. Moreover, iterative calculations allow the adjustment of the permeability of each layer to take into account saturation.

Lastly, by knowing the distribution of the fields in the various layers of the linear induction motor, the characteristics and the performances of SLIM can be evaluated.

### **3.5 Analytical Modeling of Single-sided Linear Induction Motor by Using Method of Layer**

In this section, the analytical modeling of the single-sided linear induction motor object on two-dimensional (2D) assumption is carried out by using method of layer. From a point of view computing time, determination of the distribution of the electromagnetic fields in 2D through longitudinal section of a SLIM is preferable with a complete three-dimensional analysis and is entirely adequate for the

performance evaluation of the SLIM [2]. This approach seems to be adequate to implement an analysis tool to be incorporated in computer aided design tool.

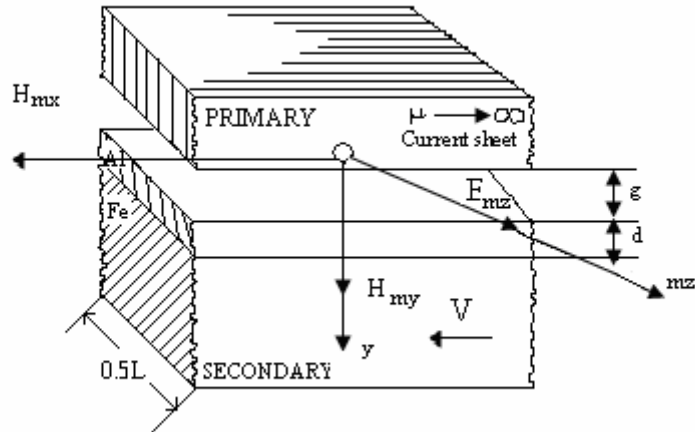


**Figure 3.4** Model of Single-sided Linear Induction Motor with double layer secondary

The two-dimensional assumption (2D), the currents and the magnetic potential vector have only one component according to axis ( $z$ ). Magnetic induction has two components: one is principal or normal and noted  $B_y$ , it creates the push and it is directed along axis ( $y$ ); and the other tangential is noted  $B_x$ , it gives rise to a normal force and it is directed along axis ( $x$ ). The longitudinal section of the SLIM to be analyzed is schematized in figure 3.4 [2]. The secondary is supposed to be composed of two layers, one is conducting (out of aluminum generally) and the other out of laminated or massive ferromagnetic steel. Ferromagnetic steel makes it possible to channel flow in the secondary and reduces the magnetizing current of the machine [7].

Moreover, the magnetic permeability of secondary steel (back-iron) has non linear characteristics due to the magnetic saturation. And it has also hysteresis losses which influence significantly secondary impedances. In order to get high precision result in the analysis and effective design of SLIM, these effects should be taken into account. So the analysis tool for SLIM based on the method of the layers is presented by taking into account of [2].



- 1) Skin effect in the secondary,
- 2) Reaction of the eddy currents of the secondary on the primary magnetic field,
- 3) Saturation and hysteresis effects in the ferromagnetic steel of the secondary,
- 4) Longitudinal ends and transverse of edges effects.

The effects of saturation and hysteresis in two-dimensional electromagnetic fields distribution are included by means of an equivalent relative magnetic permeability of the steel of the secondary, expressed by [7]:

$$\mu_{re} = \mu_{rs} (\mu' - j\mu'') \quad (3.21)$$

Where,  $\mu_{rs}$  is the surface permeability of the secondary steel on the side of the primary. The real and imaginary components are described in [7], such as:

$$\mu' = a_R a_x; \mu'' = 0.5(a_R^2 - a_x^2) \quad (3.22)$$

$a_R$  and  $a_x$  coefficients depend on the magnetic field on the surface of the secondary steel and take into account of the saturation and the effect of hysteresis.

In addition, the Carter coefficient ( $k_c$ ) which is for taking into account slot effect (its formula is given in A2), and saturation factor ( $k_\mu$ ) which is for taking into account back iron saturation effect (its formula is also given in A3), are used to obtain the equivalent air gap [7],

$$g' = k_c k_\mu g \quad (3.23)$$

The transverse edges effect in the layer of the primary ferromagnetic steel is included by a correction factor. Moreover, the factor of correction of Russel and Norsworthy (given in A4) is used to take account of the edges effect in the

conducting aluminum plate, by correcting the electric conductivity of this layer in the following way [7].

$$\sigma'_{Al} = k_{RN} \sigma_{Al} \quad (3.24)$$

In order to take account of the longitudinal end effects in an analytical model, several techniques were proposed in the literature. This effect can be taken into account;

- 1) By superposition of travelling wave at synchronous speed and two end effect waves [5],
- 2) By postulating a periodic distribution of SLIM's and representing the resultant space harmonics by Fourier series [48],
- 3) By modifying the electromotive force (EMF) across the mutual impedance of a T-type equivalent circuit [2].

The mentioned above techniques for taking into account the end effect are some of them in the literature. The technique (3) is considered to give the best results and is the simplest analytically and computationally. The end effect factor (given in A5) is defined as [2].

$$k_e = \frac{E_{me}}{E_{ms}} \quad (3.25)$$

Where  $E_{ms}$  is the maximum value of the electromotive force induced in a primary phase winding by a magnetic wave of induction being propagated at the synchronous speed.  $E_{me}$  is the maximum value of the electromotive force induced by the attenuated wave at the entry of SLIM. This attenuated wave occurs due to the limited longitudinal length of the primary. This factor expressing the end effect is used to modify the electromotive force of the magnetizing branch.

### 3.5.1 Two-dimensional (2D) electromagnetic field distribution of SLIM with double layer secondary

Two-dimensional electromagnetic field distribution equations lead to determine the mutual and secondary impedances in the equivalent circuit. These electromagnetic field equation obtained from the method of layer in the longitudinal section of SLIM which consist of three isotropic layers; the first layer is steel half place, the second layer is aluminum with thickness,  $d_{al}$ , the third layer is equivalent air gap,  $g'$ .

These assumptions are applied in Figure 3.4. Then, the electromagnetic fields expressions in a longitudinal section of the SLIM are established within the framework of the following assumptions [2]:

- 1 - The steel of the primary consists of ferromagnetic infinite permeability and perfectly laminated sheets (i.e. electric conductivity is null in the transverse direction ( $z$ ));
- 2 - The primary phase winding is represented by a thin current sheet which contains space harmonics of winding;
- 3 - The analyzed longitudinal section consists of three homogeneous and isotropic parts: an air-gap a thickness  $g'$ , an aluminum plate  $d_{al}$  thickness and a secondary ferromagnetic layer  $d_{ir}$  thickness;
- 4 - The active surface of the primary is parallel to that of the secondary;
- 5 - The equivalent magnetic permeability of the back iron is defined so that the saturation and the hysteresis loop are taken into account;
- 6 - The equivalent magnetic permeability of the secondary ferromagnetic is the same one for the fundamental one and the harmonics of space of the magneto motive force of the primary of high row;

7 - The space period of the distribution of the electromagnetic fields in the longitudinal direction (x) is of  $2\tau$  ;

8 - All electromagnetic fields are sinusoidal functions of time;

9 - The motor is supplied by a presumedly perfect power source (one neglects the harmonics of current due to the order by Multi Line Inverter of the inverter supplying the motor).

If the above assumptions and appropriate boundary conditions are applied to the equation (3.20), the following distribution of the electromagnetic are obtained [2]:

1 - For the area of the air-gap ( $0 < y < g'$ ):

$$H_{mx3} = \sum_{v=1}^{\infty} \frac{1}{M_v} \left\{ \begin{aligned} & \left[ \frac{K_{v2}}{\beta_v} \left[ \frac{K_{v1}}{K_{v2}} \cosh(K_{v2}d_{a1}) + \mu_{re} \sinh(K_{v2}d_{a1}) \right] \cosh[\beta_v(y - g')] \right] - \\ & \left[ \mu_{re} \cosh(K_{v2}d_{a1}) + \frac{K_{v1}}{K_{v2}} \sinh(K_{v2}d_{a1}) \right] \sinh[\beta_v(y - g')] \end{aligned} \right\} \\ \left[ - (A_{mv}^+ e^{-j\beta_v x} + A_{mv}^- e^{j\beta_v x}) \right] \quad (3.26)$$

$$H_{my3} = \sum_{v=1}^{\infty} \frac{1}{M_v} \left\{ \begin{aligned} & \left[ \frac{K_{v1}}{K_{v2}} \sinh(K_{v2}d_{a1}) + \mu_{re} \cosh(K_{v2}d_{a1}) \right] \cosh[\beta_v(y - g')] - \\ & \left[ \frac{K_{v2}}{\beta_v} \left[ \mu_{re} \sinh(K_{v2}d_{a1}) + \frac{K_{v1}}{K_{v2}} \cosh(K_{v2}d_{a1}) \right] \sinh[\beta_v(y - g')] \right] \end{aligned} \right\} \\ \left[ j (A_{mv}^+ e^{-j\beta_v x} - A_{mv}^- e^{j\beta_v x}) \right] \quad (3.27)$$

$$E_{mz3} = \sum_{v=1}^{\infty} \frac{1}{M_v} \left\{ \begin{aligned} & \left[ \frac{K_{v1}}{K_{v2}} \sinh(K_{v2}d_{a1}) + \mu_{re} \cosh(K_{v2}d_{a1}) \right] \cosh[\beta_v(y - g')] - \\ & \left[ \frac{K_{v2}}{\beta_v} \left[ \mu_{re} \sinh(K_{v2}d_{a1}) + \frac{K_{v1}}{K_{v2}} \cosh(K_{v2}d_{a1}) \right] \sinh[\beta_v(y - g')] \right] \end{aligned} \right\} \\ \left[ \frac{j\omega\mu_0}{\beta_v} (A_{mv}^+ e^{-j\beta_v x} - A_{mv}^- e^{j\beta_v x}) \right] \quad (3.28)$$

2 - For the area of the conducting layer out of aluminum ( $g' < y < dal + g'$ ):

$$H_{mx2} = \sum_{v=1}^{\infty} \frac{1}{M_v} \frac{K_{v2}}{\beta_v} \left\{ \frac{K_{v1}}{K_{v2}} \cosh[K_{v2}(y - d_{al} - g')] - \mu_{re} \sinh[K_{v2}(y - d_{al} - g')] \right\} \left[ - \left( A_{mv}^+ e^{-j\beta_v x} + A_{mv}^- e^{j\beta_v x} \right) \right] \quad (3.29)$$

$$H_{my2} = \sum_{v=1}^{\infty} \frac{1}{M_v} \left\{ \mu_{re} \cosh[K_{v2}(y - d_{al} - g')] - \frac{K_{v1}}{K_{v2}} \sinh[K_{v2}(y - d_{al} - g')] \right\} \left[ j \left( A_{mv}^+ e^{-j\beta_v x} - A_{mv}^- e^{j\beta_v x} \right) \right] \quad (3.30)$$

$$E_{mz2} = \sum_{v=1}^{\infty} \frac{1}{M_v} \left\{ \mu_{re} \cosh[K_{v2}(y - d_{al} - g')] - \frac{K_{v1}}{K_{v2}} \sinh[K_{v2}(y - d_{al} - g')] \right\} \left[ \frac{j\omega_v \mu_0}{\beta_v} \left( A_{mv}^+ e^{-j\beta_v x} + A_{mv}^- e^{j\beta_v x} \right) \right] \quad (3.31)$$

3 - For the area of the ferromagnetic steel of the secondary ( $y > dal + g'$ ):

$$H_{mx1} = \sum_{v=1}^{\infty} \frac{1}{M_v} \frac{K_{v1}}{\beta_v} e^{jk_{v1}(y - dal - g')} \left[ - \left( A_{mv}^+ e^{j\beta_v x} - A_{mv}^- e^{j\beta_v x} \right) \right] \quad (3.32)$$

$$H_{my1} = \sum_{v=1}^{\infty} \frac{1}{M_v} e^{-jK_{v1}(y - dal - g')} j \left( A_{mv}^+ e^{-j\beta_v x} - A_{mv}^- e^{-j\beta_v x} \right) \quad (3.33)$$

$$E_{mz1} = \sum_{v=1}^{\infty} \frac{1}{M_v} e^{-jK_{v2}(y - dal - g')} \frac{j\omega_v \mu_0 \mu_{re}}{\beta_v} \left( A_{mv}^+ e^{-j\beta_v x} + A_{mv}^- e^{-j\beta_v x} \right) \quad (3.34)$$

Where

$$M_v = \left\{ \begin{array}{l} \frac{K_{v2}}{\beta_v} \left[ \frac{K_{v1}}{K_{v2}} \cosh(K_{v2} D_{al}) + \mu_{re} \sinh(K_{v2} D_{al}) \right] \cosh(\beta_v g') + \\ \left[ \mu_{re} \cosh(K_{v2} D_{al}) + \frac{K_{v1}}{K_{v2}} \sinh(K_{v2} D_{al}) \right] \sinh(\beta_v g') \end{array} \right\}; \beta_v = \frac{v\pi}{\tau}$$

$$K_{v1} = \sqrt{a_{v1}^2 + \beta_{v1}^2} = (a_{RvFe} + ja_{xvFe})k_{vFe}; K_{v2} = \sqrt{a_{v2}^2 + \beta_{v2}^2} = (a_{RvA1} + ja_{xvA1})k_{vA1};$$

$$a_{RvFe} = \frac{\text{Re}[K_{v1}]}{k_{vFe}}; a_{xvFe} = \frac{\text{Im}[K_{v1}]}{k_{vFe}};$$

$$a_{RvA1} = \frac{\text{Re}[K_{v2}]}{k_{vA1}}; a_{xvA1} = \frac{\text{Im}[K_{v2}]}{k_{vA1}};$$

$$k_{vFe} = \sqrt{\frac{\omega_v \mu_0 \mu_{rs} \sigma_{Fe}}{2}}; k_{vA1} = \sqrt{\frac{\omega_v \mu_0 \sigma'_{A1}}{2}};$$

$$\alpha_{v1} = \sqrt{j\omega_v \mu_0 \mu_{rs} \sigma_{Fe}} = (a_R + ja_x)k_{vFe}; \alpha_{v2} = \sqrt{j\omega_v \mu_0 \sigma'_{A1}} = (a_{R1} + ja_{x1})k_{vA1}.$$

Time factors  $\exp(j\omega_v^+)$  in  $A_{mv}^+, H_{mx}^+, H_{mz}^+, E_{my}^+$  and  $\exp(j\omega_v^-)$  in  $A_{mv}^-, H_{mx}^-, H_{mz}^-, E_{my}^-$  have been eliminated. The peak values of the line current density of the primary A, angular frequency  $\omega$ , and slips  $s$ , are given the following formulae.

a) For the forward traveling fields:

$$A_{mv}^+ = \frac{mNk_{wv} \sqrt{2I}}{p\tau} \exp\left[-j(v+1)\frac{m-1}{m}\pi\right]; \quad (3.35)$$

$$\omega_{mv}^+ = s_v^+ \omega = 2\pi f s_v^+; \quad s_v^+ = 1 - v(1-s).$$

b) For the backward traveling field:

$$A_{mv}^- = \frac{mNk_{wv} \sqrt{2I}}{p\tau} \exp\left[-j(v+1)\frac{m-1}{m}\pi\right]; \quad (3.36)$$

$$\omega_{mv}^- = s_v^- \omega = 2\pi f s_v^-; \quad s_v^- = 1 + v(1-s).$$

All calculations are carried out by the assumption of taking into account of the fundamental space harmonics of the primary magneto motive force (i.e.  $v=1$ ) [18]. The electromagnetic equations for the first space harmonic ( $v=1$ ) of the magneto motive force of the primary are obtained from above equations. They are as follow:

1 - For the area of the air-gap ( $0 < y < g'$ ):

$$H_{mx3} = -\frac{A_m e^{-j\beta x}}{M} \left\{ \begin{array}{l} \frac{K_2}{\beta} \left[ \frac{K_1}{K_2} \cosh(K_2 D_{a1}) + \mu_{re} \sinh(K_{2v1} D_{a1}) \right] \cosh[\beta(y - g')] - \\ \left[ \mu_{re} \cosh(K_{2v1} D_{a1}) + \frac{K_1}{K_2} \sinh(K_{2v1} D_{a1}) \right] \sinh[\beta(y - g')] \end{array} \right\} \quad (3.37)$$

$$H_{my3} = \frac{jA_m e^{-j\beta x}}{M} \left\{ \begin{array}{l} \left[ \mu_{re} \cosh(K_2 d_{a1}) + \frac{K_1}{K_2} \sinh(K_2 d_{a1}) \right] \cosh \beta(y - g') - \\ \frac{K_2}{\beta} \left[ \frac{K_1}{K_2} \cosh(K_2 d_{a1}) + \mu_{re} \sinh(K_2 d_{a1}) \right] \sinh \beta(y - g') \end{array} \right\} \quad (3.38)$$

$$E_{mz3} = \frac{j\omega\mu_0 A_m e^{-j\beta x}}{\beta M} \left\{ \begin{array}{l} \left[ \mu_{re} \cosh(K_2 d_{a1}) + \frac{K_1}{K_2} \sinh(K_2 d_{a1}) \right] \cosh[\beta(y - g')] - \\ \frac{K_2}{\beta} \left[ \frac{K_1}{K_2} \cosh(K_2 d_{a1}) + \mu_{re} \sinh(K_2 d_{a1}) \right] \sinh[\beta(y - g')] \end{array} \right\} \quad (3.39)$$

2 - For the area of the conducting layer out of aluminum ( $g' < y < dal + g'$ ):

$$H_{mx2} = -\frac{A_m K_2 e^{-j\beta x}}{M\beta} \left\{ \frac{K_1}{K_2} \cosh[K_2(y - d_{a1} - g')] \mu_{re} \sinh[K_2(y - d_{a1} - g')] \right\} \quad (3.40)$$

$$H_{my2} = \frac{jA_m e^{-j\beta x}}{M} \left\{ \mu_{re} \cosh[K_2(y - d_{a1} - g')] - \frac{K_1}{K_2} \sinh[K_2(y - d_{a1} - g')] \right\} \quad (3.41)$$

$$E_{mz2} = \frac{j\omega\mu_0}{\beta M} A_m e^{-j\beta x} \left\{ \mu_{re} \cosh[K_2(y - d_{a1} - g')] - \frac{K_1}{K_2} \sinh[K_2(y - d_{a1} - g')] \right\} \quad (3.42)$$

3 - For the area of the ferromagnetic steel of the secondary ( $y > dal + g'$ ):

$$H_{mx1} = -\frac{K_1 A_m}{M\beta} e^{-j\beta x} e^{-K_1(y - D_a - g')} \quad (3.43)$$

$$H_{my1} = -\frac{jA_m}{M} e^{j\beta x} e^{-K_1(y-D_a-g)} \quad (3.44)$$

$$E_{mz1} = \frac{j\omega\mu_{re}A_m}{M\beta} e^{-j\beta x} e^{-K_1(y-D_a-g)} \quad (3.45)$$

Such as:

$$M = \frac{K_1}{\beta} \left[ \frac{K_1}{K_2} \cosh K_2 D_{a1} + \mu_{re} \sinh K_2 D_{a1} \right] \cosh \beta g' + \left[ \mu_{re} \cosh K_2 D_{a1} + \frac{K_1}{K_2} \sinh K_2 D_{a1} \right] \sinh \beta g'$$

$$\beta = \frac{\pi}{\tau}; K_1 = \sqrt{\alpha^2_{11} + \beta^2}; K_2 = \sqrt{\alpha^2_{22} + \beta^2}; \alpha_1 = \sqrt{j\omega\mu_0\mu_{re}\sigma_{Fe}};$$

$$\alpha_2 = \sqrt{j\omega\mu_0\sigma'_{Al}}.$$

and

$$A_m = \frac{3\sqrt{2}kwNI}{p\tau} \quad (3.46)$$

### 3.6 Summary

In this chapter, the electromagnetic modeling of SLIM has been presented. The presented model is developed by means of the method of layer. Hence, two-dimensional (2D) electromagnetic field distribution by considering the fundamental space harmonic is described by the equations which take into account the skin effect and reaction of the secondary eddy current. Other electromagnetic phenomena during the operation of SLIM (such as the longitudinal end effect, transverse edge effect, and slot effect) are integrated into the model by means of the corrected factors. Because the transversal and longitudinal dimension effects of the primary applying to the electromagnetic field analysis of a linear induction motor is the difficulty.

The electromagnetic equations, which are obtained from the electromagnetic analysis using the method of layer, will be used in the next chapter to obtain the equivalent circuit parameters and the electromagnetic investigation of SLIM.



## CHAPTER 4

### EQUIVALENT CIRCUIT TECHNIQUE

#### 4.1 Introduction

The single-sided linear induction motors (SLIM) are widely utilized in industrial applications and transportation due to their simple structure, ease of implementation in manufacturing, high reliability and speed, low energy consumption and pollution [1]. Generally, a double layer reaction rail SLIM is made up of two major parts; a primary and a secondary. The former part, i.e., the primary, consists of slots which hold primary windings. The secondary of the SLIM holds a conducting plate which is backed by a ferromagnetic material, 'back iron' or 'secondary iron' [16]. While the motor operates, some essential electromagnetic phenomena occur because of the structure of the motor and its physical properties. To take into account these phenomena in performance calculations, several corrections should be introduced thereafter in the form of reiterated calculations or of correction factors [2].

The equivalent circuit technique (ECT) is assessed numerous studies [1-3] in the literature and it is shown that the method is appropriate to utilize the ECT for the steady state performance calculation of the SLIM where particularly the T-type equivalent circuit is usually preferred. In order to employ the T-type equivalent circuit, primary resistance, primary reactance, magnetizing branch, magnetizing reactance and secondary impedance should be considered. The magnetizing branch reactance and secondary impedance are obtained by solving the field equations which are acquired from the electromagnetic field analysis through the layer method. Although, the layer method is widely used for the electromagnetic analysis of the SLIM [3], [48] the analytic results obtained via this method are not adequately close to the values measured over a wide range of operating conditions. The main reason of the mentioned problem is actually the inadequate treatment of the saturation effect and the depth of penetration, which is related to the permeability of the secondary

iron, in the back iron for high frequency applications. An adequate consideration of such parameters in addition to the others will provide the correct calculation of the secondary impedance; moreover, it will present more precise performance prediction for both analysis and design stages as well. Thus, research over the mentioned problem is still essential.

For this purpose, in this chapter, the following tasks are performed: a) Saturation level of the back iron is determined by iteration. Having accomplished aforementioned tasks, we calculate secondary iron impedance by using a linear approximation that is novel in the calculation of secondary iron impedance. The developed model with this novel approach is then applied to the Canadian Guided Ground Transportation (CIGGT) LIM to assess its performance under the above mentioned conditions. The results are compared with those given in the experiments of the previous studies.

#### 4.2 Longitudinal end effect and saturation factor

The Longitudinal end effects in the linear induction motor are due to the limiting longitudinal length of the motor. It influences the speed on the non uniform distribution of the induction in the air gap of the LIM and current induced in the secondary. This effect is taken into account by a factor  $k_e$  given on the basis of a distribution of induction in the air gap of SLIM made up of a slipping field. The end effect can be expressed as a summation of two air gap flux density waves [1]

$$B(x, t) = B_{ms} \sin\left(\omega t - \frac{\pi}{\tau} x\right) + B_{me} e^{-\frac{x}{\tau_e}} \sin\left(\omega t - \frac{\pi}{\tau} x + \delta\right) \quad (4.1)$$

The electromotive force induced in a primary phase is the superposition of two electromotive forces, one due to the fundamental field and the other is induction due to the end effect and it can be expressed in the form [47]:

$$e_p(t) = e_s(t) + e_e(t) = -E_{ms} \cos(\omega t) - E_{me} \cos(\omega t) = -E_{ms} (1 - k_e) \cos(\omega t) \quad (4.2)$$

where

$$k_e = -\frac{k_{we}}{k_w} \frac{\frac{\pi}{\tau_e^2}}{\frac{1}{t_e^2} + \left(\frac{\pi}{\tau_e}\right)^2} f(\delta) e^{\frac{-p\tau_e}{t_e}} \frac{\sinh\left(\frac{p\tau_e}{t_e}\right)}{p \sinh\left(\frac{\tau_e}{t_e}\right)} \quad (4.3)$$

Since the ferromagnetic material (back iron) exists in the secondary, the saturation should be considered at some operating conditions. The classical theory of the electric motors defines the saturation factor of the magnetic circuit as being the relationship between the total magneto motive force and that of the air gap by pole pairs. The magnetic permeability of the primary is assumed infinite. So the magneto motive force in the primary can be neglected. Under this condition, the saturation factor [2] of the magnetic circuit of SLIM can be expressed as.

$$k_\mu = \frac{V_v}{2(V_{gv} + V_{dv})} \approx 1 + \frac{V_{sv}}{2(V_{gv} + V_{dv})} \quad (4.4)$$

where  $V_v$  is the magneto motive force (MMF) per poles pair,  $V_{gv}$  is the magnetic voltage drop in the air gap,  $V_{dv}$  is the magnetic voltage drop in the conducting plate,  $V_{sv}$  is the magnetic voltage drop in the secondary back iron. The details for equations (4.3) and (4.4) are given in Appendix A5 and A3 respectively.

### 4.3 Wave penetration depth concept

The performance prediction of the SLIM has been carried out by the electromagnetic field analysis together with the ECT which include special phenomena (transverse edge effect, longitudinal end effect, saturation, hysteresis and non-linear complex magnetic permeability) presented in section 2. In ECT, the secondary parameters are evaluated from two dimensional (2-D) field analyses. Thereby, the layering model has been developed by paralleling the layer impedances of the motor considering the wave impedance concept [16].

In the layering model, the secondary iron has two regions; the conducting surface ferromagnet, which has the uniform field distribution in the normal direction ( $y$ ), and

the nonconducting ferromagnet. As regards to the wave penetration concept, the wave with frequency  $f$  penetrates into the layers of the secondary iron having the permeability  $\mu$  and the conductivity  $\sigma$  where the amount of penetration depth is calculated according to the (4.10). Thus, the thickness of the conducting surface region is assumed to be equal to the penetration depth of the wave that is in accordance with the wave penetration concept. It is observed that the penetration depth increases as the secondary frequency ( $sf$ ) decreases. Note that, the average distance value of flux penetration is limited to be the half of the layer thickness even though the penetration depth value is calculated to be greater than the half of the layer thickness of the secondary iron ( $d_{ir}/2$ ) as seen in Figure 4.1.

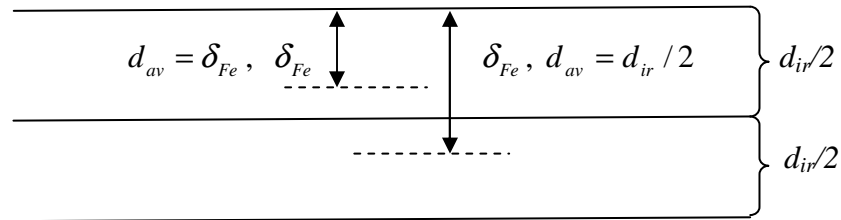


**Figure 4.1.** Back iron half space layer modeling

#### 4.4 Calculation of saturation level

The following iterative algorithm is used to obtain equivalent magnetic permeability of the back iron, in other words, the saturation level.

- It is assumed that the surface magnetic field intensity at the boundary between the solid iron and the aluminum is equal to the line current density of the primary

$$H_{s1} = A_m$$

where  $A_m = \frac{3\sqrt{2}k_wNI}{p\tau}$  (4.5)

and the saturation factor  $k_\mu$  is assumed to be equal to one

- Extract the surface permeability of the back iron from  $B-H$  curve data and calculate the equivalent magnetic permeability by using the (3.21) and (3.22)

- Then, the effective air gap  $g'$  (3.23) and the attenuation factors  $\alpha_1$ ,  $\alpha_2$  and the propagation constants  $K_1$ ,  $K_2$  are calculated by using the following expressions [2]

$$K_1 = \sqrt{\alpha^2_1 + \beta^2} \quad (4.6)$$

$$K_2 = \sqrt{\alpha^2_2 + \beta^2} \quad (4.7)$$

$$\alpha_1 = \sqrt{j2\pi fs\mu_0\mu_{re}\sigma_{Fe}} \quad (4.8)$$

$$\alpha_2 = \sqrt{j2\pi fs\mu_0\sigma'_{Al}} \quad (4.9)$$

where  $\beta = \frac{\pi}{\tau}$

- Next, in order to determine effective depth ( $d_{av}$ ) of the induced currents in the secondary iron layer, the penetration depth of magnetic flux into the back iron is calculated by using the equations given below [7]:

$$\delta_{Fe} = \frac{1}{\sqrt{\pi fs\mu_0\mu_{rs}\sigma_{Fe}}} \quad (4.10)$$

$$d_{av} = \begin{cases} \delta_{Fe} & \text{if } \delta_{Fe} < 0.5d_{ir} \\ 0.5d_{ir} & \text{if } \delta_{Fe} > 0.5d_{ir} \end{cases} \quad (4.11)$$

- Later, tangential and normal magnetic field intensity is calculated by the use of the (4.12) and (4.13) to obtain the average magnetic permeability,  $\mu_{av}$ , from the  $B$ - $H$  curve data of the back iron.

$$H_x = -\frac{K_1 A_m}{M\beta} e^{-j\beta x} e^{-K_1(y-d_{Al}-g')} \Big|_{y=g+d_{Al}+d_{av}} \quad (4.12)$$

$$H_y = -\frac{jA_m}{M} e^{j\beta x} e^{-K_1(y-d_{Al}-g')} \Big|_{y=g+d_{Al}+d_{av}} \quad (4.13)$$

where  $M$  is the factor required for the two dimensional analysis of SLIM [7]

- The new saturation factor is then calculated by equation (4.4)

- As a last step, the magnetic field intensity ( $H_{s2}$ ) value at the surface of the back iron is updated by using the (4.12) and (4.13) with  $y=g+d_{Al}$ . The above mentioned computation are carried out until a sufficient convergence between the  $H_{s1}$  and  $H_{s2}$  is attained where each of the magnetic field intensity values can be calculated with the following:

$$\text{where} \quad H_s = (H_x^2 + H_y^2)^{1/2} \quad (4.14)$$

As a consequence of the iterations, the saturation level is determined for each slip value with the consideration of the nonlinear characteristics of the secondary iron as mentioned above. Through the iterations the wave penetration depth is calculated according to the wave penetration depth concept which is explained in Section 4.3.

#### 4.5 Simulating the CIGGT LIM

For the CIGGT SLIM with the given design data in Table 4.1, the variation of the wave penetration depth with linear speed at different input frequencies ( $f$ ) is shown in Figure 4.2. As expected, the depth of the penetration into the secondary iron increases as the slip decreases.

**Table 4.1** Data on CIGGT LIM

Number of Phase, $m$	3
Number of pole pairs, $p$	3
Rated phase current, $I$	200 A
Pole pitch, $\tau$	0.25 m
Air gap length, $g$	0.015 m
Number of primary turn/phase, $N$	108
Width of the aluminum layer, $W+2h_{ov}$	0.201 m
Width of the secondary iron layer, $W$	0.111 m
Thickness of the aluminum layer, $d_{al}$	0.0025 m
Thickness of the secondary iron layer, $d_{ir}$	0.0254 m

Conductivity of secondary iron, $\sigma_{Fe}$	4.46 MS/m
Conductivity of secondary iron, $\sigma_{Al}$	32.3 MS/m

The penetration depth value, which is dependent on the frequency of the secondary, goes up to the half of the layer thickness about the synchronous speed. Additionally penetration depth goes up to the total thickness of the secondary iron near the synchronous speed. The thickness of the passing path, that the induced current on the secondary iron flows on, also increases as the depth value of the penetration increases. This thickness should be fixed to a certain value according to the wave impedance concept.

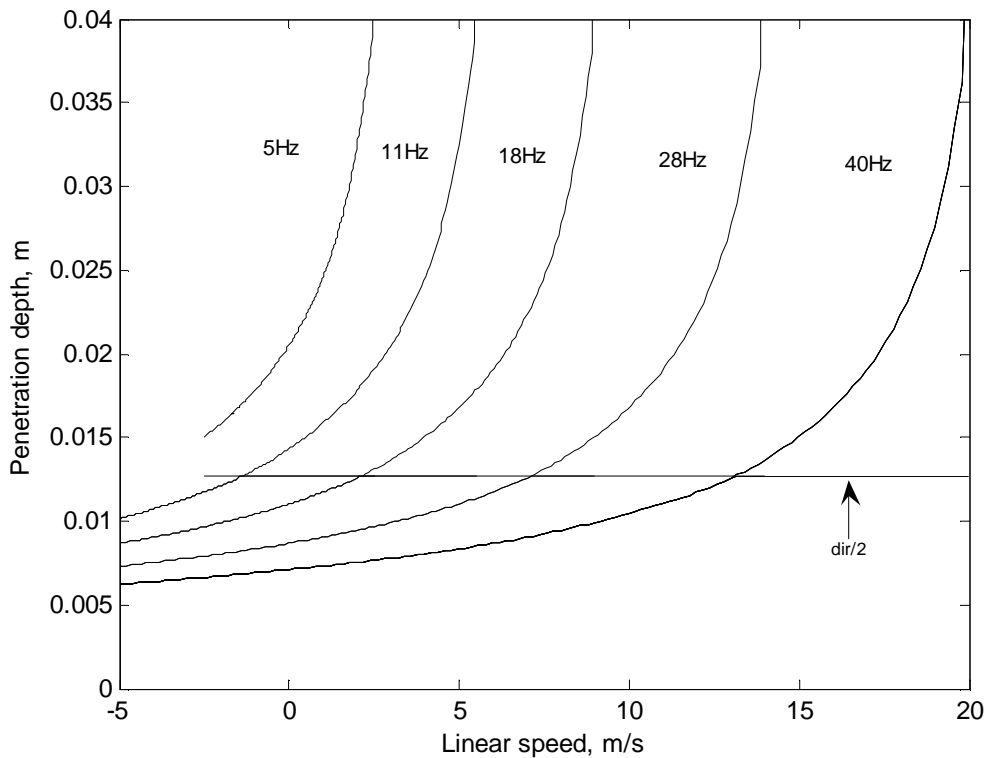


**Figure 4.2** Linear speed vs. penetration depth at different constant input frequency

The changes of the penetration depth have an influence on the equivalent relative permeability as well. The relation between the penetration depth and the equivalent relative permeability is depicted in Figure 4.3. As the secondary frequency decreases, the penetration depth increases. Therefore, the equivalent relative permeability also increases as well. Additionally, the penetration depth shows regular variation along

with the speed and the variation equivalent relative permeability against speed which is observed to be slight between zero and synchronous speed.

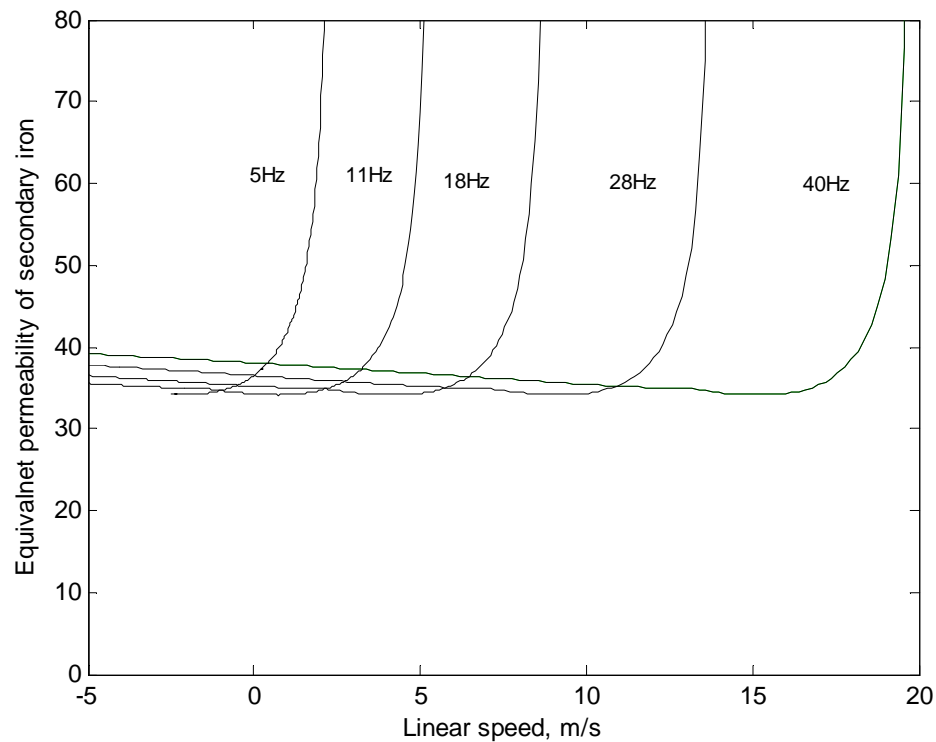


**Figure 4.3** Variation of the equivalent permeability vs. linear speed at different input frequencies

At each iteration of the algorithm, the change in the equivalent permeability value of the secondary iron is calculated to be so small that current slip value in the iteration is nearly the same with the previous one, until speed approaches near the synchronous speed. Note that, the linear speed is obtained by multiplying the synchronous speed ( $2f\tau$ ) with the expression  $(1-s)$  where  $s$  denotes the slip value.

#### **4.6 Obtaining the Equivalent Circuit Parameters of SLIM from Electromagnetic Equations**

The secondary and mutual impedances in equivalent circuit diagram of Figure 4.4 are derived from the two-dimensional electromagnetic field equations. Unit secondary impedance due to the first space harmonic is given by the ratio of



tangential electric and magnetic field components, as given by equations (3.40) and (3.42):

$$z_y = \frac{E_{mz2}}{H_{mx2}} \Big|_{y=g'} = Z_{Fe} \cdot z_{12} \quad (4.15)$$

where:  $Z_{Fe}$  is the unit impedance of the solid steel plate, and  $z_{12}$  is the unit equivalent impedance of nonmagnetic layer which is dependent of parameters of solid steel reaction plate. In order to take account of transverse edge effect,  $Z_{Fe}$  is multiplied by  $k_z > 1$  [2].

$$Z'_{Fe} = Z_{Fe} k_z \quad (4.16)$$

And the electric conductivity of nonmagnetic layer should be multiplied by Russel and Norsworthy's factor  $k_{RN} < 1$ .

$$Z'_{Fe} = - \frac{j\omega\mu_0\mu_{re}}{K_1 \tanh(K_1 d_{ir})} k_z \quad (4.17)$$

$$z_{12} = \frac{- \frac{j\omega\mu_0}{z_1 K_2} \sinh(K_2 d_{a1}) + \cosh(K_2 d_{a1})}{\cosh(K_2 d_{a1}) - \frac{K_2}{j\omega\mu_0} z'_1 \sinh(K_2 d_{a1})} \quad (4.18)$$

where :

$$K_2 = (a_{RAI} + ja_{xAL}) \sqrt{\omega\mu_0 \sigma_{Al} k_{RN} / 2}$$

Let us note that this expression of  $z_{12}$  depends on the parameters of the layer of the secondary steel. While making tighten the impedance of ferromagnetic secondary towards the infinite, the expression from the impedance of the aluminum conducting layer is deduced. So  $Z_{Al}$  is:

$$Z_{Al} = \frac{-j\omega\mu_0}{K_2 \tanh(K_2 d_{a1})} \quad (4.19)$$

So the secondary branch impedance of a single-phase equivalent circuit diagram in Figure 4.4 can be expressed as follows:

$$Z_2 = \frac{R_2}{s} + j \frac{X_2}{s} = \frac{Z'_{Fe} Z_{Fe}}{Z'_{Fe} + Z_{Al}} \frac{1}{s} \quad (4.20)$$

The secondary impedance referred to primary winding is expressed by:

$$Z'_2 = \frac{R'_2}{s} + j \frac{X'_2}{s} = \frac{Z'_{Fe} Z_{Al}}{Z'_{Fe} + Z_{Al}} \frac{1}{s} k_{trv} \frac{L}{\tau} \quad (4.21)$$

$$\text{where: } k_{trv} = \frac{2m(Nk_{wv})^2}{vp}$$

Now let us express the impedance seen on the primary side. It can be expressed in the following way (for  $y=0$ ):

$$z = \left. \frac{E_{mz3}}{H_{mx3}} \right|_{y=0} = z_1 \cdot z_{12} \cdot z_{123} = z_y \cdot z_{123} \quad (4.22)$$

where:

$$z_{123} = \frac{-\frac{j\omega\mu_0}{z_y \beta} \sinh(\beta_v g') + \cosh(\beta_v g')}{\cosh(\beta_v g') - \frac{\beta_v}{j\omega\mu_0} z_y \sinh(\beta_v g')} \quad (4.23)$$

If the secondary impedance of the  $z_y$  is made tighten towards the infinite, the magnetizing reactance expression is obtained:

$$Z_m = -jX_m = -\frac{j\omega\mu_0}{\beta \tanh(\beta g')} \quad (4.24)$$

The magnetizing reactance referred to primary winding is

$$X_m = \frac{\omega\mu_0}{\beta \tanh(\beta g')} k_{trv} \frac{L}{\tau} \quad (4.25)$$

In addition, the resistance of a phase of the primary education is expressed by:

$$R_1 = \rho_{cuo} (1 + \alpha_{cu} \Delta T) \frac{2(L + L_f)}{N_b \frac{\pi D_b^2}{4}} N \quad (4.26)$$

As regards the leakage reactance of the primary (due to the leakage in the slots), it is calculated by using one of the methods used in the conventional rotary machines presented as below:

$$X_1 = \omega \left\{ \left( \frac{N^2}{3} \right) \frac{\mu_0 W_p h_e}{s_w} + \frac{N^2 \mu_0 w_c}{8} \ln \left( \frac{\pi w_0^2}{4 h_e s_w} \right) \right\} \quad (4.27)$$

To take account of the end effect, the amplitude of the electromotive force induced referred to primary winding is modified as follows:  $E_{me} = E_{ms} (1 - k_e)$ , as it is illustrated on the equivalent circuit diagram of Figure 4.4.

#### 4.6.1 A new approach to obtaining the secondary impedance of SLIM in ECT

By solving the electromagnetic field equation which is obtained from the electromagnetic analysis by using the layering method, the following secondary iron layer impedance, aluminum layer impedance and magnetizing reactance equations are obtained respectively [2].

$$Z_{Fe} = -\frac{j2\pi f s \mu_0 \mu_{re} k_z}{K_1} \quad (4.28)$$

$$Z_{Al} = \frac{-j2\pi f s \mu_0}{K_2 \tanh(K_2 d_{al})} \quad (4.29)$$

$$Z_m = -jX_m = -\frac{j2\pi f s \mu_0}{\beta \tanh(\beta g')} \quad (4.30)$$

The secondary iron layer impedance depends on the equivalent permeability as shown in (4.28). Diverse from the methods in the literature, the secondary iron impedance is calculated with the consideration of the variations of the equivalent permeability with the slip. This novel approach, which aims to calculate the secondary iron impedance more sensitive by utilizing a linear approximation method, is given in this section.

Together with the following approximation (such as  $K_l = \alpha_1$ ,  $\tanh(K_2 d_{al}) = K_2 d_{al}$ ), the secondary iron layer and aluminum layer impedance equation for the above mentioned purpose can be written as

$$Z_{Al} = \frac{-j2\pi f s \mu_0}{K_2^2 d_{al}} \quad (4.31)$$

$$\begin{bmatrix} Z_{Fe}(s_0) \\ Z_{Fe}(s_1) \\ Z_{Fe}(s_2) \\ Z_{Fe}(s_3) \\ \vdots \\ Z_{Fe}(s_{max}) \end{bmatrix} = -j2\pi\mu_0 k_z \begin{bmatrix} \frac{s_0 f}{\alpha_2(s_0)} \mu_{re}(s_0) & 0 & 0 & 0 & 0 & 0 \\ \frac{s_1 f}{\alpha_2(s_1)} \mu_{re}(s_0) & \frac{s_1 f}{\alpha_2(s_1)} \mu_{re}(s_1) & 0 & 0 & 0 & 0 \\ \frac{s_2 f}{\alpha_2(s_2)} \mu_{re}(s_0) & \frac{s_2 f}{\alpha_2(s_2)} \mu_{re}(s_1) & \frac{s_2 f}{\alpha_2(s_2)} \mu_{re}(s_2) & 0 & 0 & 0 \\ \frac{s_3 f}{\alpha_2(s_3)} \mu_{re}(s_0) & \frac{s_3 f}{\alpha_2(s_3)} \mu_{re}(s_1) & \frac{s_3 f}{\alpha_2(s_3)} \mu_{re}(s_2) & \frac{s_3 f}{\alpha_2(s_3)} \mu_{re}(s_3) & 0 & 0 \\ \vdots & \vdots & \vdots & \vdots & \vdots & \vdots \\ \frac{s_{max} f}{\alpha_2(s_{max})} \mu_{re}(s_0) & \frac{s_{max} f}{\alpha_2(s_{max})} \mu_{re}(s_1) & \frac{s_{max} f}{\alpha_2(s_{max})} \mu_{re}(s_2) & \frac{s_{max} f}{\alpha_2(s_{max})} \mu_{re}(s_3) & \dots & \frac{s_{max} f}{\alpha_2(s_{max})} \mu_{re}(s_{max}) \end{bmatrix} \quad (4.32)$$

In order to take transverse edge effect into account, the impedance of secondary iron is multiplied by [7]:

$$k_z = 1 - \frac{g}{L} + \frac{2}{\pi} \frac{\tau}{W} \left[ 1 - \exp\left(-\frac{\pi W}{2 L}\right) \right] \quad (4.33)$$

In (4.32), each column vector represents the secondary iron layer impedance which corresponds to each slip value that is between zero and an appropriate value (1 or 2). The length of the column vector depends on the step value of slip. Consequently, maximum length of the column vector ( $l$ ) can be defined as:

$$l = \frac{s_{\max} - s_0}{\text{step value}} \quad (4.34)$$

Where  $s_0$  denotes the minimum value of the slip and  $s_{\max}$  stands for the maximum value of the slip that this value is chosen as 2 in this study.

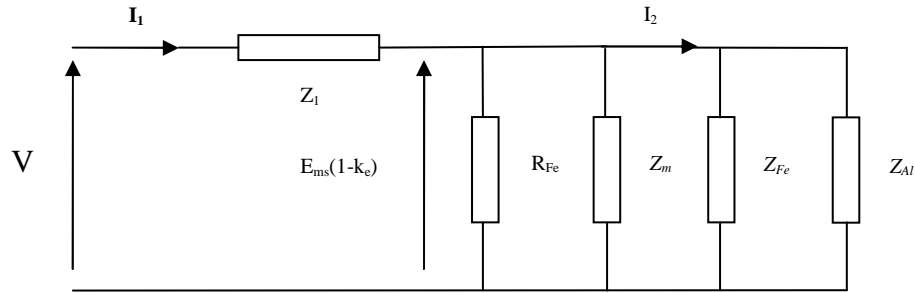


**Figure 4.4** Per-phase equivalent circuit of SLIM

Figure 4.4 depicts the T-type equivalent circuit of the SLIM with double-layer secondary where aluminum and secondary iron layer impedances are connected in parallel. Hence, equivalent secondary impedance referred to primary winding can be found by using classical circuit theory as below.

$$Z_2(s_n) = \frac{Z_{Fe}(s_n)Z_{Al}(s_n)}{Z_{Fe}(s_n) + Z_{Al}(s_n)} k_{tr} \frac{L}{\tau} \quad (4.35)$$

where;  $n=0,1,2,\dots,l$

The equivalent secondary impedance depends on the slip and should be determined for each slip value in the case of the different operating conditions. To do this, each column vector obtained from (4.32) is substituted into (4.35). However, it is not appropriate to calculate the secondary equivalent impedance in this way due to the

mathematical constraints. After some required algebraic manipulation, the secondary impedance model has the form:

$$A^{(n)}y = d^{(n)} \quad (4.36)$$

$$\text{where } A^{(n)} = \left( X^{(n)} + \frac{s_n f}{K_2(n)d_{al}} \right) \quad \text{and} \quad d^{(n)} = \frac{-j2\pi\mu_0 X^{(n)}(s_n f)^2}{K_2^2(n)d_{al}} k_{tr} \frac{L}{\tau}$$

where  $X^n$  represents each column vector obtained from the equation (4.32) and  $y$  is the equivalent secondary impedance value. The column vector  $X^n$ , which actually holds secondary impedance values for each slip, can be shown as:

$$Z_{Fe}(s_n) = X^{(n)} \quad (4.37)$$

So, this model represents the secondary iron impedance and can now be evaluated by the least square solution for the equivalent secondary impedance. To utilize the least square solution,  $A^n$ , which represents column vector, should be transposed. Then, the (4.38) is obtained to solve the  $y$  value that stands for the secondary impedance by the use of least square solution.

$$y = \left( (A^{(n)})^T A^{(n)} \right)^{-1} (A^{(n)})^T d^{(n)} \quad (4.38)$$

The rest of the parameters required to evaluate equivalent circuit technique, i.e., the specific primary iron losses, primary impedance and air gap voltage, should be obtained. The specific primary iron core loss, which is represented with  $R_{Fe}$ , is characterized in (4.39).

$$R_{Fe} = \frac{mE^2}{\Delta P_{Fe}} k_{ad} \quad (4.39)$$

Where  $\Delta P_{Fe}$  is the core loss of the primary. On the other hand, the other required parameter, i.e., the primary impedance,  $Z_1$ , is calculated with the same way as in the rotary induction motor. As for the air gap voltage, which has to be calculated to take the end effect into account, the air gap voltage is obtained and multiplied by  $(1-k_e)$ .

Thus, to validate of the proposed method, the steady-state thrust of the SLIM is calculated to compare the experimental results where the calculation is carried out by using the following equations.

$$F_x(s_n) = \frac{mR'_2(s_n)[I'_2(s_n)]^2}{s_nVs} \quad (4.40)$$

where

$$R'_2(s_n) = \text{real}(y) \quad (4.41)$$

$$I'_2(s_n) = \frac{E(1-k_e)}{y} \quad (4.42)$$

Now let us express the electromagnetic power transmitted of the primary to the secondary:

$$P_{em} = \frac{m(I'_2)^2 R'_2}{s} \quad (4.43)$$

The mechanical power can be deduced from this expression:

$$P_{me} = P_{em}(1-s) \quad (4.44)$$

And the efficiency is expressed as:

$$\eta = \frac{P_{me}}{P_{em} + \Delta P_{prim}} = \frac{P_{me}}{P_a} \quad (4.45)$$

$P_{em}$  and  $P_{me}$  are the total electromagnetic and mechanical powers respectively. They are calculated by taking account of the most dominating space harmonics;  $P_a$  is the total electric output absorptive by the motor and  $\Delta P_{prim}$  is the total active losses in the primary such as:

$$\Delta P_{prim} = mR_{prim}I^2 + \Delta P_{Fe} \quad (4.46)$$

In addition, the efficiency and power factor ( $\eta \cos \varphi$ ) is also a performance characteristic of SLIM, which also noted ( $KW/KVA$ ), can be defined as:

$$KW / KVA = \eta \cos \varphi = \frac{P_{me}}{S_a} \quad (4.47)$$

For the calculation of the normal force, an empirical formula suggested in [2] is used and it is given by:

$$F_{vy} = \frac{B_{vmyg}^2}{4\mu_0} A_p - \frac{B_{vmxg}}{B_{vmyg}} F_{vx} \quad (4.48)$$

Where  $A_p$  is the equivalent transverse surface of the primary which takes account of the semi slot filled in the linear machines. It is expressed by (one adds  $\Delta x$  if the length of the primary of the linear motor is larger than  $2\tau p$  in the longitudinal direction (x)):

$$\begin{aligned} A_p &= (2\tau p + \Delta x) & W < L + 2g' ; \\ A_p &= (2\tau p + \Delta x)(L + 2g') & W > L + 2g' . \end{aligned} \quad (4.49)$$

and  $B_{myg}$  it is the amplitude of normal induction in the air-gap by taking account of the saturation and the longitudinal end effect. It is empirically given by [2]:

$$B_{vmyg} = \frac{E_{vms}(1 - k_e)}{4\sigma_k \alpha_i f N k_w \tau L} \quad (4.50)$$

where

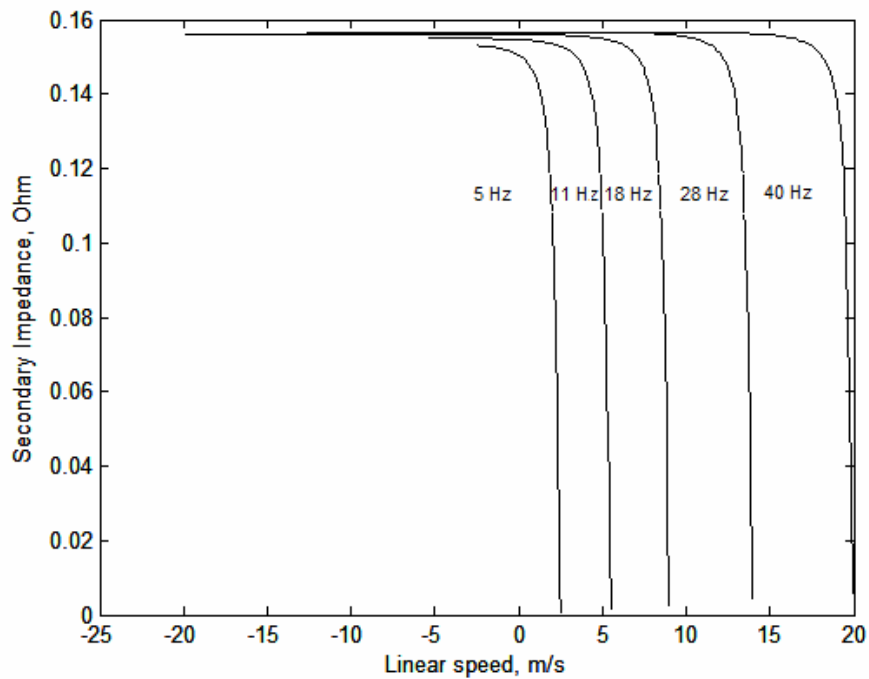
$$\sigma_k \cong \frac{\pi\sqrt{2}}{4} \exp\left(\frac{1 - k_\mu}{18}\right) \quad \text{and} \quad \alpha_i \cong \frac{2}{\pi} k_\mu^{1/3}$$



## 4.7 Conclusions and Remarks

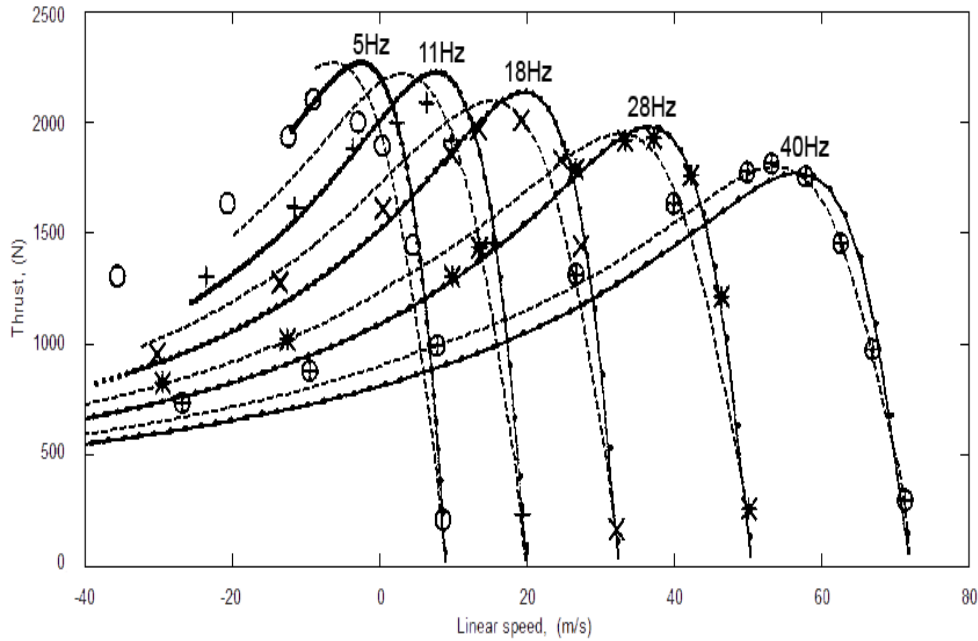
Here, an attempt has been done to develop a new approach to obtain the secondary impedance of the SLIM. Section 4.6.1 presents the details of the novel approach and this section will study the relationship between the obtained secondary impedance with speed and thrust variations as a consequence of the adequate treatment of the saturation effect and permeability.

The relevancy between the secondary impedance which is obtained by using the proposed approach and speed is depicted in Figure 4.5. As can be seen in the figure, when approaching the synchronous speed, the secondary impedance stays nearly constant; however, it decreases sharply near the synchronous speed. This is an expected effect of the wave impedance concept since the change in the permeability of the iron is minimal until the penetration depth reaches the half of the thickness of the iron. Moreover, when the penetration depth passes the half of the thickness of the iron and approaches the exact thickness of the iron, a decrease in the secondary impedance initiates. Once the penetration depth reaches the exact thickness of the iron, a sharp decrease occurs.



**Figure 4.5** Secondary impedance vs. linear speed of CIGGT SLIM

Since the secondary impedance is not a value that can be measured during the operation of the SLIM, hence, thrust value should be employed in evaluation of the secondary impedance. As a result, the proposed approach can only be validated through the thrust values of the SLIM.



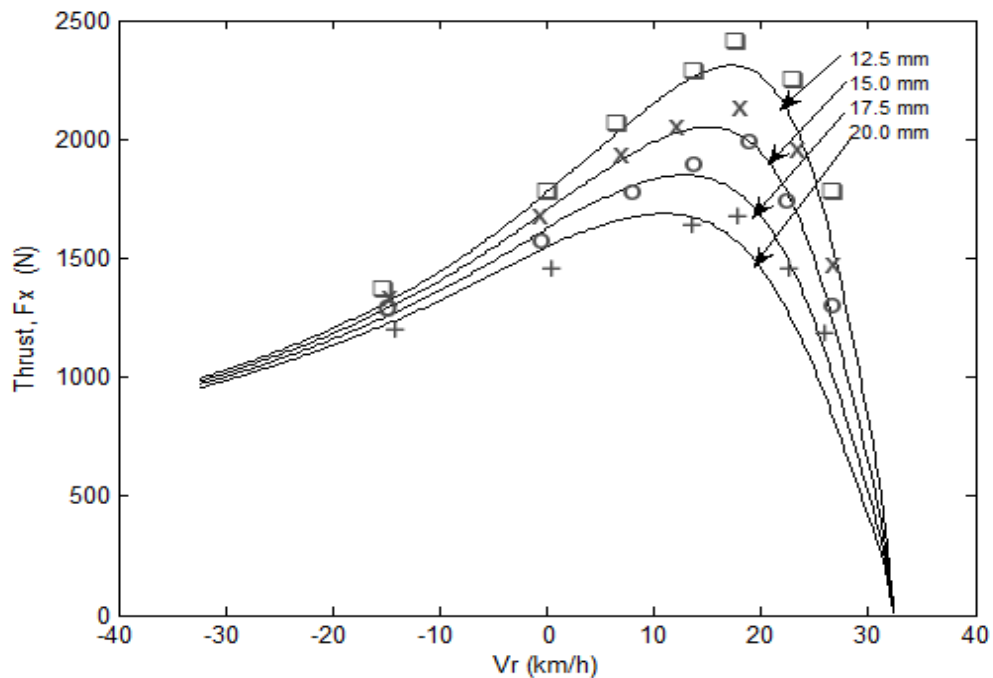
**Figure 4.6** Simulation results for performance of the CIGGT SLIM  
 Experimental points: + 40 Hz, x 28 Hz, o 18 Hz, \* 11 Hz, Δ 5 Hz

Figure 4.7 depicts the curves of thrust values according to linear speed for constant frequency, e.g., 5 Hz, 11 Hz, 18 Hz, 28 Hz and 40 Hz where experimental results at each frequency is given with a separate symbol; circles correspond to the results at 5Hz, plus signs to 11Hz, crosses to 18 Hz, stars to 28 Hz and circled-plus signs to 40Hz. The dashed lines represent the results of our method and straight lines correspond to the results of the CIGGT SLIM study [1] from the literature. The results of proposed method are observed to be in good accordance with the experimental results of the CIGGT SLIM. Notice that, as seen in the figure, there is a good match between the objective model and the result of the proposed method in 40 Hz frequency. As far as similar studies in the literature are concerned, as to the authors' knowledge, the proposed approach is the most efficient method studied in this frequency while it sacrifices computational speed on behalf of a more precise performance. At frequencies below 40Hz such as 18Hz and 28Hz, however, the results of the proposed method are observed to be slightly poorer than the results of

the CIGGT SLIM study. This is mainly caused by the errors during the linear approximation to estimate the secondary iron impedance at lower frequencies.

As a result, a new approach has been introduced that might be efficient when used for design and analysis of the SLIM with a wide-range of applications by adequately treating the electromagnetic phenomena. The novel contribution is the utilization of the least squares approach for linear approximation in order to calculate the secondary impedance. The simulation results suggest that the proposed approach is efficient to improve the accuracy in thrust calculations. Since the proposed method is observed to be computationally intense, future studies of the method will include the evaluation of the optimization techniques to overcome this disadvantage.

In Figure 4.7, while the variation between thrust values and speed are given, the results of the proposed method are compared with the experimental results and it is observed that our results are satisfactorily in accordance with the objective model. Whereas, Figure 4.8 depicts the curves of the relationship between thrust and speed for the proposed method. It is seen that the results of the method are also close to the points that correspond to the experimental results.



**Figure 4.7** Simulation results for performance of the CIGGT SLIM at different air gaps. Experimental points: + 20mm, o 17.5mm, x 15mm, □ 12.5mm

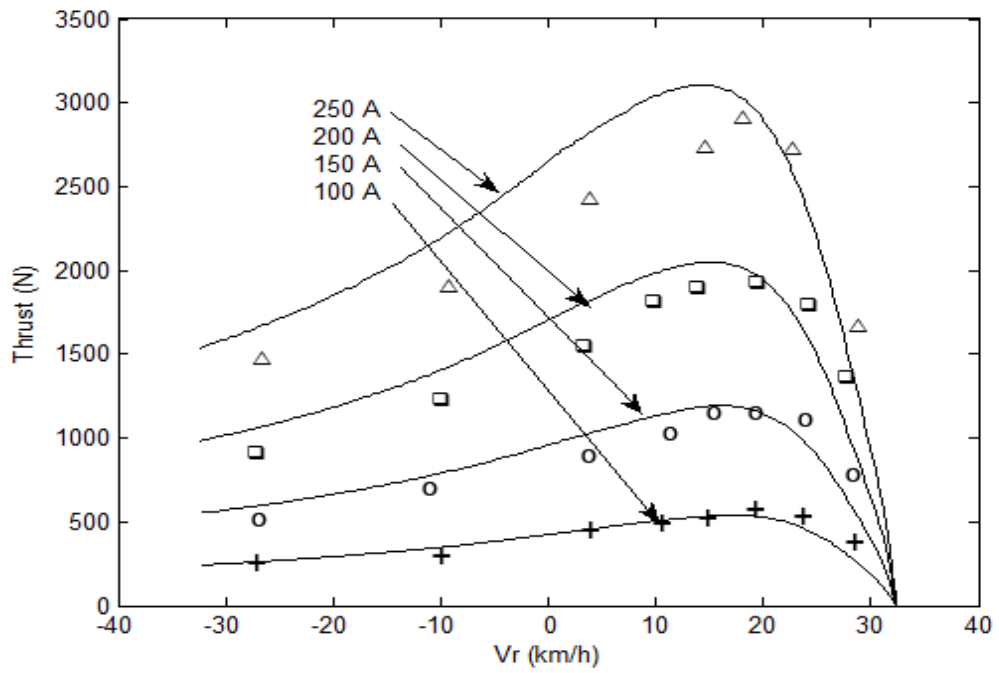


**Figure 4.8** Simulation results for performance of the CIGGT SLIM at different constant current. Experimental points: + 100A, o 150A, □ 200A, Δ 250A

## CHAPTER 5

### ANALYTICAL DESIGN OF SLIM with the AIDED of COMPUTER

#### 5.1 Introduction

In fact, the design of the electric motors is difficult task due to the having non-linear structure and complex geometry. This task can be carried out by the aid of the computer nowadays. The computer aided design for electric machine consists of two elementary stages. One of them is the selection of the structure and another is the dimensioning of the motor. The structure selection in the first stage of the design is chosen according to the condition of use. The second stage of the design is to dimension of motor which is generally not linear and does not have a single solution.

In this study, the first stage of the electric motor design with the aid of computer is deduced. The second stage of this task is the objective of this thesis. This means that the dimensioning and the performance of the motor obtained from these geometrical dimension and electrical specifications are determined by the help of computer.

The design of the single-sided linear induction motor is regarded as a problem of synthesis. The analysis can be performed by analytic software, and then the design can be achieved by using the analytic software in the way of the synthesis. In chapter 4, the analytic tool was developed for the analysis of SLIM. And this software is significantly validated with the experimental results obtained from large linear induction motor (CIGGT). Thus, this analysis tool was developed thereafter to implement the computer aided design software. The computer aided design, which is primarily based on the developed analytical tool, allow the simulation and finding the best design for the necessary characteristics and performance to be optimized with respect to technical constraints required by the specifications.

In order to obtain more competitive and effective design, all chosen parameters for constraints should be related to the performance of the motor and an objective function to be optimized. The dimensioning of the motor by the help of computer is treated by an iterative process based on the searching all possible solutions space in the case of the objective. All solutions are stored in the memory and searching the required parameter in it according to an objective function. The design with the aid of the computer make the automatically exploration possible in all possible solution set for the objective function to be optimized. Obtaining the required parameters respecting all considerable constraints is easy with the aid of computer. Nowadays, design optimization of SLIM is carried out taking into account the various electromagnetic, thermal, and mechanical phenomena within the motor to be designed and optimize the performances by seeking a better solution. The improving the efficiency and power factor product for low speed SLIM was studied [55] for the initial motor design using multi objective optimization method. In this study, the longitudinal end effect and core loss has not been taken into account due to the low speed. In the design of the SLIM, the magnetic saturation, the longitudinal end, transverse edge, skin, hysteresis effects within the SLIM should be taken into account, because a computer-aided design requires a powerful tool for the electromagnetic analysis within SLIM.

The enumeration method is used to get the required parameter for the design of SLIM. Nevertheless, if the high number of parameters are selected to optimize for better designing of an electric motor and in addition to that if each of the parameters have different values, the computing time increases very much with the increase in the iterative processes. Because of that, the parameters to be optimized should be determined by being familiar with know-how relating to the design of the motor. If the schedule of condition is too constraining or unrealistic, the existence solutions cannot always guaranteed. Moreover, the necessary characteristics and performances must be optimized, with respect to all technical and/or economic constraints required by the specifications.

MATLAB package software (Release 14) has been used to develop new analytic design software of SLIM by using M-file programming according to the explained above realistic estimations in this study. This is why; it includes lot of facility tool

and flexibility to develop the engineering applications. The developed software with the MATLAB is embedded into VC# .NET framework 2008 to be user interactive. For this aim, the user interfaces is prepared for ergonomic usage by using C# framework 2008. A SLIM is designed by the newly developed user interactive software.

## **5.2 Electric machine design**

The design of the electric machine is not an easy task to realize. Because the model of the electric machines generally have complex structure and mathematical model. In the standard process of electric machine design with the aid of computer is shown in figure 5.1 [58]. The designer has to change every input data in the standard procedure until getting best design results with trial and error. The computer is being used as calculator. There is no automatic exploration in the design and optimization process. In addition to that, the optimization process is time consuming in the manual case.

The design procedure shown in figure 5.1 is not suitable for the design of the electric machine with the aided of computer. The computer aided design of electric machine should be used more effective. This effective usage is shown in figure 5.2 [58]. The computer does most of the work of the electric machine design. The designer must input a set of parameters and their bounds (min. /max. values) only.

## **5.3 Design methodology of SLIM**

The design stages for SLIM is the same as other electric machine design. The structure of the SLIM with double layer secondary has been presented in the chapter 4. The second stage is the dimensioning of the SLIM structure. The original dimension of the SLIM can be determined by the treating the seizing equations [2] in a logical order and the optimization method is applied to the original design of the SLIM to improve the objective function respecting the considerable constraints required by predetermined specifications.

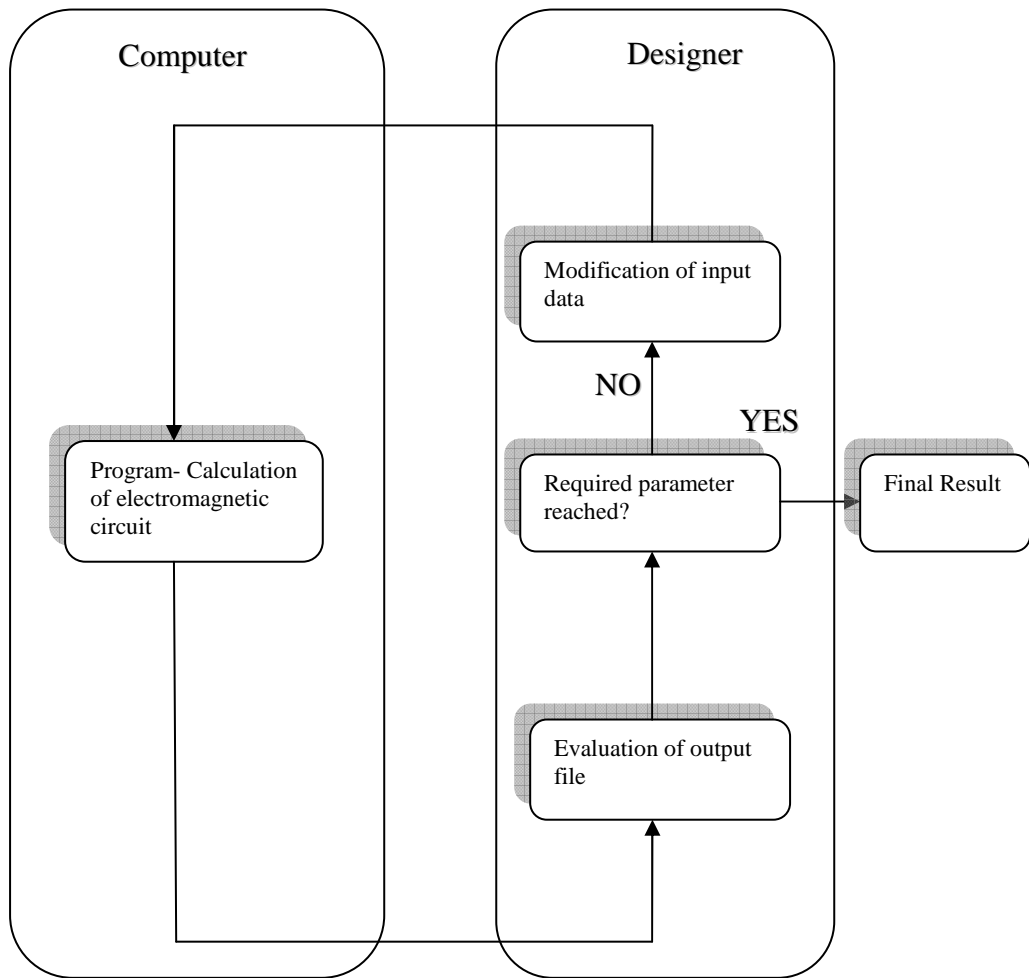


**Figure 5.1** Classical procedure of Electric machine design

### 5.3.1 Dimensioning of SLIM

Together with determination of the structure of the SLIM with double layer which is presented in the chapter 3, the dimensioning can be performed. The design of SLIM begins with the calculation of the main dimensions of the primary side and secondary side. The determining geometrical parameters satisfying the performances and relating to the constraints previously defined in the listed of conditions. The geometrical parameters to be able to optimize is given in figure 5.4. These geometrical parameters consist of the pole pitch  $\tau$ , the primary core length  $L$ , width of the primary core  $W_p$  and air gap  $g$ . As for the secondary side consists of width of



the back iron  $W$ , overhang width  $h_{ov}$ , overhang thickness  $t_{ov}$ , the thicknesses of the conducting plate  $d_{al}$  and the back iron  $d_{ir}$ .

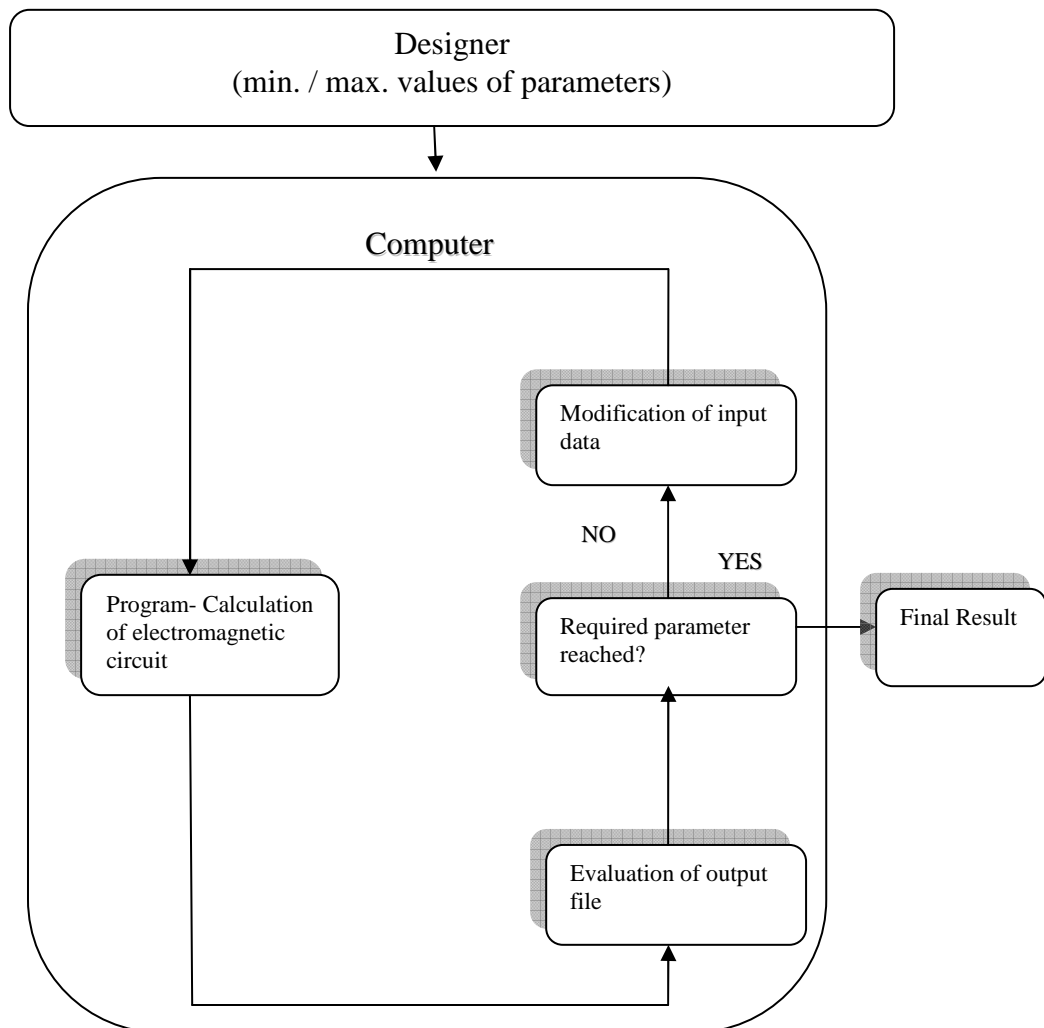


**Figure 5.2** The more effective design procedure of Electric machine design

In fact, design is regarded as a problem of synthesis. This means that the operation  $Y=AX$  should be performed [7].  $X$  represents set of input data and  $Y$  is the set of output results. In this system,  $A$  is the mathematical model. The dimensioning problem is the reverse operation according to this approach. In order to calculate the dimension of SLIM and its performances, the proposed method in the equivalent circuit technique presented in the chapter 4 has been used. This model allows the quantitatively to join the expressive parameters of a system (geometrical and

physical) with the characteristics parameter of SLIM (power factor, efficiency, output power etc.).

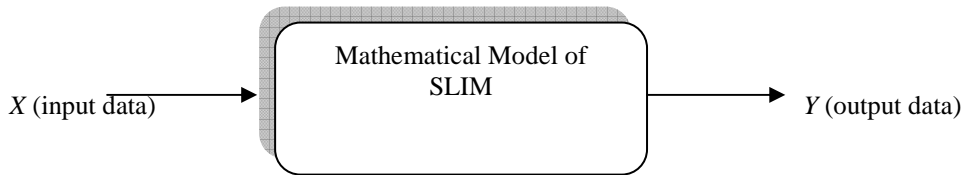


**Figure 5.3** The simple block diagram of the SLIM system

### 5.3.2 Procedural calculation of the dimensioning

An algorithm can be developed to dimension of SLIM by the treating the seizing equations in a logical order [7]. The dimensioning can be obtained from this equation by using simple mathematical problems instead of complicated numerical algorithm. In order to improve dimensioning, the correct calculation of the dimension is made with the test and loop. This algorithm is usually used in the design of the electric machine

### 5.3.3 Optimization of the dimensioning

Another alternative algorithm is the optimization one which is used to dimensioning the electric machine. Indeed, if the schedule of conditions is realizable, there are infinity solutions to dimensioning of electric machine in general. But it is tried to seek the best design in the solution set by optimizing a performance or a characteristic of the electric machine to be dimensioned such as output power, power factor, efficiency etc....

The optimization problem in electric machine is composed of the objective function to be made extreme (minimal /maximal) and of all constraints in the form of equalities and/or inequalities, which can be linear or not linear, implicit or explicit, to respect.

An optimization algorithm starts from the initial design ( structural or dimensioned) then adjusts all of the parameters by iteration until the objective function reaches its optimum while respecting all constraints imposed by scheduled conditions. This approach is appropriate for improving an objective function for the initial design.

The optimization problem can be formulized as mathematically. The optimum design of an electric machine means the finding a combination of the independent variables  $x=(x_1, x_2, \dots, x_m)$  in such a way that  $F(x_1, x_2, \dots, x_m)$  is an extremum [7] and

$$P(x_1, x_2, \dots, x_m) \in D \quad (5.1)$$

where:  $F$  is the objective function,  $m$  is the number of variables,  $P$  is the point in the space of independent variables and  $D$  is the set of feasible designs which satisfy the constraints. A solution set is determined with the aid of constraint functions which described as;

$$g_j(x_1, x_2, \dots, x_m) \leq 0 \quad (5.2)$$

for  $j= 1,2,3,\dots,l$  and  $l$  is the number of constraints.

The criterion for the optimization depends on the requirements and can be the power output per mass, cost or volume of a machine. A large number of independent variables can be limited to the dimension of the magnetic and electric circuit in the case of the induction machine [7]. The efficiency product power factor, tooth flux density, starting thrust, material weight and volume can be also the optimization criterion. The defined above equations for the optimization problem, which are presented in general way, can be also formulated with the other optimization techniques for particular design optimization problem.

The objective of this study is to get the initial design of the SLIM. In order to get local optimum value in the design of SLIM for the given specifications, the optimization procedure can be obtained from the above one in simple manner.

Linear induction motor suffer from two major drawbacks, such as low efficiency and power factor which cause more energy consumption, a rise input current and occupation of transmission lines capacity [31]. Although in most cases improving the efficiency or power factor has an adverse effect on the other one, the objective function can be selected as efficiency product power factor ( $\eta \cos \varphi$ ).

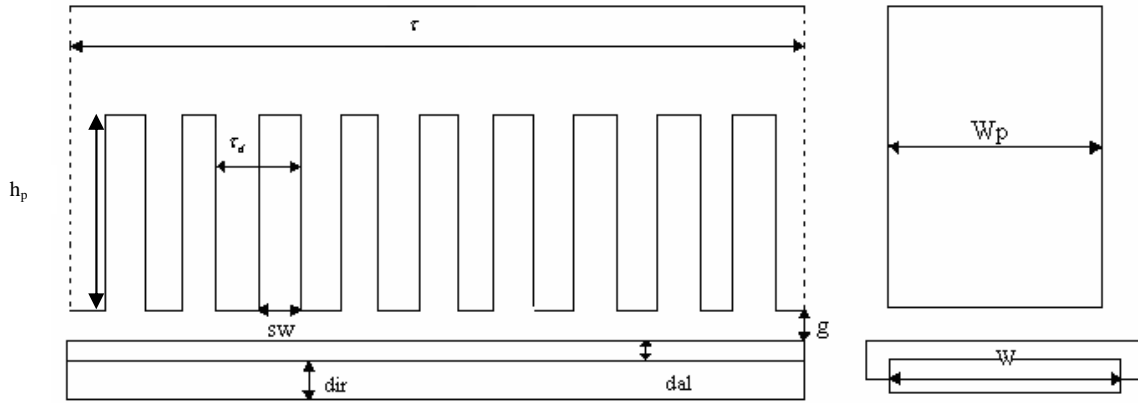


**Figure 5.4** The structure of the SLIM with double layer and its geometrical parameters for constraints

During the optimization process, the optimization algorithm can be adjusted to find the rest desired structural parameters which influence considerably with the characteristics of SLIM. These parameters are namely; air gap ( $g$ ), pole pitch ( $\tau$ ), thickness of the conducting plate ( $d_{al}$ ), thickness of the back iron ( $d_{ir}$ ), transverse length of the back iron ( $W$ ) and slot height ( $h_p$ ). The remainder parameters of SLIM can be expressed in terms of standard value or design variables [18].

Choosing the variables to be optimized and their beach of variation are important. The variables to be optimized can be various nature and it can be its geometrical dimensions, parameter of food etc.. . In this study, the objective function is chosen in order to maximize the average of  $\eta \cos \varphi$  of SLIM in the stable area. The stable area is between zero and critical slip value which correspond to maximum thrust value. The structural parameters which influence on the performance of SLIM should be investigated for choosing design variables in optimization process.

### 5.3.3.1 The Influence of some design parameters on the performance of SLIM

The influence of the some design parameters on the performance of SLIM is investigated by means of the simulation results getting from the design data of Canadian Institute of Guided Ground Transportation (CIGGT) LIM. These simulation results are obtained by using the analytic tool for the analysis of SLIM which is developed and significantly validated. The effect of some design parameters on the performance of SLIM is investigated by changing their values around the design ones. These design parameters are taken as the thickness of the back iron ( $d_{ir}$ ), thickness of the conducting plate ( $d_{al}$ ) and the air gap ( $g$ ). These parameters change in the normal direction and belong to secondary side of SLIM. While one parameter is changing, others remain at the design values. The influences of the chosen design parameters on the thrust, efficiency, power factor and efficiency product power factor are evaluated for constant current  $I=200$  A, frequency  $f=40$  Hz, overhang width  $h_{ov}=33.9$  mm, the back iron width  $W=111$  mm. In this investigation, the parameters to be investigated vary around the optimum design values while the rest of them remain the original design values.

In order to obtain the target thrust value at the rated speed in case of optimization, the design variables and its increment in the range of constraint should be determined. For this aim, this investigation is accomplished by means of the simulations using the developed analytic tool for analysis of SLIM. In fact, it can be interested in a great number of design variables but solution cannot be guaranteed and computing time is enormous. Because of that, more sensitive parameters to performance of the SLIM should be chosen to reach the target thrust in case of optimizations.

In order to evaluate the back iron thickness, its discrete values are taken around optimum value. In Figure 5.5 shows the influence of the back iron thickness on the thrust vs. speed characteristics of SLIM. It may be noted that the variation of the performance for these discrete values is less sensitive. This situation can be clearly seen in table 5.1. The values in table 5.1 are obtained at 0.21 value of slip which corresponds the maximum available thrust value for CIGGT LIM. As the thickness of the back iron decreases, the maximum available thrust decreases.

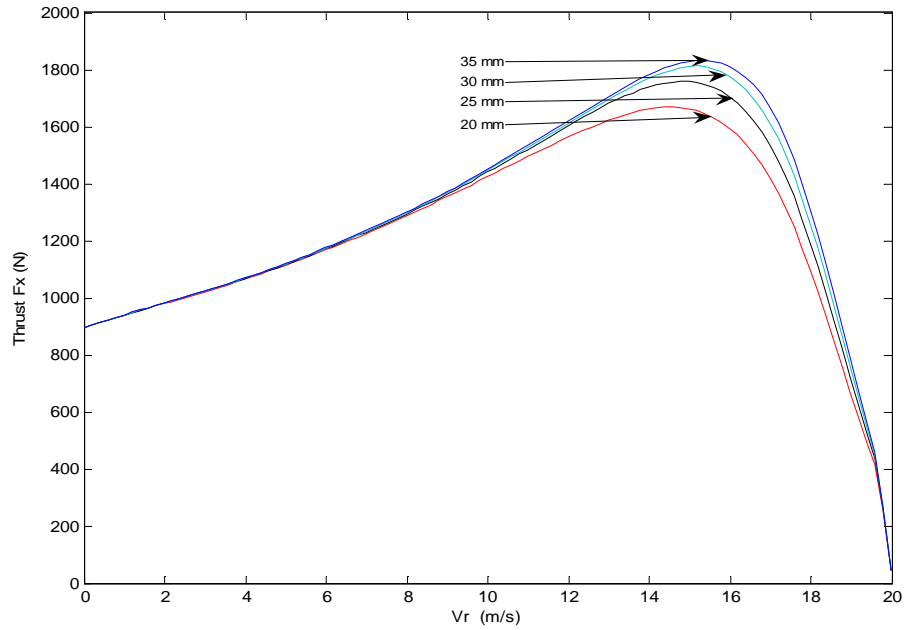


**Figure 5.5** Variations of *Thrust vs. Vr* (linear speed) curves at different thickness of back iron ( $d_{ir}$ ).

Because the back iron serves to carry the air gap flux and reduces the magnetizing current. Hence, reducing the thickness of the back iron thickness means that secondary current increases. This leads to increase in thrust of SLIM in accordance with the equation 4.40.

In Figure 5.6-5.8 are shown the variations the power factor, efficiency product power factor and efficiency with the back iron thickness respectively. It is observed that the variations of these performance values at 0.21 value of slip is less sensitive to the variation of the back iron thickness around its optimum value.

**Table 5.1** The performance values at discrete values of thickness of the back iron

$d_{ir} (mm)$	Efficiency	Power factor	Thrust (N)	$\eta \cos \phi$
20	0.5774	0.5772	1616	0.3332
25	0.5872	0.6081	1724	0.3571
25.4	0.5878	0.6100	1730	0.3585
30	0.5930	0.6279	1792	0.3724
35	0.5954	0.6363	1821	0.3788

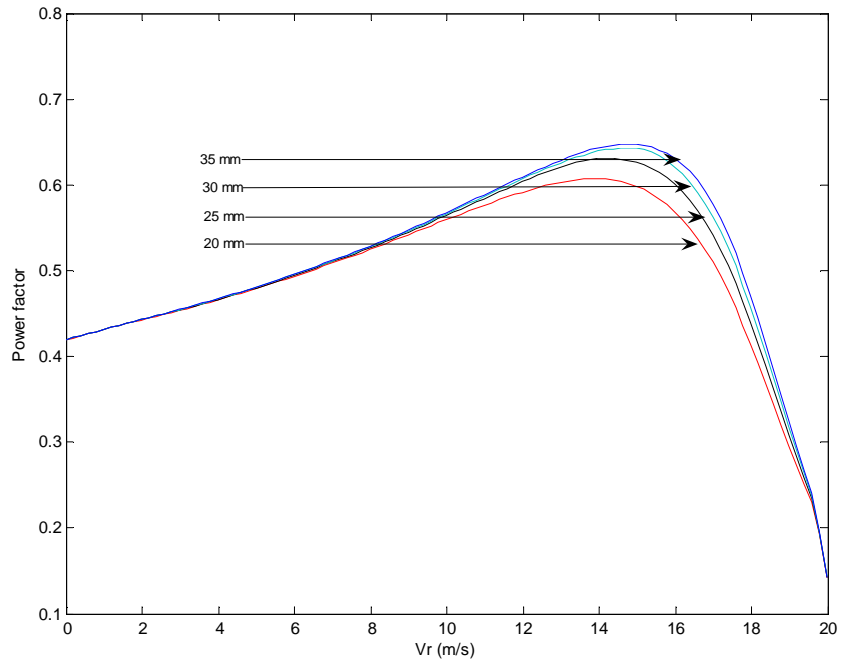


**Figure 5.6** Variations of *Power factor* vs. *Vr* (linear speed) curves at different thickness of back iron ( $d_{ir}$ ).

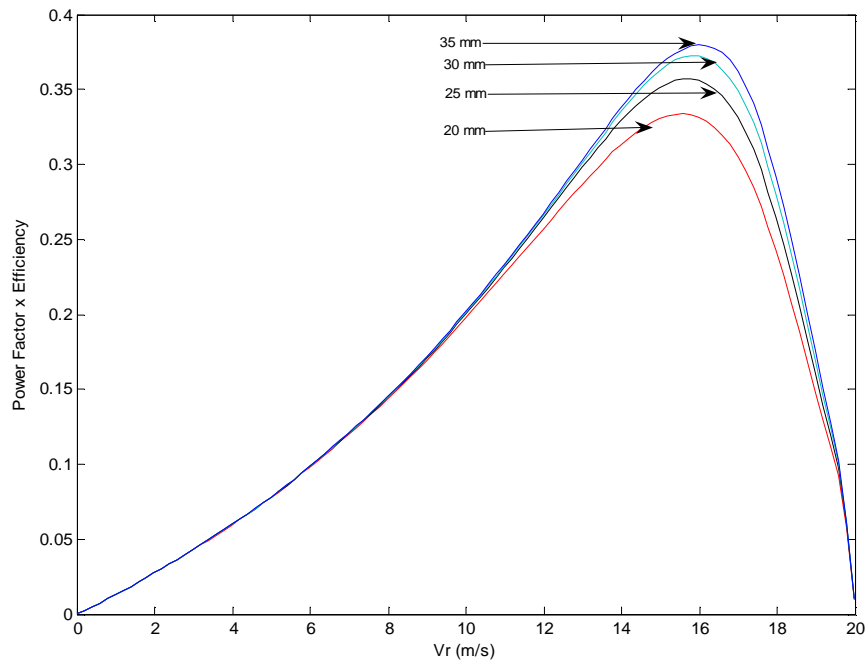


**Figure 5.7** Variations of *Power factor product efficiency* vs. *Vr* (linear speed) curves at different thickness of back iron ( $d_{ir}$ ).

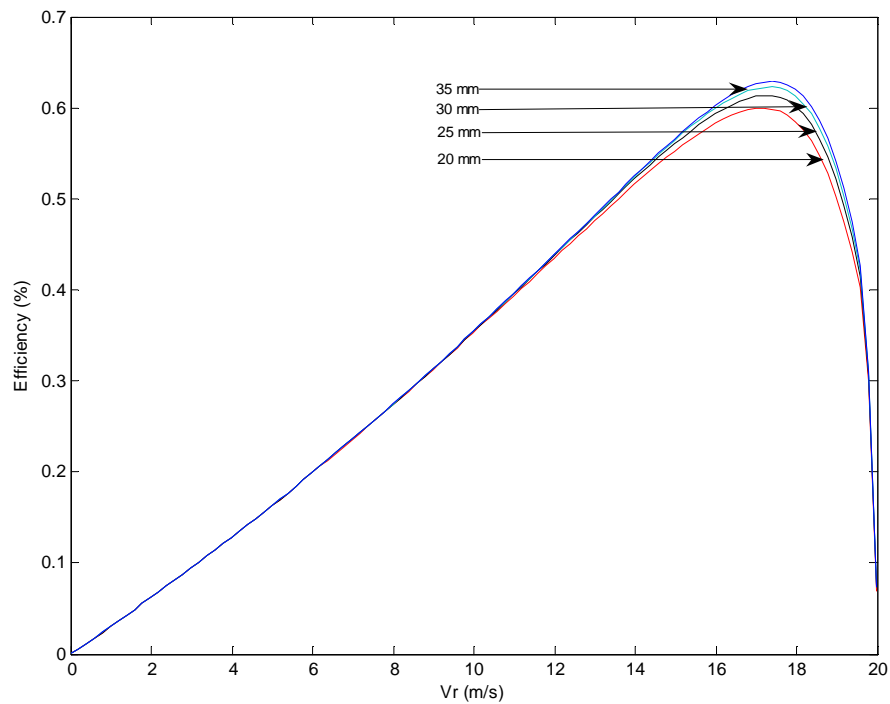


**Figure 5.8** Variations of *Efficiency* vs. *Vr* (linear speed) curves at different thickness of back iron ( $d_{ir}$ ).

In figure 5.9-5.12 shows the influence of the thickness of the conducting plate on the performance of SLIM. It is also clearly seen that the variations of the thickness of the conducting plate at discrete value is less sensitive in the stable area. But it is sensitive for the starting thrust. It can be evaluated for the optimization of the starting thrust. If the thickness of the conducting plate increases, then secondary resistance is also increases. This situation affects the end effect resistance. The end effect resistance increases with the increasing the secondary resistance so that the maximum available thrust decreases with the increasing the thickness of the conducting plate. But it is also observed that the thrust value at 0.21 value of slip is around the designed value (1700 N). The variation of the performance is shown in Figure 5.2 at discrete value of the design parameters.



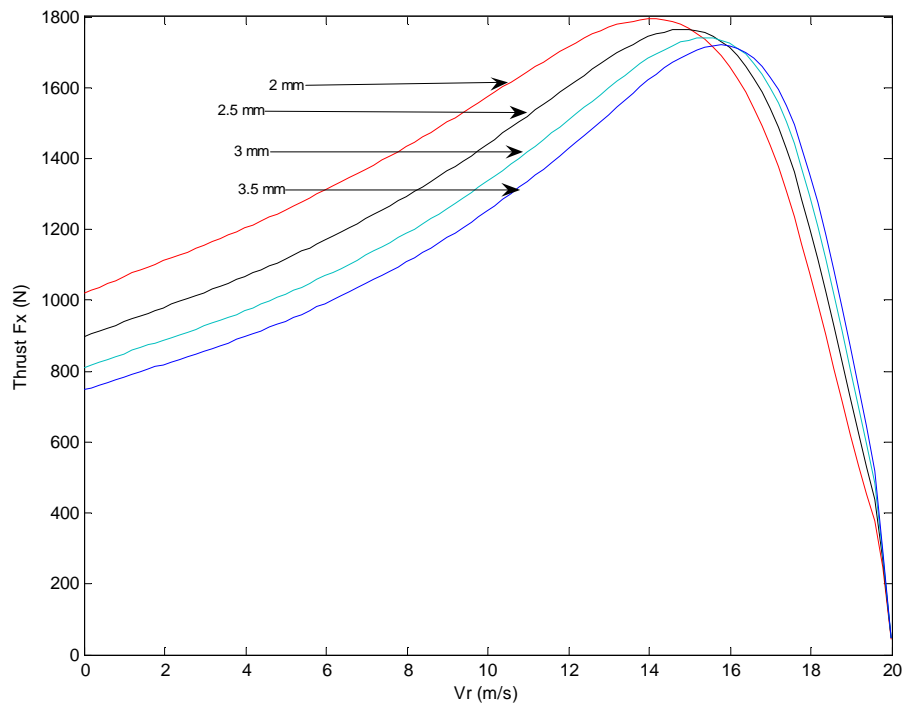


**Figure 5.9** Variations of *Thrust* vs. *Vr* (linear speed) curves at different thickness of conducting plate ( $d_{al}$ ).

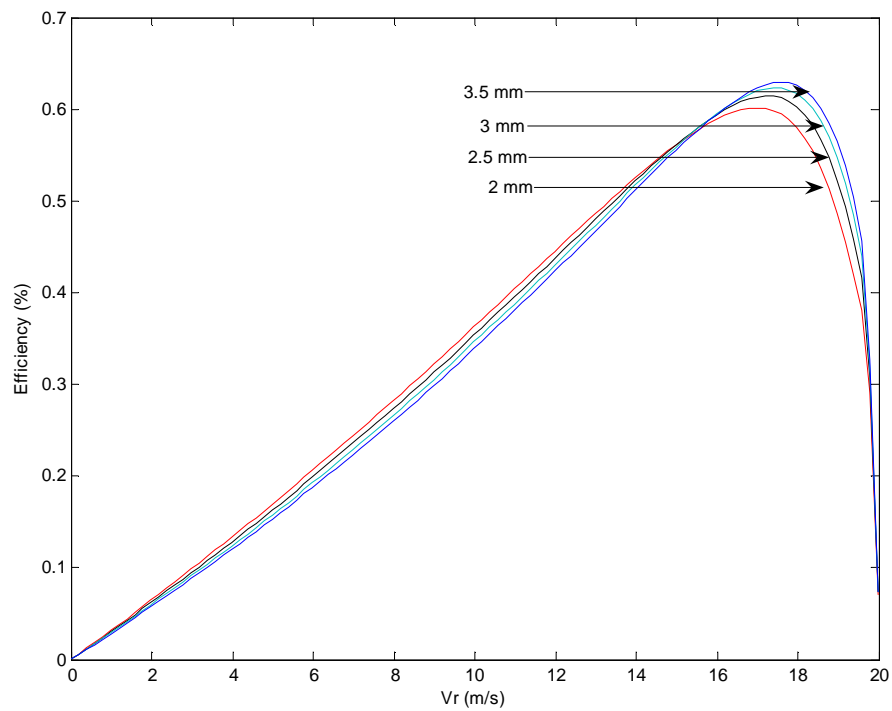


**Figure 5.10** Variations of *Efficiency* vs. *Vr* (linear speed) curves at different thickness of conducting plate ( $d_{al}$ ).

**Table 5.2** The performance values at discrete values of the conducting plate thickness

$d_{al} (mm)$	Efficiency	Power factor	Thrust (N)	$\eta \cos \phi$
2	0.5841	0.6068	1689	0.3545
2.5	0.5878	0.6100	1730	0.3585
3.0	0.5881	0.6048	1734	0.3557
3.5	0.5869	0.5959	1720	0.3497

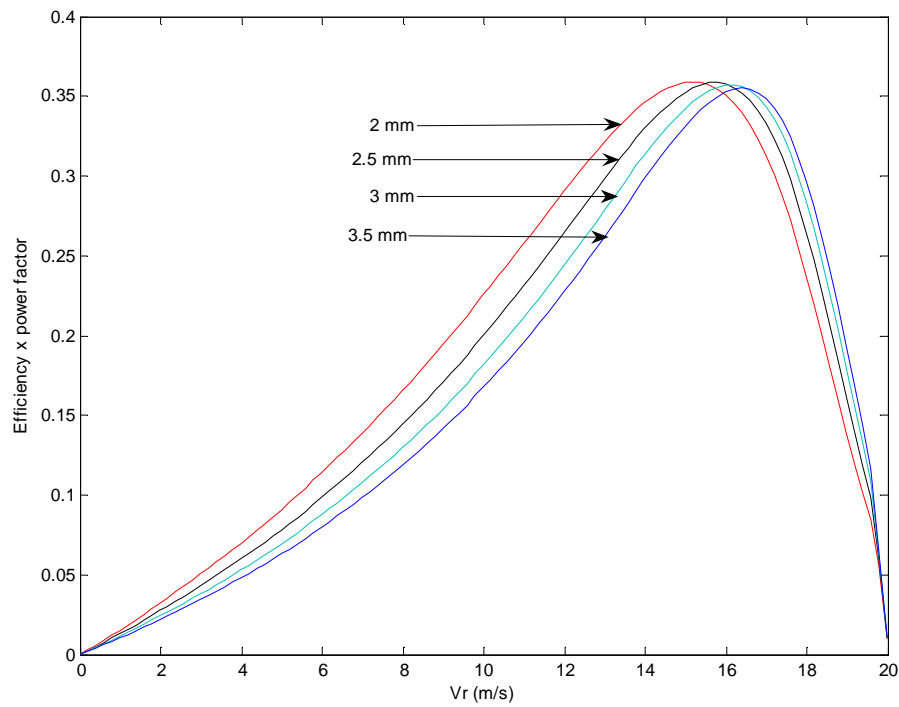


**Figure 5.11** Variations of *Efficiency product power factor* vs.  $V_r$  (linear speed) curves at different thickness of conducting plate ( $d_{al}$ ).

In Figure 5.13-5.16 shows the influence of the air-gap on the performance parameters of SLIM. In table 5.3 shows that while the air gap increases, thrust value decreases. In fact, there is the relationship between the effective air-gap ( $g'$ ), pole pitch ( $\tau$ ) and magnetizing reactance. This relation is shown in equation 4.25. If the air-gap increases while the pole pitch remains constant, the magnetizing reactance increases. Hence, the magnetizing current becomes smaller and the power factor improves. Depending on this results, Thrust value also increases with the increasing

the secondary current (equation 4.40). The efficiency is also increases when air-gap increases. In point of fact, the air-gap is generally large compared to rotary induction motors in order to maintain safety and primary and secondary supporting structure. Consequently, if the air gap cannot be made sufficiently small, the pole pitch should be smaller. However, the size of  $\tau$  is limited in accordance with the length of the motor. Finally, the air-gap is more sensitive to the performance parameters of SLIM. It is also noted that air-gap and the pole pitch can be taken into account as design variable in optimization.

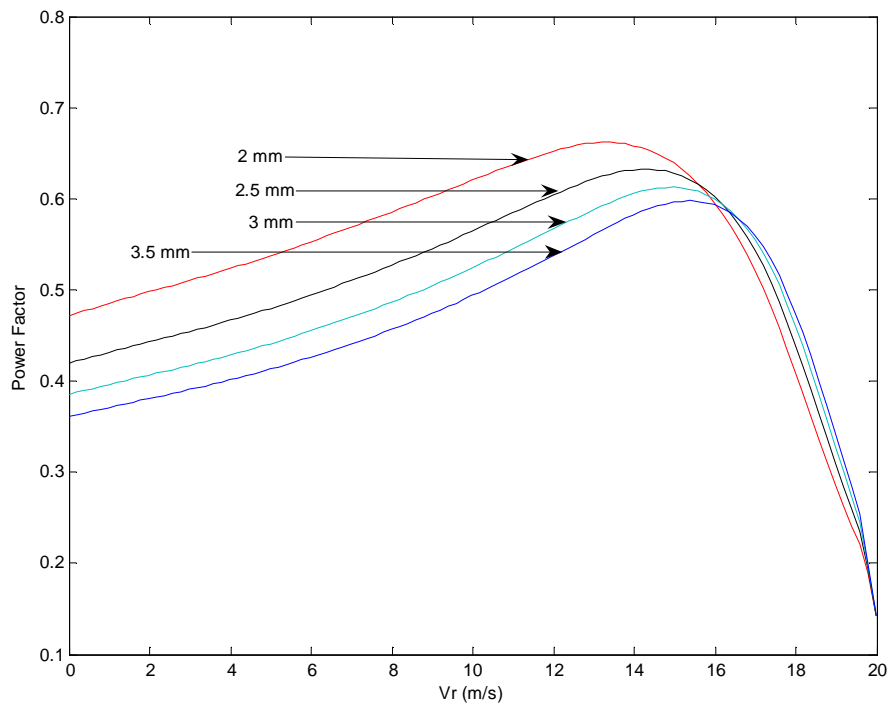


**Figure 5.12** Variations of *power factor* vs. *Vr* (linear speed) curves at different thickness of conducting plate ( $d_{al}$ ).

It is also observed that the high thrust is achieved with the smaller air gap and increased the secondary back iron thickness and conducting plate thickness. The efficiency product power factor is around the optimum value even the variation the thickness of the conducting plate and of back iron. But the variation of the air gap affects the all performance parameters. This means that air gap is more sensitive to performance parameters.

**Table 5.3** The performance values at discrete values of the air gap

$g$ (mm)	Efficiency	Power factor	Thrust (N)	$\eta \cos \phi$
10	0.6269	0.7729	2291	0.4846
15	0.5878	0.6100	1730	0.3585
20	0.5433	0.4902	1310	0.2663
25	0.4964	0.4052	1005	0.2011

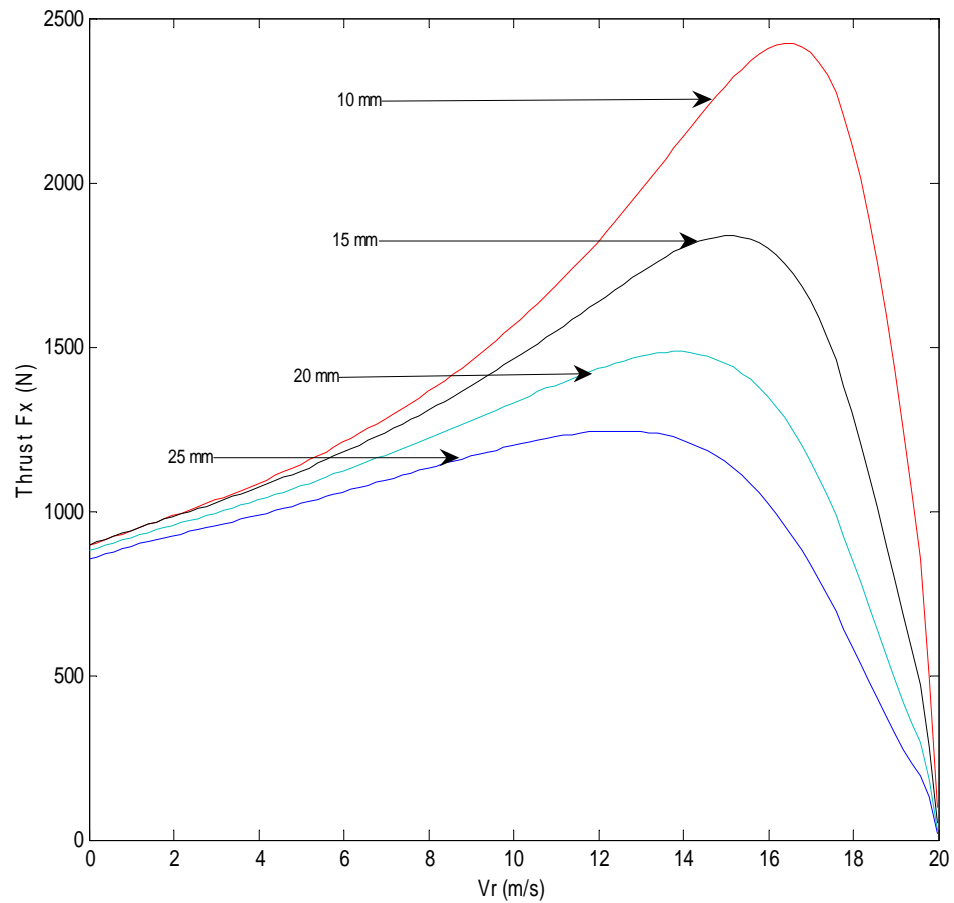


**Figure 5.13** Thrust vs.  $V_r$  (linear speed) curves at different air gap ( $g$ ).

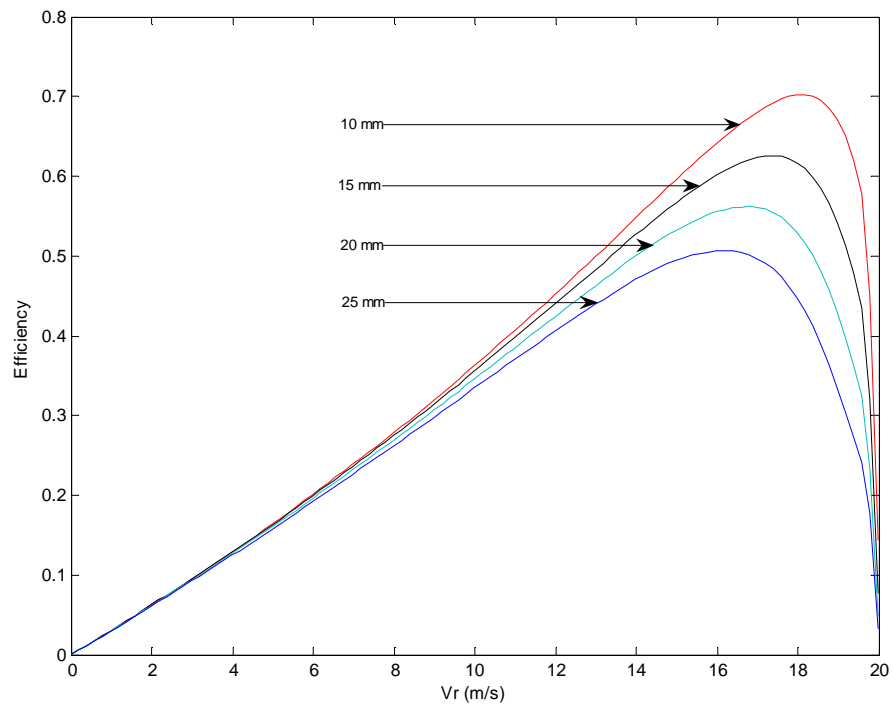


**Figure 5.14** The variations of *Efficiency* vs. *Vr* (linear speed) curves at different air gap (*g*).

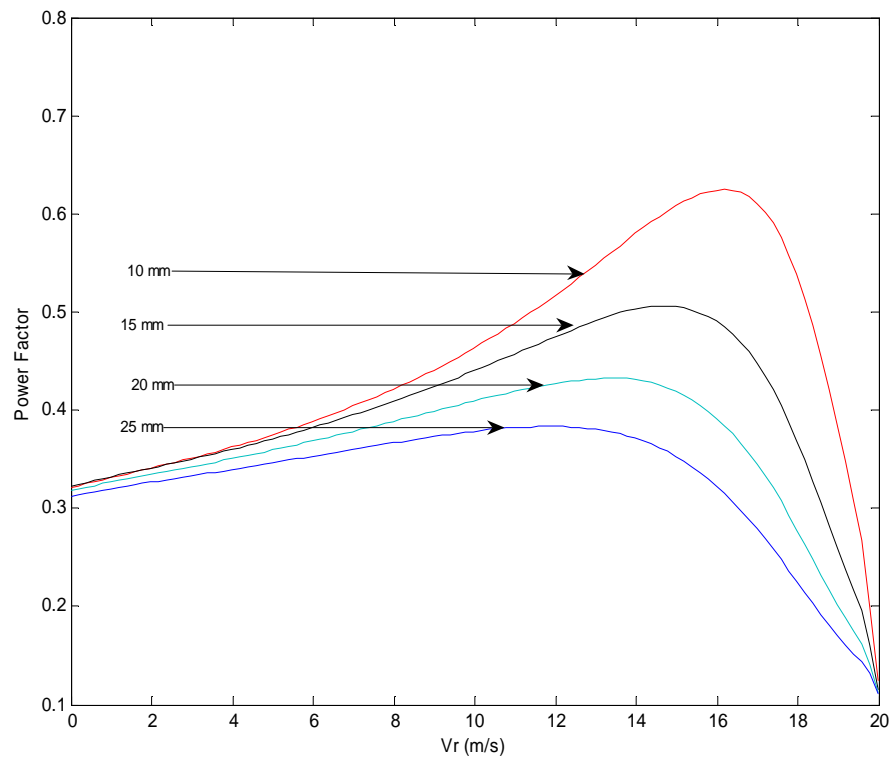


**Figure 5.15** The variations of *power factor* vs. *Vr* (linear speed) curves at different air gap (*g*).

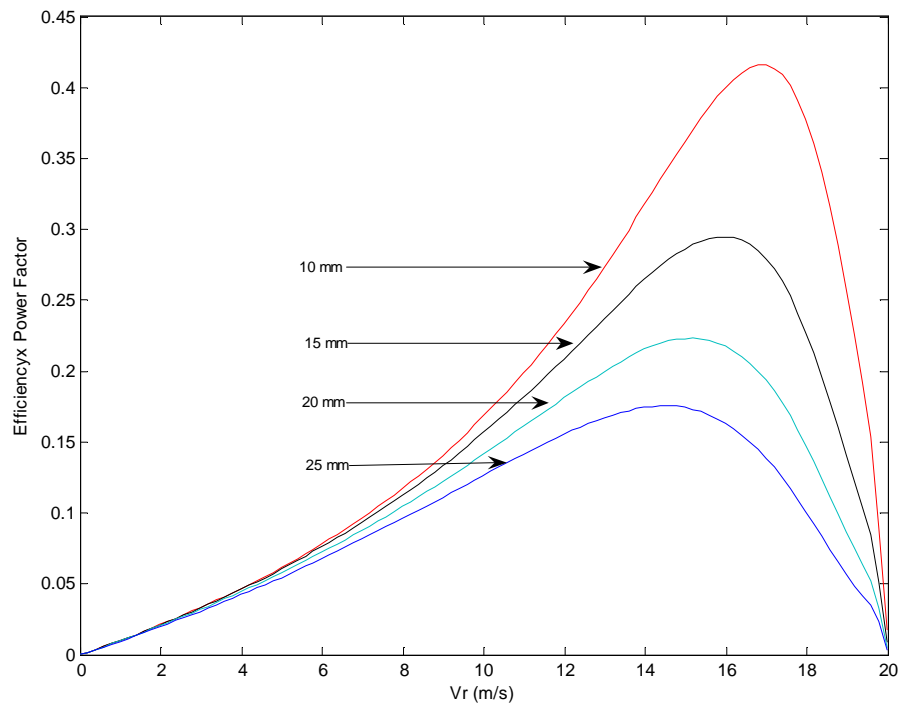


**Figure 5.16** The variations of *Efficiency product power factor* vs.  $V_r$  (linear speed) curves at different air gap ( $g$ ).

### 5.3.3.2 Design Optimization in the SLIM by using Enumeration method

The Enumeration method have simple principle that is limited space search or infinite but discrete. Enumeration algorithm evaluates the value of function to be optimized in each point of the feasible space solutions. The use of such an algorithm is interesting when the number of points is not very important. But in practice much of research spaces are too large so that computing time is very much. The disadvantages of this method are that it is not appropriate for great dimensions. And also this kind of methods is not guided by reasoning or an intelligent process without sweeping all the space solutions to find a good solution [49].

In this method, the discrete space exploration which is delimited by the feasibility intervals imposed on the parameters to be adjusted by incrementing the variables to be optimized. If the number of variables is four (for instance  $g$ ,  $W$ ,  $dir$  and  $dal$ ) and the number of incrementation for each variable is ten, the space of solution is too vast. Total combination is 10000 for this situation. The computing time will be large

even in the space of solutions. It takes about one hundred sixty six minutes even computing time is only one second for each combination. This time can be acceptable for optimization software but not for the software to be developed in this study due to the initial design consideration. Because of that, the number of the geometrical or physical parameters to be optimized should be chosen as possible as less.

This optimization method can be applied to locate the optimal solution of the design problem among the explored combinations in the case of the objective function in the existing geometrical constraints. In the discrete space solutions for each point, which is obtained by taking into account of the steps of variation of the variables to optimize, is explored for the best result according to the objective function. The structural parameters and some characteristics of SLIM can be optimized for different target thrust values by using this method in the presence of the constraints. These constraints can be summarized in table 5.4. The structural constraints can be expanded to other structural and physical parameters (such as  $\tau$ , the ratio of slot opening to slot pitch). According to the investigation of influence of the design parameters on the performance SLIM, the air gap is most critical design variable imposed on the efficiency product power factor (see figure 5.16).

**Table 5.4** Some structural constraints (u.b. =upper bound, l.b=lower bound)

Mechanical air gap (mm)	$l.b.<g<u.b.$
Secondary back iron thickness ( <i>mm</i> )	$l.b.<d_{ir}<u.b.$
Secondary conducting plate thickness (mm)	$l.b.<d_{al}<u.b.$
Secondary back iron width (mm)	$l.b.<W<u.b.$

This method seems to be implemented easily for design software to be developed. The air-gap is determined as the design variable to be optimized for objective function (efficiency product power factor). It can be expanded the design variables to be optimized.

## 5.4 Design of SLIM with the aided of computer

A new design algorithm of SLIM is developed based on the developed analytical tool for analysis which is presented in chapter 4. In order to design of SLIM, two different design algorithms can be considered depending on excitation type; i) Constant current excitation, ii) Constant voltage excitation. In this design concern of SLIM, it is assumed that source of feed is good filtered from the space harmonics. These two algorithms are applied by using MATLAB package software release 14. The purpose of these algorithms is to get the good design according to the given specifications. This developed software for design of SLIM consists of five different functions. They are as follow: i) Independent of Slip (IOS) ii) Boundary, iii) Maxwell, v) End effect, vi) Equivalent circuit. The main function reads the input data and calls these functions in consistent order and produces results for the input desired values. The user inputs the target thrust ( $F_x$ ) and linear velocity ( $V_r$ ) then this program calculates required geometrical parameters to dimensioning of SLIM and calculate the performance characteristics of SLIM at the given specifications. All results are stored in the main memory, and then performance characteristics are simulated.

The flowcharts of the developed software with the using of M-file programming for the design of SLIM are presented for constant current excitation and constant voltage excitation.

### 5.4.1 Independent of slip function (IOS)

In this function, the primary winding resistance (eqn. 4.26), primary winding leakage reactance (eqn. 4.27), the differential leakage reactance neglecting the saturation of the magnetic circuit, Carter's coefficient (eqn. A.1), equivalent conductivities (eqn. A.9) and other parameters that independent of slip variables are calculated. These calculations are performed by using formulas which are given in appendix.



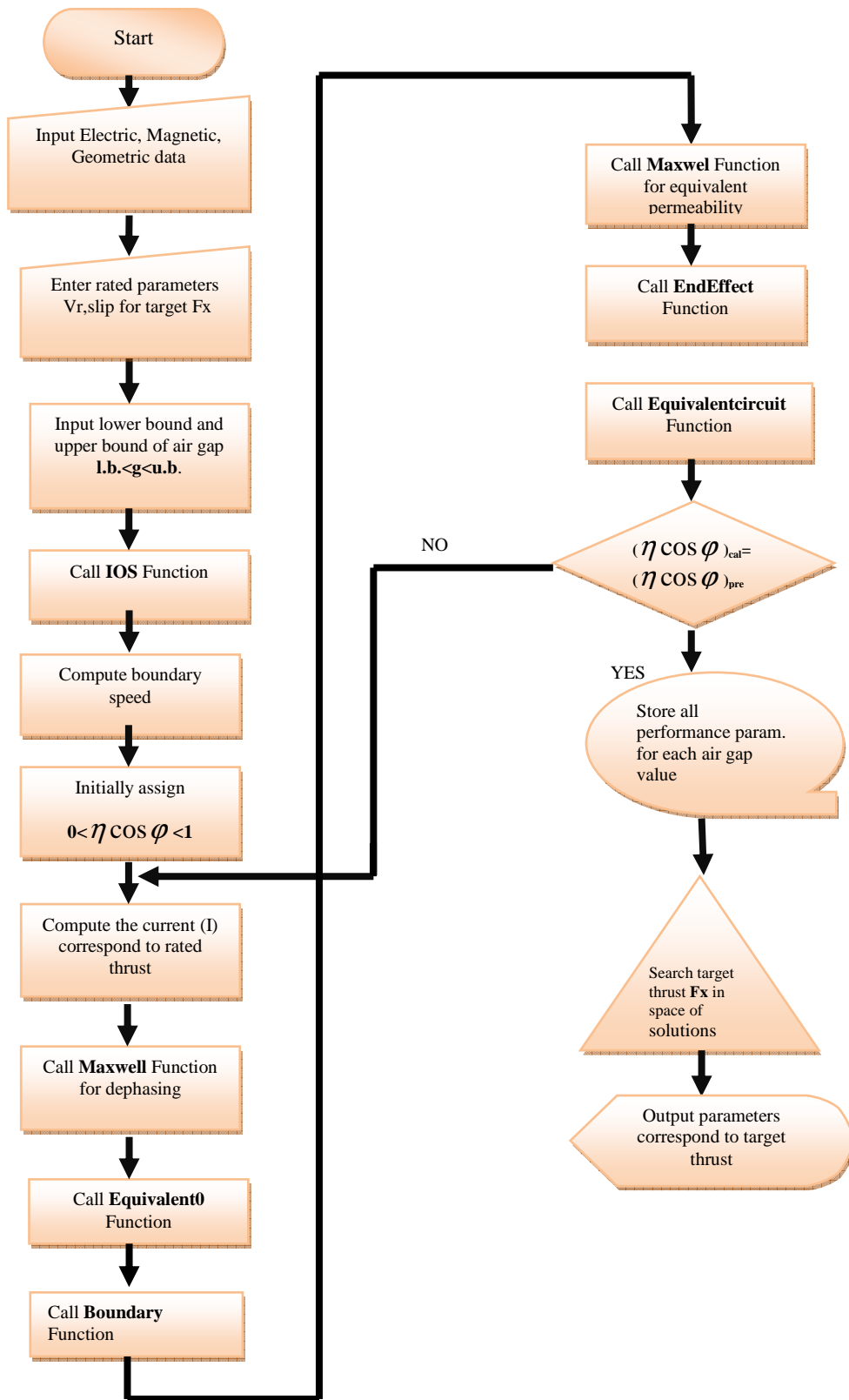


**Figure 5.17** Flowchart of design algorithm of SLIM at the Constant Voltage excitation

### 5.4.2 Boundary function

In order to get high precision for the calculation of the performance of SLIM, the longitudinal end effect must be taken into account. The longitudinal end effect can be included in the calculation of the performances in two ways. In the equivalent circuit of SLIM, The end effect can be represented either as an end effect impedance which is connected parallel with the magnetizing branch or reducing electromotive force (emf) on primary phase winding with the coefficient  $k_e$ . ( see on figure 4.4). In this study, the longitudinal end effect is represented with the reducing electromotive force on the primary phase winding. The calculations are performed according to this representation. In fact, there is no difference between these two representing for the calculation of the performances of SLIM. The end effect factor must be calculated correctly. In the SLIM, there is a certain speed which is between the zero and synchronous velocity. This is called boundary speed. In the calculation of the performance of SLIM, the longitudinal end effect doesn't take into account until the velocity is reached the boundary speed. In general, this speed is determined the formula which is given in appendix. But in CIGGT linear induction motor, this is determined as half of the synchronous speed ( $V_0 = 0.5V_s$ ). There is a phase angle difference between the fundamental wave produced by primary phase winding and the entry end wave which is represented by  $\delta_o$  ( the details are given in A5) . In this function,  $\delta_o$  is calculated as an input to the end effect function.

### 5.4.3 Maxwell function

The saturation factor and non-linear complex magnetic permeability of secondary back iron are calculated in this function. To calculate these factors, two-dimensional distribution of the electromagnetic field in the air gap, in the conducting plate and in the secondary back iron should be calculated first. The obtaining peak values of electric and magnetic components are sufficient at all boundaries. Since the electric and magnetic quantities are necessary for calculating the equivalent circuit parameters. The primary resistance and reactance are calculated as in the rotary induction motor. However, the calculated parameters ( such as equivalent relative

permeability, propagation constant..) in this function are related to the calculations of the secondary impedance and magnetizing reactance.

The solution of the electromagnetic equations in the solid back iron is very complicated because of the non linear magnetization characteristics. In the calculation of the non linear complex magnetic permeability of the secondary back iron, two coefficients ( $a_R$  and  $a_x$ ) should be determined.  $a_R$  and  $a_x$  represent the active power and reactive power loss in the secondary back iron. These coefficients for the used material in the secondary back iron are determined by the interpolation techniques in this function. In order to take into account non linear magnetic permeability and hysteresis effect,  $a_R$  is multiplied by the resistance or active power loss of secondary back iron and represents the active power loss and  $a_x$  is multiplied by reactance or reactive power loss of secondary back iron. But in general these coefficients are taken into account in calculations with the average values.

The saturation factor and the non linear magnetic permeability are calculated in this function together. First of all, the saturation factor is initialized with 1 ( $k_\mu = 1$ ) and magnetic field intensity at the surface of the secondary back iron on the side of the primary is assumed to be equal to the line current density. The corresponding magnetic permeability is found by interpolation using the magnetization data of the secondary back iron. The new magnetic field intensity at the surface of the secondary is calculated and compared to initial value and the difference is leveled in an iterative loop with the maximum error of 0.1 %. The convent iteration technique is used and the assuming the relaxation factor is equal to unity. In that assumption, fast convergence is obtained. This function is summarized with the below algorithm;

- 1) Initialize the  $k_\mu = 1$  and  $H = A_m$ .  $A_m$  is the line current density and  $H$  is the magnetic field intensity at the surface of the secondary back iron.
- 2) Find the magnetic flux density and active ( $a_R$ ) and reactive loss ( $a_x$ ) coefficient correspond to magnetic field intensity from magnetizing data.

- 3) Calculate the complex magnetic permeability of secondary back iron correspond to initial value of magnetic field intensity.
- 4) Calculate the magnetic field new magnetic field intensity with using obtained magnetic permeability.
- 5) Calculate magnetic voltage drop for each part of motor
- 6) Calculate saturation factor using the equations given in appendix.
- 7) Compared the calculated and assumed magnetic field intensity with the 0.1% error ( $(H_c - H_i) > 0.1\%$ ).
- 8) Until the convergence is attained, the iteration is continued.

The details in this function has been given in section 4.4.

#### **5.4.4 End effect function**

The longitudinal end effect factor is calculated in this function. This factor must be taken into account to get the high accuracy in performance calculations. In fact, the longitudinal end effect can be taken into account in two ways as mentioned previously. The end effect factor is represented by  $k_e$  which is calculated using the equations given in A.5. In calculations of the end effect factor, some sub functions are used. The secondary resistances and reactance is also calculated to find the equivalent thickness of the conducting plate. In the literature, three methods are developed for the determining of the equivalent thickness of conducting plate ( $d_R'$ ). In the end effect calculations, the first method which is given in A.5, has been used. In this method, the real part of impedance of a hypothetical layer (A.29) with thickness  $d_R'$  is made equal to the real part of the equivalent impedance of two iron and aluminum parts (4.35).

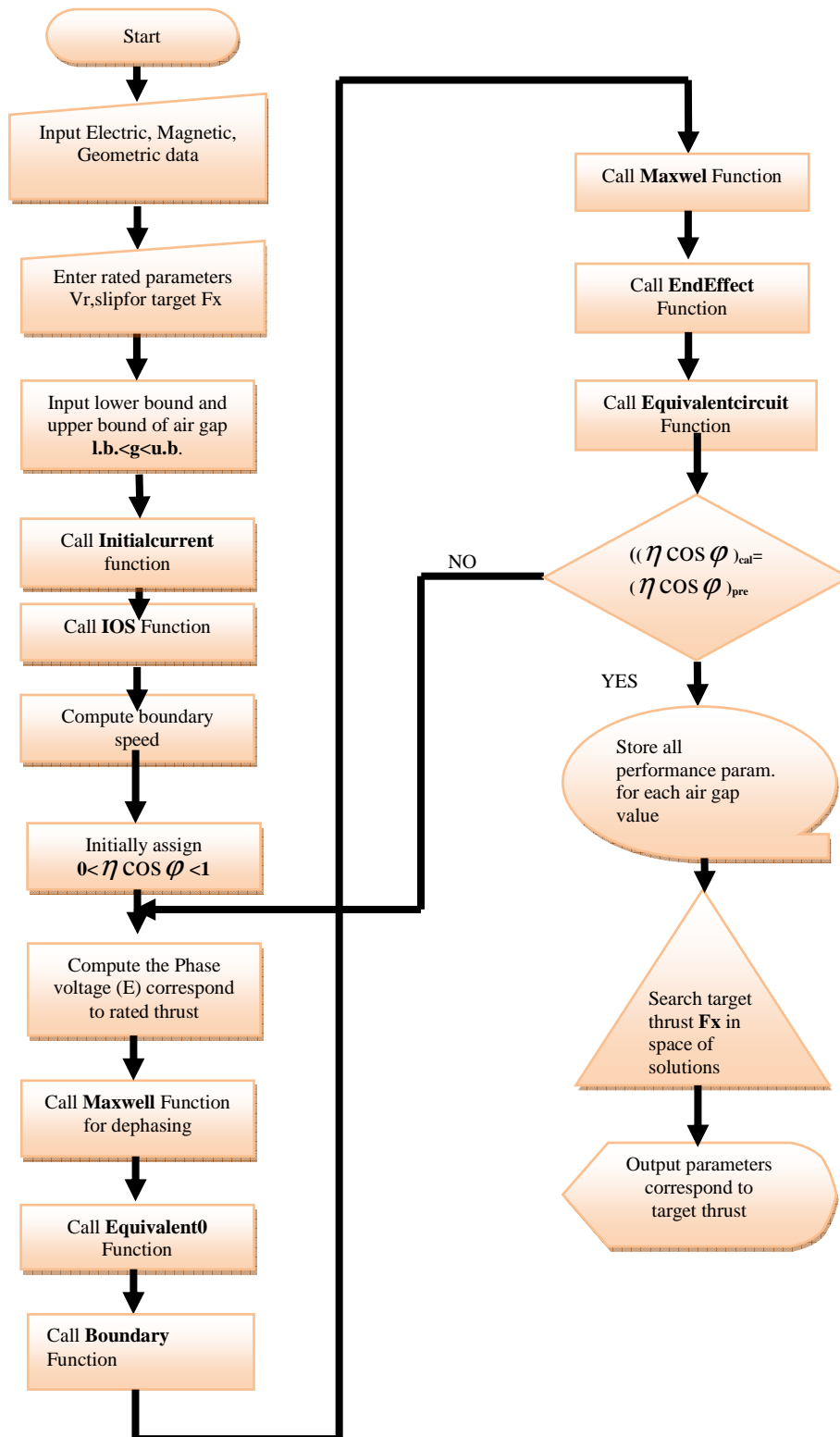


**Figure 5.18** Flowchart of design algorithm of SLIM at the Constant current excitation

#### **5.4.5 Equivalent circuit function**

To calculate the performance of the SLIM, the equivalent circuit parameters are used. Before the performance calculations, the equivalent circuit parameters are calculated. The magnetizing reactance and secondary impedance are depending on the slip. These parameters for each slip value is calculated taking into account the longitudinal end effect, saturation effect, hysteresis effect in the secondary, slot effect, non-linear magnetic permeability in this function. The longitudinal end effect factor in T-type equivalent circuit of SLIM is used for the reducing electromotive force on the primary phase winding. These equivalent circuit parameters are used to calculate the performance parameters. The input current, secondary current, thrust, normal force, input power, output power, losses, efficiency and power factor are also calculated as a function of slip.

#### **5.4.6 Initial current function**

For constant current excitation type design, constant input current is estimated on the basis of input voltage ( $V$ ), the primary resistance  $R_1$  and the primary leakage reactance  $X_1$  where magnetic saturation is not taken into account. This function estimated the primary constant current. This value remains constant for each value of slip.

### **5.5 The software infrastructure of LIMCAD**

The core of the Limcad (Linear induction motor with the computer aided design) program is constructed with MATLAB package software (Release 14) since MATLAB offers more scientific facilities than any other programming tool does. On the other hand, it is more appropriate not to use MATLAB for the task of preparing the user-interface of Limcad. The main reason behind this decision was the MATLAB is a powerful programming tool designed to develop academic software in which the main focus is the algorithm itself neither the user-interface nor the user-friendliness of the developed software. Moreover, MATLAB does not include as rich user-interface options as many of the visual software development tools provide nowadays. Thus, it is decided to implement the core of the program

with MATLAB and Graphical User Interface (GUI) of the program with a visual programming environment.

The GUI of the Limcad application, thus, is prepared with Visual C#.NET. The Visual Studio .NET 2008 is selected for the Integrated Development Environment (IDE) for developing VC# programs. VC# is the one of the choices that it can be deployed into MATLAB applications after creating M-Files and packaging the application into the exportable format. The other choices are Java and Excel environments. MATLAB can package any M-File into a Windows DLL file that VC# environment can handle. In fact, MATLAB prepares the M-File as an Object that some Object-Oriented Programming (OOP) languages such as Java, VB.NET and C# can utilize. As a result, VC# as an OOP and high-level language is a good choice of visual programming and embedding MATLAB programs into a GUI.

The Limcad applications require the .NET Framework 2.0 and the MATLAB Component Runtime software packages to be installed. Limcad is tested against .NET Framework 3.5 and is observed to successfully work with it, as well.

### **5.5.1 The User-Interfaces of LIMCAD**

The Limcad software is organized for the ergonomic usage. It consists of the title bar, menu bar and project area. “File”, “Material”, “Run”, “Curve”, “Post Process” and “Help” menus exist in the menu bar. In “File” menu has the submenus consists of ‘New, Open, Save, Save as, and Exit’. These submenus have functions of opening existing project or new design project, saving existing design project and exit to program. These submenus are shown in Figure 5.19.

In “Material” menu, three submenus exist. They are Core loss, Wire and B-H submenus. These submenus are prepared for the materials used in the SLIM’s primary side and secondary side. The material database is constructed for the materials used in the primary and secondary side. These databases contain the data for primary core loss data, wire data for used in primary winding and secondary

back iron material data used in the reaction rail. These submenus are shown in Figure 5.19.

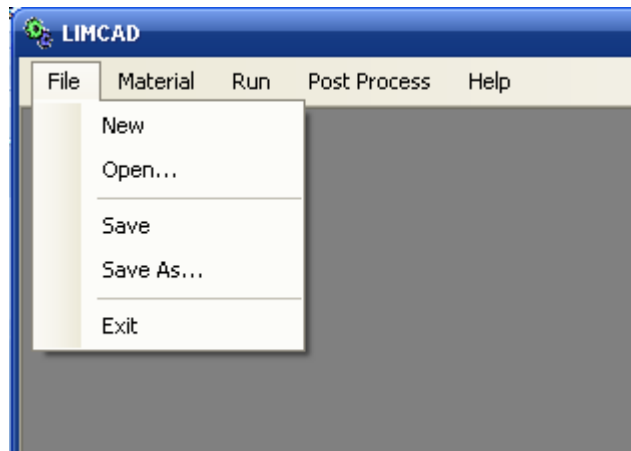


**Figure 5.19** Submenus of “Menu”

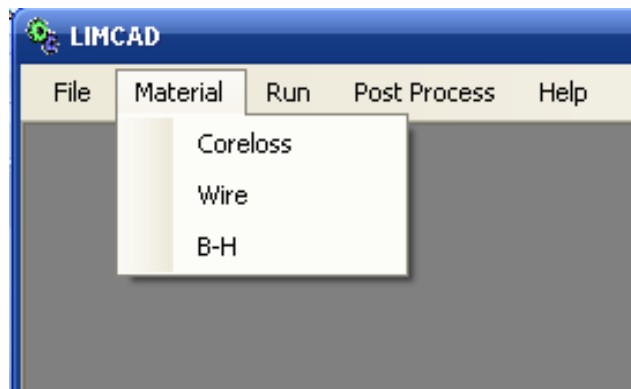


**Figure 5.20** Submenus of “Material”

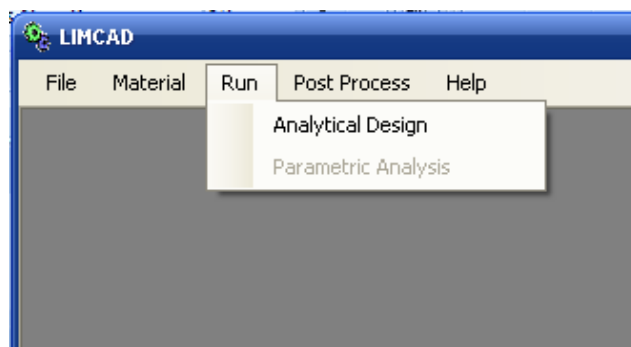


**Figure 5.21** Submenus of “Run”



Once the required parameters for the design of SLIM input the program via User Interface, these submenus will be active. These submenus are shown in Figure 5.21. “Analytical Design” submenu is launched the design routine in the program. Parametric Analysis submenu is also launched the analysis routine in the main routine.

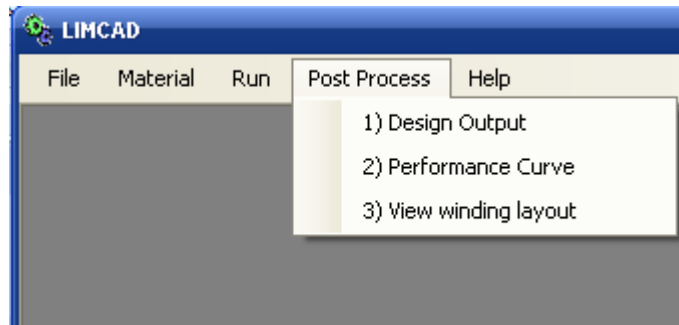


**Figure 5.22** Submenus of “Post Process”

In” Post Process” menu contains three submenus. They are Design Output, Performance Curve and View winding layout. These submenus are also shown in Figure 5.22. When the required parameters input the program, the analytical design is launched from the Analytical Design submenu in Run menu. Then the program produces some outputs such as efficiency, power factor, rated thrust, normal force, weight of the motor, the dimensions of the motor. One of them is the design output into a file. This file contains the design data for the SLIM at the given specifications.

### **5.5.1.1 The new project interfaces of LIMCAD**

The design of SLIM is based on the project in this software. The input parameters for SLIM input the program via the user interface shown in Figure 5.23. The user input the required parameters to the program in the four headers. They are General data, Stator, Winding and reaction rail. Under General data header, the rated parameters, air gap boundaries, input frequency, input voltage, number of pole, stray loss, stacking factor and operating temperature can be entered into program. Stator

header contains the parameters to input the stator data. They are as follow; primary core width, height and number of slot are the input parameters. And primary slot dimension is also input parameters under the stator header. The dimension of two slot structure can be selected for the design of SLIM. In fact, open and semi open slot is used for SLIM. These slot structures are shown in Figure 5.23 ad 5.24.

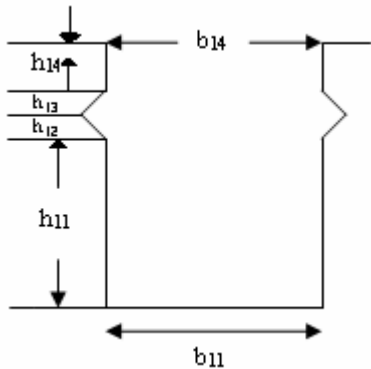


**Figure 5.23** Open slot structure

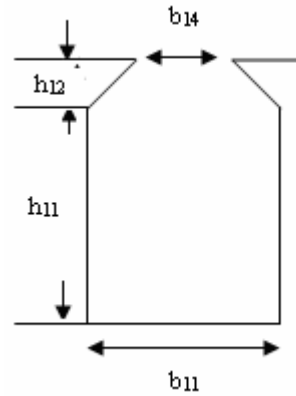


**Figure 5.24** Semi-open slot structure

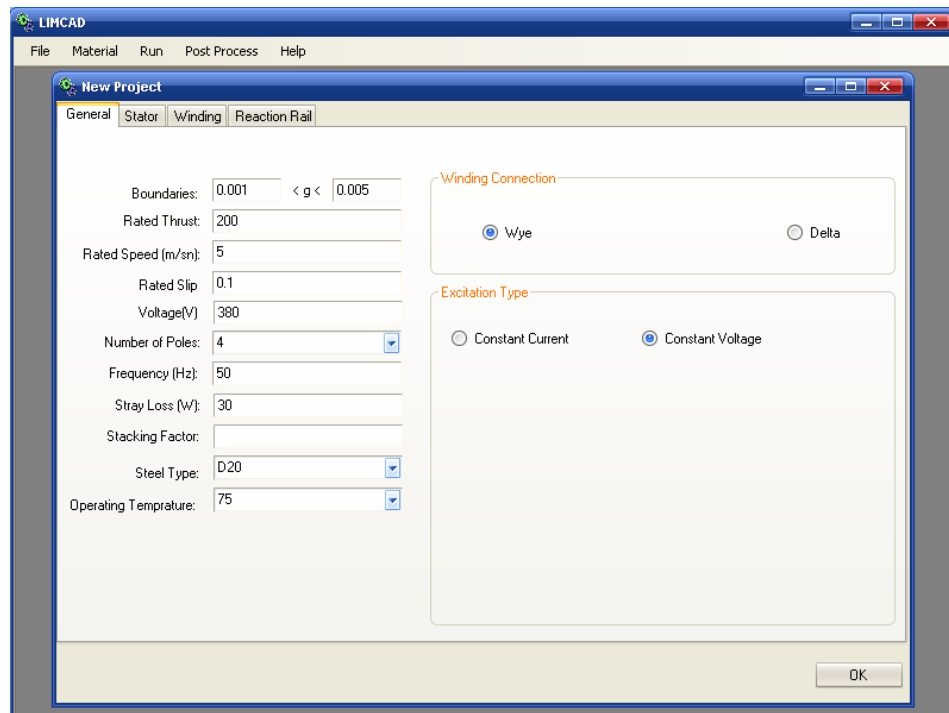


**Figure 5.25** User interface of General header

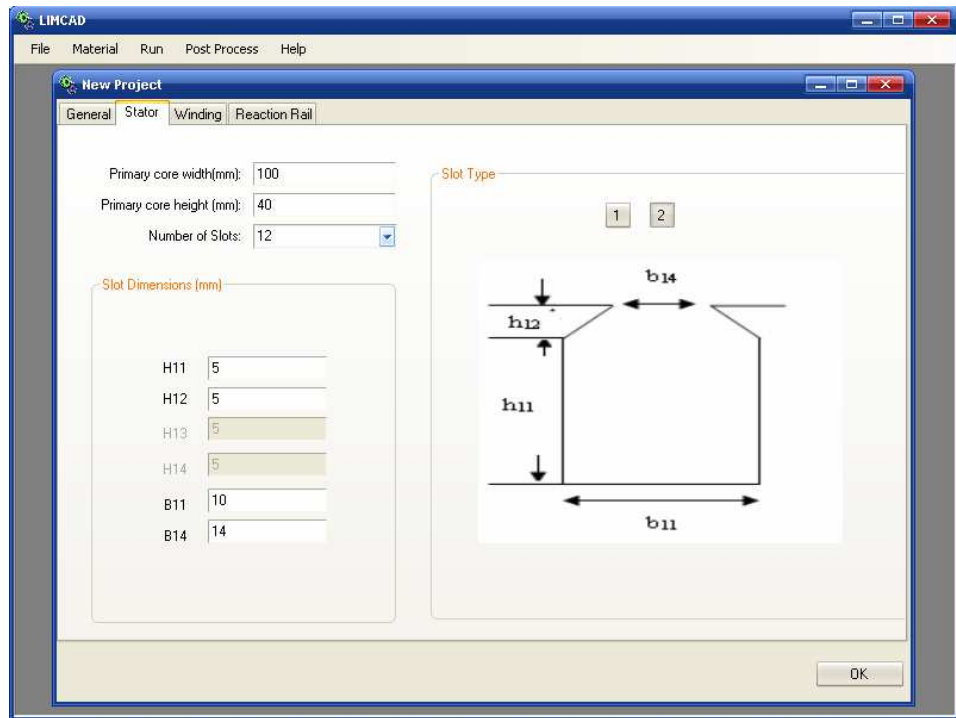


**Figure 5.26** User interface of Stator header

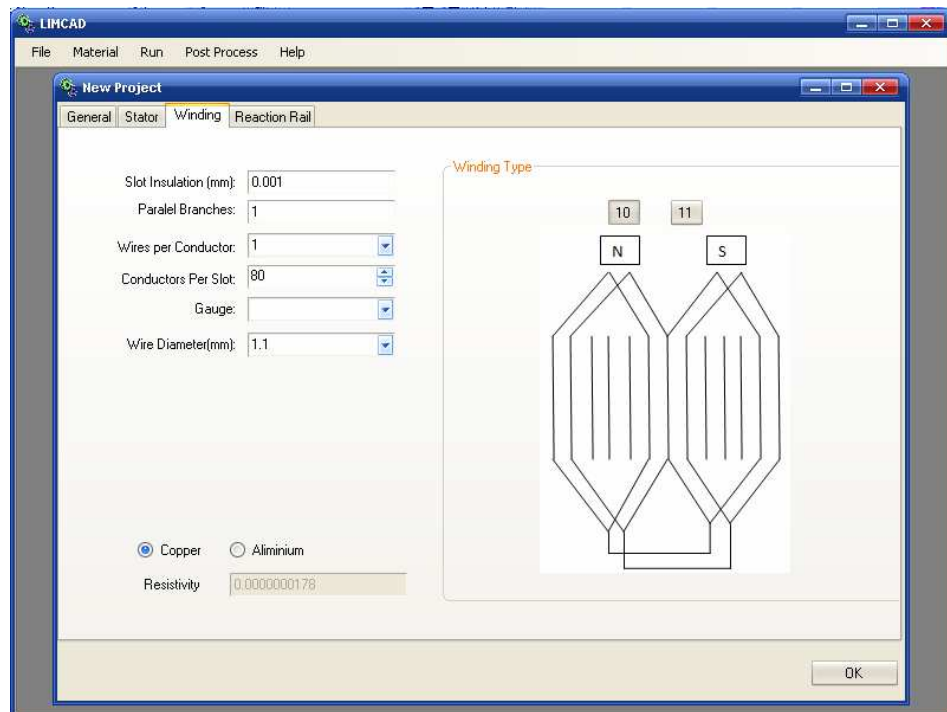


**Figure 5.27** User interface of Winding header

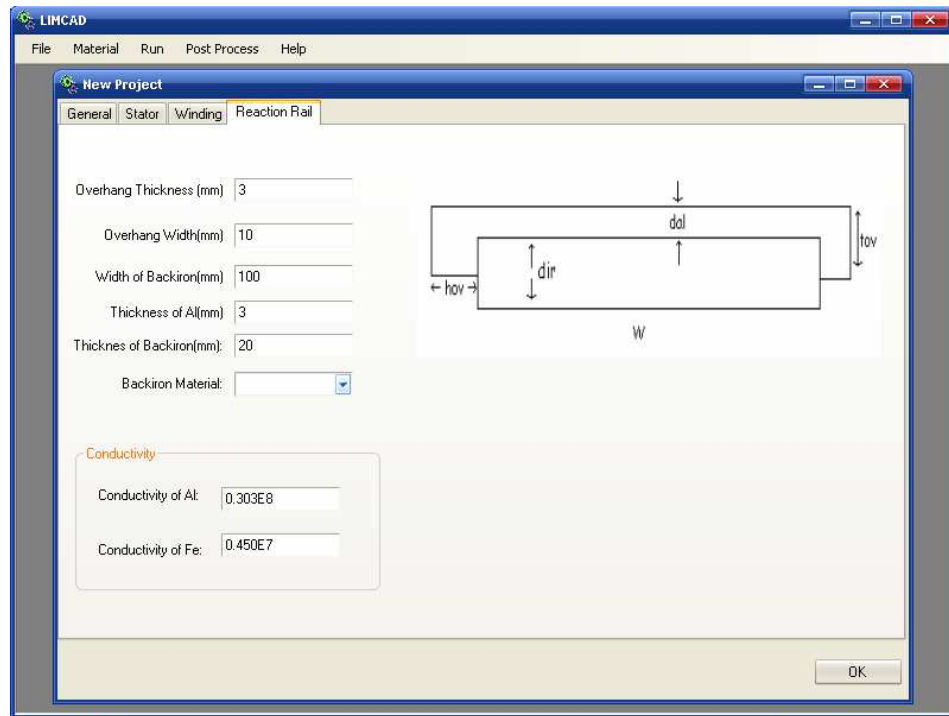


**Figure 5.28** User interface of Reaction Rail header

In the winding header, there are two winding configurations. One of them is full pitch, single layer and number of slot per pole per phase is one ( $q=1$ ) and ( $q=2$ ). These two winding configurations can be selected for the primary winding. As for the Reaction rail header, the dimension of the secondary structure and the material properties can be entered into program via this user interface. In order to run the analytical design processing, pressing the “OK” button is enough and then click “Analytical design” submenu under the “Run” menu. After the program runs, the design output and performance curves are produced by the program. The output for construction of the designed of SLIM is also produced by the program such as winding layout and lamination.

### 5.5.2 A design application using developed software

We have been tried to design a SLIM by using developed the analytical design software. The required parameters for the design of SLIM are shown in Figure 5.23-5.26. In order to obtain 200 N thrust, linear speed 5 m/s at 0.1 of rated slip value at constant voltage excitation, the program runs and the output results are produced by

the developed software. The design output can be shown in design output format of the program and of MS Excel format. Design output can be exported to the MS Excel. Both design output format are given in Figure 5.29 and Table A.2. The performance curves are also produced by the program and performance curves of the designed SLIM by this software are presented in Figure 5.27-5.32.

The screenshot shows a software window titled "LIMCAD - [Design Output]" with a menu bar containing "File", "Material", "Run", "Post Process", and "Help". The main area displays a table of design variables and their values, organized into three sections: GENERAL DATA, PRIMARY DATA, and REACTION RAIL DATA. An "Export" button is visible next to the "H14(mm)" row in the PRIMARY DATA section.

Variable	Value
<b>GENERAL DATA</b>	
Given Rated Thrust(N)	198.7582
Given Rated Speed(m/s)	5
Rated Voltage(V)	219.3931
Winding Connection	Wye
Number of Poles	4
Frequency(Hz)	50
Stray Loss(W)	30
Excitation Type	Constant Voltage
Operating Temperature	75
<b>PRIMARY DATA</b>	
Number of Stator Slots	12
Primary Length(m)	0.2222
Teeth Width(m)	0.0085
Dimension of Stator Slot	
H11(mm)	5
H12(mm)	5
Export	5
H14(mm)	5
B11(mm)	10
B14(mm)	14
Number of Conductor per Slot	80
Number of Parallel Branches	1
Type of Coils	11
Coil Pitch	0.0556
Wire Diameter(mm)	0.0011
<b>REACTION RAIL DATA</b>	
Aluminium Thickness(mm)	0.0030
Air Gap(mm)	1
Backiron Thickness	0.0200
Backiron Width	0.1000

**Figure 5.29** Design output in program format

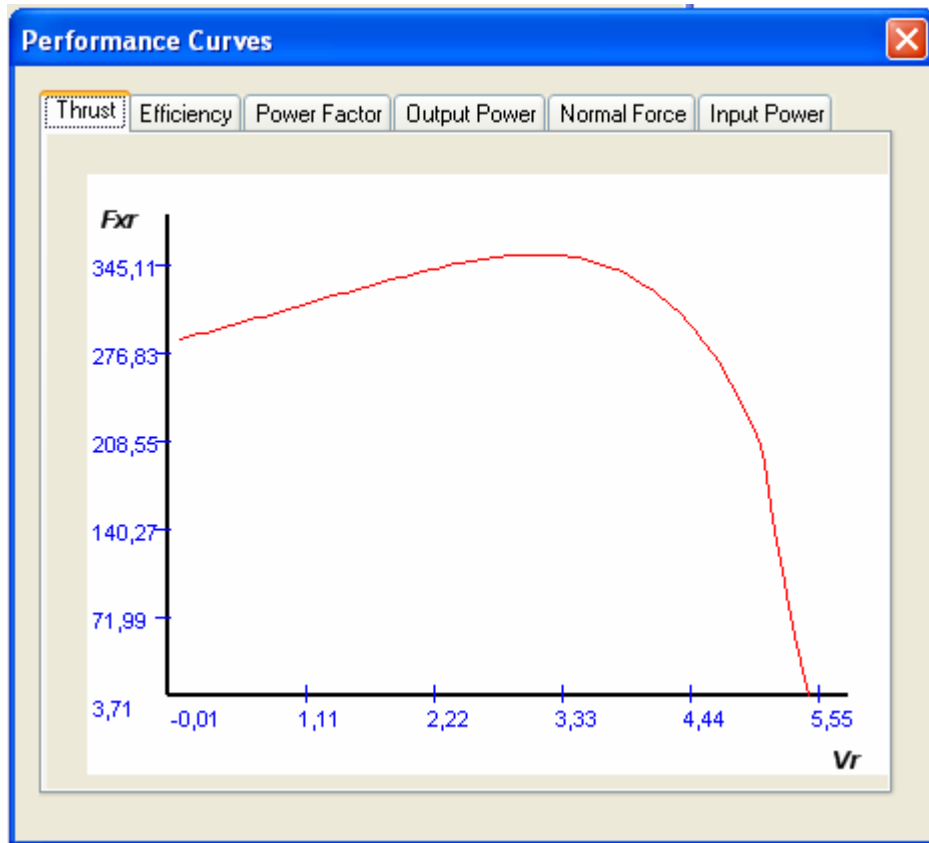


Figure 5.30 Thrust vs. linear speed

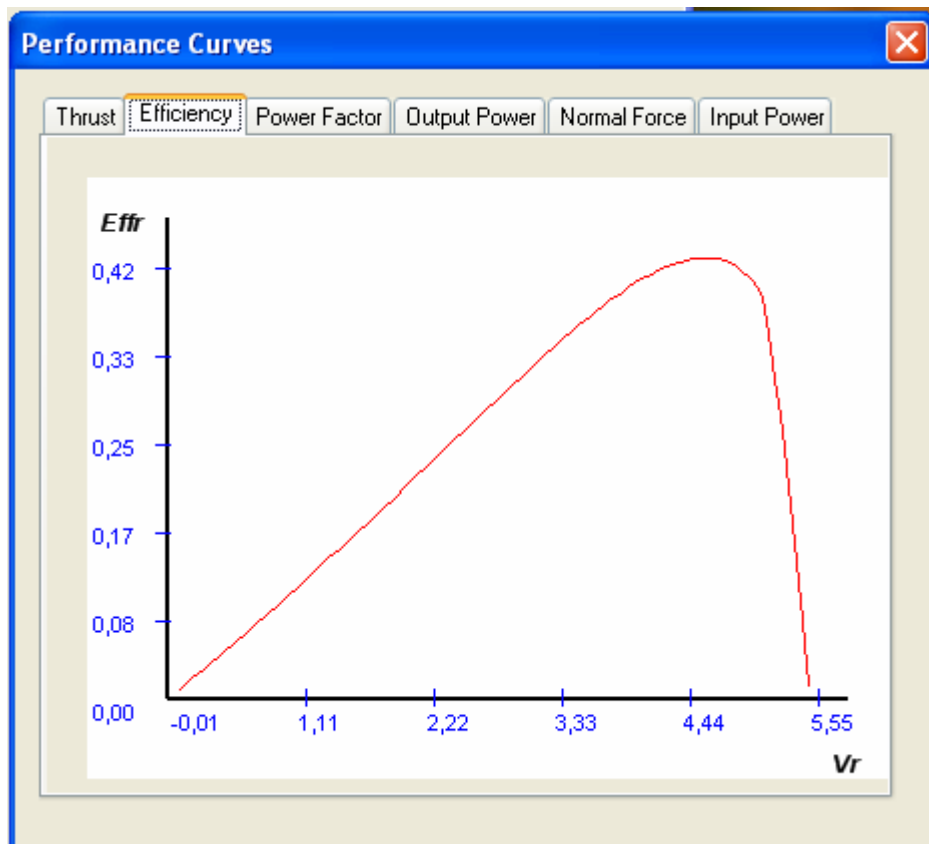
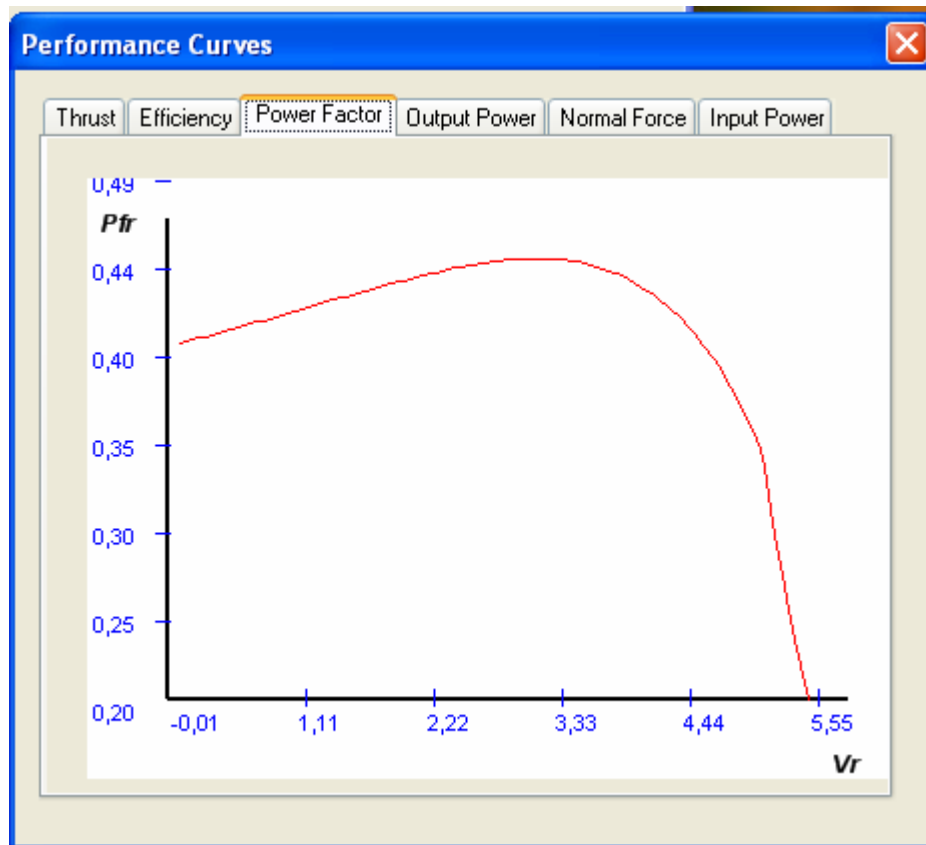
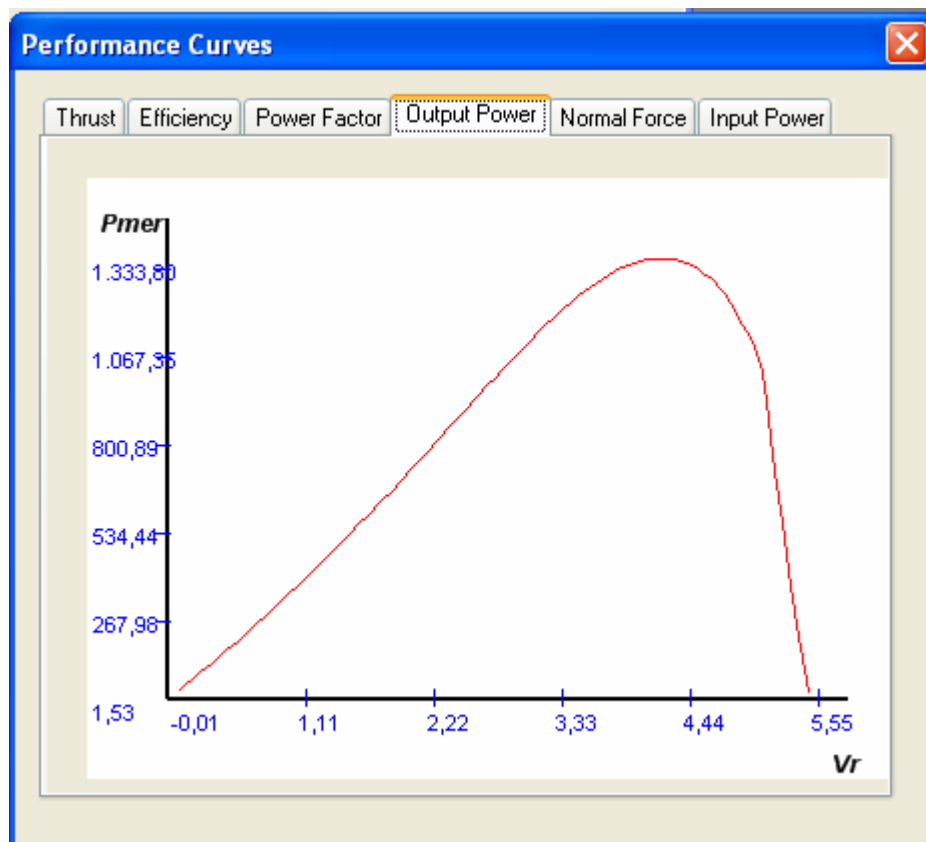


Figure 5.31 Efficiency vs. linear speed



**Figure 5.32** Power factor vs. linear speed



**Figure 5.33** Output power vs. linear speed

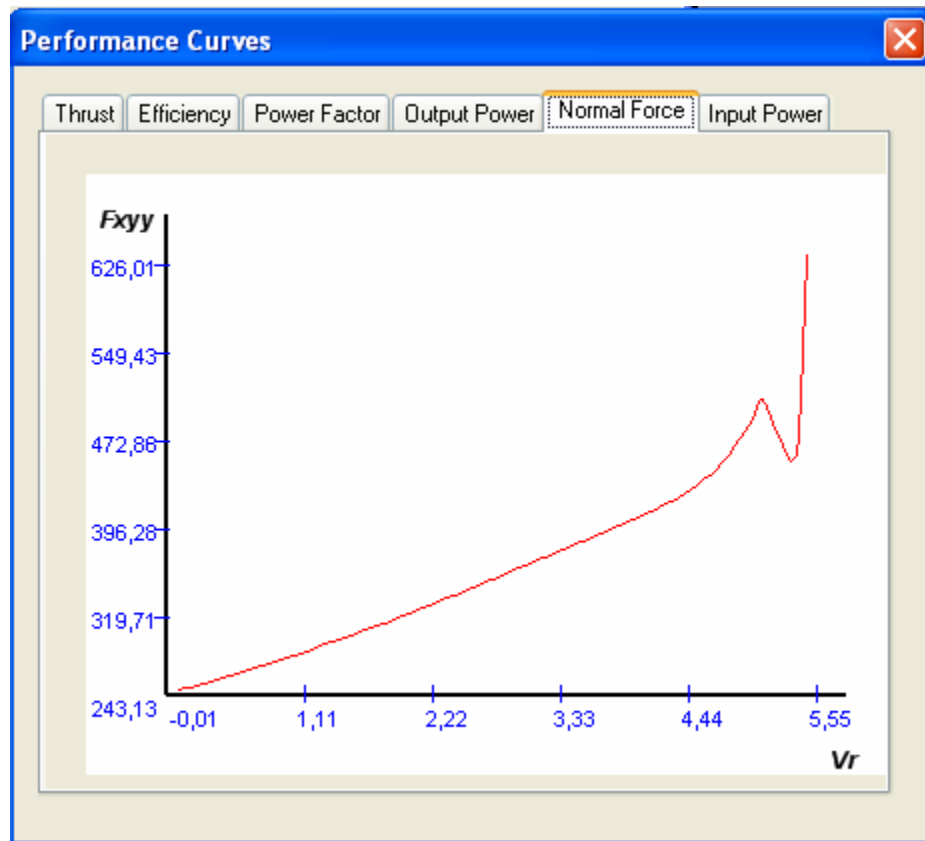


Figure 5.34 Normal forces vs. linear speed

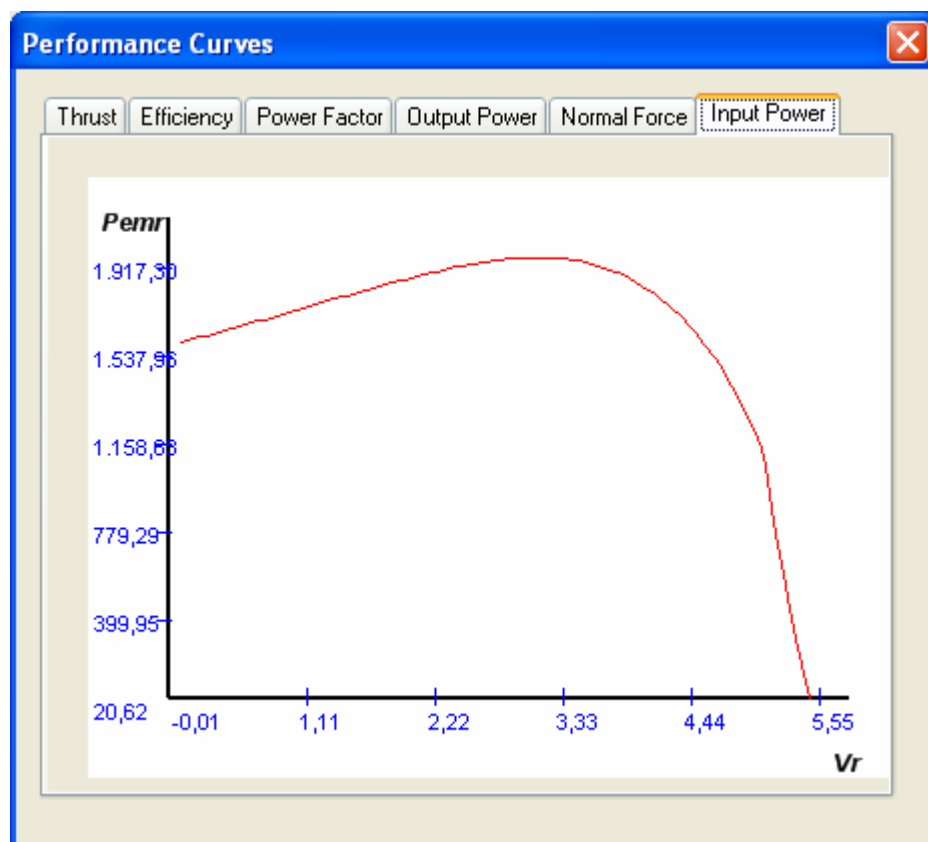


Figure 5.35 Input power vs. linear speed



## 5.6 Summary

In this chapter, the electric machine design methodology with the aid of computer is presented. The dimensioning of the electric machine has been carried out by procedural approach and optimization. Enumeration method, which has been used in the optimization of the dimensioning of SLIM in this study, has been presented. In order to determine the descriptive geometrical parameters, the influence of the geometrical parameters on the performances of SLIM is investigated by using the significantly validated developed analytical tool for analysis. As a result of this investigation, the air gap is more sensitive parameter in performance calculations. This parameter is chosen as the design variable. The air gap should take the possible smallest value by critical constraint. And the efficiency product power factor is chosen as an objective function.

With this estimation, new analytical design algorithm is developed for the finding optimum value of efficiency product power factor, air gap and thrust. The software is developed by using the MATLAB package software. Then, this software is embedded into VC# .NET. An example design is carried out and simulated by new developed software. It can be designed a SLIM over a wide range operating conditions at various power ratings using this developed software.

## CHAPTER 6

### CONCLUSION AND RECOMMENDATIONS

#### 6.1 Summary and Conclusion

Here, analytic design software for a single sided linear induction motor with a double layer reaction rail has been developed. In this software, given secondary geometrical dimension constraints, i.e. aluminum thickness, back iron thickness and air gap, the optimum value of efficiency product power factor is to be calculated to obtain the LIM's target thrust and linear speed. To facilitate this objective, we have used a two step approach, namely electromagnetic analysis and equivalent circuit technique.

In the electromagnetic analysis phase of LIM, we have examined the electromagnetic phenomena having ignored other harmonics rather than the fundamental space harmonics. The reason to take into account only the fundamental space harmonics is to decrease heavy computational load of algorithm. Through this approach, the considerable cause of longitudinal end effects on the performance of LIM has been evaluated. And following the result of this assessment, the effect on the performance of LIM has been noticed to change with variations in input frequency. As the frequency increases, this effect becomes significant on the performance of the LIM. In addition to the other effects, saturation and hysteresis effects have been the main focus of this study to obtain the secondary impedance parameters in the equivalent circuit technique. While examining these two effects, depth of the penetration of the wave that is produced by the primary of the LIM is evaluated according to the wave penetration depth concept. While the permeability is obtained by a conventional iterative method, the estimation of the secondary impedance is done with a new contribution of this study. Secondary impedance is actually a hard or nearly impossible phenomenon to measure. As a result of its highly accurate consideration, performance calculations have been accomplished in high precision and correctness. The proposed method accomplishes this by using a modified Least Squares statistical

learning method, which is actually a linear approximation, to estimate the secondary impedance. The relevancy between the secondary impedance which is obtained by using the proposed approach and speed is observed and it is seen that while approaching the synchronous speed, the secondary impedance stays nearly constant; however, it decreases sharply near the synchronous speed. This is an expected effect of the wave impedance concept since the change in the permeability of the iron is minimal until the penetration depth reaches the half of the thickness of the iron. Moreover, when the penetration depth passes the half of the thickness of the iron and approaches the exact thickness of the iron, a decrease in the secondary impedance initiates. Once the penetration depth reaches the exact thickness of the iron, a sharp decrease occurs.

Since the accuracy of the estimated secondary impedance cannot be validated during the operation of the SLIM, hence, thrust value should be employed in evaluation of the secondary impedance. As a result, the proposed approach can only be confirmed through the thrust values of the SLIM. The thrust values according to linear speed for constant frequency, e.g., 5 Hz, 11 Hz, 18 Hz, 28 Hz and 40 Hz, are compared to the experimental results of the CIGGT SLIM study [1] under different input frequencies. The thrust values of the proposed method are observed to be in accordance with the results of the CIGGT SLIM. It has been observed that there is a good match between the objective model and the result of the proposed method in 40 Hz frequency. As far as similar studies in the literature are concerned, as to the authors' knowledge, the proposed approach is the most efficient method studied in this frequency while it sacrifices computational speed on behalf of a more precise performance.

To fulfill the above mentioned requirement for further applications of the LIM, a computer software has been constructed. The core components of the software, which are computationally intensive, are implemented in MATLAB environment. In order to present the tools of the software in a user-friendly manner, Visual C#.NET is utilized to cover the core components of the software as a shell. The user is expected to give command and provide the parameters of the desired design by using the visual controls provided by the Visual C#.NET software development environment. While the target platform for the developed software is primarily Windows, by the use of the Mono project that is the effort to port the .NET environment into Linux,

our software can be ported into the Linux/Unix environment successfully. Thus, the developed software can be seen as a multi-platform tool for users. The software is appropriate for the use of motor manufacturers for various applications.

As a result, this thesis introduces a new approach and an accompany software that is efficient when used for design and analysis of the SLIM with a wide-range of applications by adequately treating the electromagnetic phenomena. The novel contribution of this work is the utilization of the least squares approach for linear approximation in order to calculate the secondary impedance. The simulation results suggest that the proposed approach is efficient to improve the accuracy in thrust calculations. Since the proposed method is observed to be computationally intense, future studies of the method will include the evaluation of the optimization techniques to overcome this disadvantage.

## **6.2 Recommendation for Future Work**

**i)** The proposed method in the chapter 4 is observed to be computationally intense, future studies of the method will include the evaluation of the optimization techniques to overcome this disadvantage

**ii)** The software can be easily converted to be a software double-sided linear induction motor

**iii)** The full pitch ( $q=1$ ) and ( $q=2$ ) single layer winding configurations has been used in this software. The winding configurations can be expended to fractional pitch double layer winding configurations.

**vi)** Thermal optimization must be included in future studies.

**vii)** A test bench for SLIM can be constructed to measure some performance parameters. This can be compared with simulations results for the designed SLIM

**viii)** Economical optimization can be included in future studies

## REFERENCES

- [1] Faiz, J., Jafari, H. (2000). Accurate Modeling of Single-Sided Linear Induction Motor Considers End, effect and Equivalent Thickness. IEEE Transaction on Magnteics, 36, 3785-3790
- [2] Gieras, J. F., Dawson, G. E., Eastham, A R. (1986a). Performance Calculation for Single-Sided Linear Induction Motors with a Double-Layer Reaction Rail Under Constant Current Excitation. IEEE Transactions on Magnetic, 22, 54-62
- [3] Pai,R.M., Boldea,I. and Nasar,A. (1988). A Complete Equivalent Circuit of a Linear Induction Motor with Sheet Secondary. IEEE Tranactions on Magnetics, 24, 639-654
- [4] Mirsalim,M., Doroudi,A., Moghani,J.S.(2002). Obtaining the Operating Characteristics of Linear Induction Motors: A New Approach. IEEE Transactions on Magnetic, 38, 1365-1370
- [5] Yamamura, S. (1979). Theory of Linear Induction Motor. New York: Wiley.
- [6] Nasar S. A., Boldea, I. (1987) . Linear Electric Motor. N.J.: Prentice-Hall Inc.
- [7] Gieras, J.F. (1994). Linear Induction Drives. Oxford, U.K.: Oxford University Press.
- [8] Sakabe, S., Iwamoto M. (1977). Experiment On High Speed Linear Induction Motor With A Saturable Iron Secondary, Electric Power Components and Systems, 2 , 25-36
- [9] Mukelera, J., Slemon, G. R. (1978). Forces in a Single-sided Linear Induction Motor. Electric Power Components and Systems, 3, 47-63.

- [10] Lee, C.H. and Chin, C.Y. (1979). A Theoretical Analysis of Linear Induction Motors. *IEEE Transactions on Power Apparatus and Systems*, *98*, 679-688
- [11] Katz, R.M., Eastham, A. R., Dawson, G.E., Atherton D. A., Schwalm, C. L. (1979). Integrated Magnetic Suspension and Propulsion of Guided Ground Transportation Vehicle with a SLIM. *IEEE Transaction on Magnetic*, *6*, 1437-1439.
- [12] Stickler, J.J. (1982). A Study of Single-Sided Linear Induction Motor Performance with Solid Iron Secondaries, *IEEE Transactions on Vehicular Technology*, *31*, 107-112
- [13] Mendrela, E. A., Gierczak, E., Kielce. (1982). Calculation of Transverse Edge Effects of Linear Induction Motor Using Fourier's Series Method. *Archive für Elektrotechnik*. *65*, 161-165
- [14] Mendrela, E. A., Fleszar, J., Gierczak, E., Kielce. (1983). A Method of Determination of the Distance Between Fictitious Primaries in Computational Model of Linear Induction Motor Used in Fourier Series Technique. *Archive für Elektrotechnik*, *66*, 151-156.
- [15] Mor, A. and Gavril, S. (1983). Influence of Hysteresis on Performance of Single-Sided Finite-Length Linear Induction Motor. *Electric Power Components and Systems*, *8*, 69-78
- [16] Gieras, J. F., Eastham, A. R., Dawson, G. E. (1985a). Influence of Secondary Solid Ferromagnetic Plate Thickness on the Performance of Single-Sided Linear Induction motors. *Electric Machines and Power Systems*, *10*, 67-77
- [17] Gieras, J. F., Eastham A. R., Dawson G. E. (1986b). The Influence of Conductive Cap Thickness on the Performance of Single-Sided Linear Induction Motors. *Electric Power Components and Systems*, *11*, 125-136.

- [18] Nonaka,S. and Higuchi,T. (1987). Elements of Linear Induction Motor Design for Urban Transit, *IEEE Transactions on Magnetics*, 23, 3002-3004
- [19] Pai, M. R., Nasar, S. A. and Boldea, I. (1987). A Hybrid Method of Analysis of Low-Speed Linear Induction Motors. *IEEE Transactions on Magnetics*, 23, 3908-3915
- [20] Zawadzki, A., Gierczak, E., Mendrela, E.A. (1988). Calculation Method of Linear Induction Motor Supplied from Symmetrical voltage Source. *Archive für Elektrotechnik*, 71, 221-227
- [21] Adamiak, K., Anathasivam, K., Dawson, G.A., Eatsham, A.R. and Gieras, J.F. (1988). The Causes and Consequences of Phase Unbalance in Single-Sided Linear Induction Motors, *IEEE Transaction on Magnetics*, 24, 3223-3233.
- [22] Gieras, J. F., Eastham, A. R., Dawson, G.E., John, G. (1990). Calculation of Thrust for a single-sided linear induction motor, taking into account phase unbalance and higher time harmonics. *Archive für Elektrotechnik*, 73, 299-308.
- [23] Gieras, J. F., (1992). Calculation of Stray losses in a single-sided linear induction motor. *Archive für Elektrotechnik*, 75, 103-107.
- [24] Idir, K., Dawson, G. E., Eatsham, A. R. (1993). Modeling and Performance of Linear Induction Motor with Saturable Primary. *IEEE Transaction on Industry Application*, 29, 1123-1128.
- [25] Nonaka,S. (1996). Investigation of Equivalent Circuit Quantities and Equations for Calculation of Characteristics of Single-Sided Linear Induction Motors (LIM). *Electrical Engineering in Japan*, 117, 107-122
- [26] Simone,G.A., Creppe,R.C., Souza,C.R.(1997). The Thrust and the Relation Factor KR in Linear Induction Machines. *IEEE Proceeding*, MB 11.1-11.3

- [27] Mirsalim, M., Doroudi, A., Menhaj, M.B. (2004). Simple Analytical Functions for the Equivalent Circuit Parameters of Linear Induction Motors. *IEEE Transactions on Magnetic*, 28, 383-388
- [28] Xu, W., Sun, G., Li, Y. (2007). Research on Performance Characteristics of Linear Induction Motor. *IEEE Proceeding*, 86-89
- [29] Man, K., Salah, B., (2007). Design, modeling and control of a linear induction motor. *International Review of Electrical Engineering*, 2, 414-424
- [30] Creppe, R.C., Ulson, J.A.C., Rodrigues, J.F. (2008). Influence of Design Parameters on Linear Induction Motor End Effect. *IEEE Transactions on Magnetics*, 23, 358-362.
- [31] Isfahani, A.H., Ebrahimi, B.M., Lesani, H. (2008). Design Optimization of a Low-Speed Single-Sided Linear Induction Motor for Improved Efficiency and Power Factor. *IEEE Transactions on Magnetic*, 44, 266-272
- [32] Furukawa, T., Ogawa, K., Nonaka, S. (1987). Finite Element Analysis of EDDY Currents Problem Subject to Convective Diffusion Equation, *IEEE Transactions on Magnetic*, 23, 2660-2662
- [33] Adamiak, K., Mizia, J., Dawson, G. E., Eastham, A. R. (1987). Finite Element Force Calculation in Linear Induction Machines, *IEEE Transactions on Magnetics*, 23, 3005-3007
- [34] Furukawa, T., Komiya, K., Muta, I. (1990). An Upwind Galerkin Finite Element Analysis of Linear Induction Motors. *IEEE Transactions on Magnetic*, 26, 662-665
- [35] Adamiak, K., Dawson, G.E., Eastham, A.R. (1991). Application of Impedance Boundary Conditions in Finite Element Analysis of Linear Motors. *IEEE Transactions on Magnetics*, 27, 5193-5195.



- [36] Laporte,B., Takorabet,N. and Vinsard,G. (1997). An Approach to Optimize Winding Design in Linear Induction Motors,IEE Transactions on Magnetics, 33, 1844-1847
- [37] Onuki,T.,Kamiya,Y.,Fukaya,K., Jeon ,W.J. (1999).Characteristics Analysis of Linear Induction Motor with Two Types of Secondary Structure Based on Electromagnetic Field and Electric Circuit Analysis, IEE Transactions on Magnetics, 35, 4002-40024
- [38] Srivastava, R.K., Mahendra, S.N. (2000). Drag Plate-Single-Sided Linear Induction Motor. IEEE Proceeding, 699-702
- [39] Hur, J., Toliyat, H.A., Hong, J.P. (2001). Dynamic Analysis of Linear Induction Motors Using 3-D Equivalent Magnetic Circuit Network (EMCN) Method. Electric Power and Component System, 29, 532-541
- [40] Kamiya, Y., Akagi, M., Wkao, S. (2002). Boundary Structure for Improving Performances of Single-Sided Linear Induction Motors. Journal of Applied Physics, 91, 6988-6991
- [41] Kang, G., Kim, J., Nam, K. (2003). Parameters estimation scheme for low-speed linear induction motors having different leakage inductances. IEEE Transaction on Industrial Electronics, 50, 708-807
- [42] Ramkumar,S., Balaji, M., Sivakumar,N., Kamaraj, V. (2006). Performance Evaluation of Single-sided Linear Induction Machine Using Finite Element Analysis. IEEE Proceeding, 36, 1080-1082
- [43] Selçuk, A.H. and Kürüm H.(2008). Investigation of End Effects in Linear Induction Motors by Using the Finite-Element Method. IEEE Transaction on Magnetics, 44, 1791-1795
- [44] Bianchi, J.,(2005). Finite Element Method for Electric Machines. Prentice Hall.

- [45] Nakata, T., Takahashi, N., Fujiwara, K. (1988). Physical Meaning of  $\text{Grad}\phi$  in Eddy Current Analysis Using Magnetic Vector Potential, *IEEE Transaction on Magnetic*, 24, 178-181
- [46] Dawson, G. E., Eastham, A.R., Gieras, J.F., Ong, R., and Ananthasivan, K. (1986). Design of Linear Induction Drives by Field Analysis and Finite Element Techniques. *IEEE Transactions on Industry Applications*, 22, 865-873.
- [47] Gieras, J.F., Dawson, G. E., Eastham, A. R. (1987). A New Longitudinal End Effect Factor for Linear Induction Motors. *IEEE Transactions on Energy Conversion*, 2, 152-159.
- [48] Boldea, I., Babescu, M. (1978). Multilayer Approach to Analysis of Single-sided Linear Induction Motor. In *Proceedings of IEE*, 125, 283-287.
- [49] <http://www.productionplanning.com>
- [50] Gieras, J. F., Eastham, A. R., Dawson, G. E. (1985b). Performance calculation for single-sided linear induction motors with a solid steel reaction plate under constant current excitation. *IEE Proceeding*, 132, 185-194
- [51] Byung Il,., Kyung K. Il, Sol, K. and Seung, C. P. (2000). Analysis for Dynamic Characteristics of a single-sided Linear Induction Motor Having Joints in the secondary Conductor and Back-Iron. *IEEE Transaction on Magnetics*, 36, 823-826
- [52] Tong, Y., Libing, Z. and Langru, L. (2008). Finite element Analysis of Linear Induction Motor for Transportation Systems. *IEEE Vehicle Power and Propulsion Conference*, September 3-5
- [53] Dae-Kyong, K., Byung, Il, K. (2006). A Novel equivalent Circuit Model of Linear Induction Motor Based on Finite Element Analysis and Its Coupling with External Circuits. *IEEE Transaction on Magnetics*, 42, 3407-3409

- [54] Byung-Jeen, L., Dae-Hyun, K. and Yun-Hyun, C. (2009). Investigation of Linear Induction Motor According to Secondary conductor Structure. IEEE Transaction on Magnetics, 45, 2839-2842
- [55] Junfei, H., Yumei, D., Yaohua, L., Nengqiang, J. (2008). Analysis of Longitudinal End Effect of Single-sided Linear Induction Motor. Proceeding of the International Conference on Information and Automation, 357-362
- [56] Gang LV, Qiang LI, Zhiming, LIU, Fan, Y., Guo-guo, L. (2008). The analytical Calculation of the Thrust and Normal Force and Force Analyses for Linear Induction Motor. ICSP Proceedings, 2795-2799
- [57] Zhao, J., Yang, Z., Liu, J., Zheng, T. Q. (2008). A Novel Performance Study for Linear Induction Motors Considering End Effects. IEEE Proceedings, 3231-3235
- [58][http://www.feec.vutbr.cz/2003/fsbornik/03GS/04\\_power\\_electrical\\_engineering/08\\_flip\\_powel.pdf](http://www.feec.vutbr.cz/2003/fsbornik/03GS/04_power_electrical_engineering/08_flip_powel.pdf)

## APPENDICES

### A.I Presentation of the test bench of CIGGT of ‘Quens’s Uninversity’

The test bench of linear induction motor was carried out with ‘Quens’s University’ in Canada. This test bench of CIGGT, which was used to validate the analytical model presented at the third chapter of this thesis, is used to compare the simulations and experimental results [2]. It consist of a revolving wheel of 7.6 m, which is provided with a system of guidance, allow a relative movement between primary and secondary with a speed up to 101 km/h. The two images of Figure A2 show the configuration of this test bench.

The primary of the linear motor which is built in test bench consists of sheet steel out of rolled silicon (M19) a 0.318 mm thickness and a factor of insulation of 0.96. The manufacturer provides unit losses iron of 0.65 W/kg (corresponding with an induction  $B=1T$  and frequency  $f=60Hz$ ). The LIM is fed by an inverter with multiline inverter (MLI) of 200 KVA. More details concerning the geometrical and physical characteristics of this LIM is recapulated in Table A1.

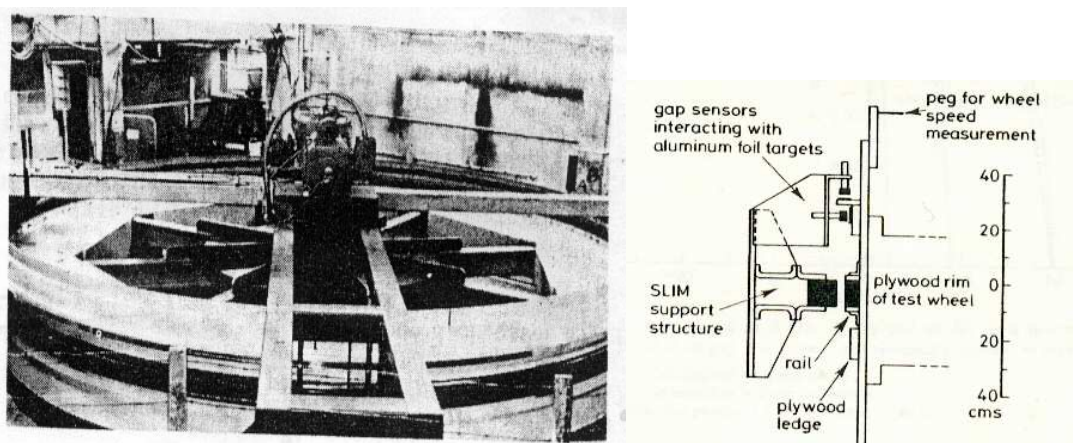


**Figure A1** Overall picture of a revolving wheel 7.6 m in diameter from 0 to 101 km/h, test bench of CIGGT and Structure of the linear motor and of its system of guidance.

**Table A.1** Design data of single-sided, three-phase LIMs for propulsion of vehicles

Quantity	CIGGT	GEC	Unit
Pull-out hrust at frequency given below, $F_x$	1.7	0.7	kN
Input frequency, $f$	40.0	60.0	Hz
Rated phase current, $I$	200.0	200.0	A
Number of poles, $2p$	6	4	-
Number of turns per phase, $N_l$	108	48	-
Equivalent diameter of conductor, $d_b$	1.115	8.1	mm
Number of paralel conductors	19	1	-
Effective width of primary core, $L_i$	0.101	0.1715	m
Pole pitch, $T$	0.25	0.20	m
Length of single end connection, $l_e$	0.2955	0.3685	m
Coil pitch, $w_c$	0.1944	0.1555	m
Airgap, $g$	15.0	18.2	mm
Number of slots, $z_l(z'_l)$	54(61)	36(43)	-
Width of slot, $b_{ll}$	15.0	13.08	mm
Width of slot opening, $b_{l4}$	10.44	13.08	mm
Depth of slot, $h_{ll}$	34.21	61.47	mm
Height of yoke, $h_{ly}$	71.63	50.0	mm
Conductivity of back iron at 20 <sup>0</sup> C, $\sigma_{FE}$	4.46	5.12	$\times 10^6$ S/m
Conductivity of Al cap at 20 <sup>0</sup> C, $\sigma_{Al}$	32.3	21.5	$\times 10^6$ S/m
Width of back iron, $w$	0.111	0.1715	m
Thickness of back iron, $h_{sec}$	25.4	47.4	mm
Thickness of Al cap, $d$	4.5(2.5)	3.2	mm
Thicknes of Al cap behind Fe core, $t_{ov}$	12.7	3.2	mm
Width of Al cap, $w+2w_{ov}$	0.201	0.2985	m
<p><b>CIGGT</b>=Canadian Inst. of Guided Ground Transport, Canada</p> <p><b>GEC</b>=General Electric Company, USA.</p>			

## A2. Carter coefficient

The carter coefficient makes it possible to take account of the primary slot effect. It increases the air gap. The actual value is the result of the multiplication mechanical clearance by this coefficient. It must be calculated by considering an air gap equal to  $(g+d_{al})$ . The general expression [7]

$$k_c = \frac{\tau_d}{\tau_d - \frac{s_w}{5(g + d_{al}) + s_w}} \quad (\text{A.1})$$

## A3. Saturation factor

The classical theory of the electric motors defines the saturation factor of the magnetic circuit as being the relationship between the total magneto motive force and that of the air gap by pole pairs. In the analytical model given in chapter 3, the magnetic permeability of the primary is infinite. So the magneto motive force in the primary can be neglected. Under this condition the saturation factor of the magnetic circuit of LIM can be expressed as [50].

$$k_\mu = \frac{V_v}{2(V_{gv} + V_{dv})} \approx 1 + \frac{V_{sv}}{2(V_{gv} + V_{dv})} \quad (\text{A.2})$$

Where  $V_v$  is the magneto motive force (MMF) per poles pair,  $V_{gv}$  is the magnetic voltage drop in the air gap,  $V_{dv}$  is the magnetic voltage drop in the conducting plate,  $V_{sv}$  is the magnetic voltage drop in the secondary back iron.

$$V_{gv} = \int_0^g H_{myv3}(x=0, y) dy = \frac{jA_{mv}}{M_v} \left\{ \left[ \mu_{re} \cosh(K_{v2}D_{a1}) + \frac{K_{v1}}{K_{v2} \sinh(k_{v2}D_{a1})} \right] \frac{\sinh(\beta_v g')}{\beta_v} \right. \\ \left. - \frac{K_{v2}}{\beta_v} \left[ \frac{K_{v1}}{K_{v2}} \cosh(K_{v2}D_{a1}) + \mu_{re} \sinh(K_{v2}D_{a1}) \right] \frac{1 - \cosh(\beta_v g')}{\beta_v} \right\} \quad (\text{A.3})$$

$$V_{dv} = \int_g^{D_{a+g}} H_{myv2}(x=0, y)dy = \frac{jA_{mv}}{M_v} \left[ \mu_{re} \frac{\sinh(K_{v2}D_{a1})}{K_{v2}} - \frac{K_{v1}}{K_{v2}} \frac{1 - \cosh(K_{v2}D_{a1})}{K_{v2}} \right] \quad (\text{A.4})$$

In order to express the magnetic voltage drop in the back iron, the average tangential component of magnetic field flow should be expressed ( $H_{mx3}$ ):

$$|\Phi_{xvsec}(x)| = W\mu_0\mu_{rs} \int_{g'+D_a}^{\infty} H_{mxv3}(x, y)dy = W\mu_0 \frac{A_{mv}}{\beta_v} \frac{1}{|M_v|} \mu_{rs} \cos(\beta_{vx}) \quad (\text{A.5})$$

The average value of the magnetic field in the back iron thickness is given by:

$$|H_{mxvav}(x)| = \frac{|\Phi_{xvsec}(x)|}{WD_{ir}\mu_0\mu_{rav}} = \frac{1}{d_{ir}} \frac{A_{mv}}{\beta_v} \frac{1}{|M_v|} \frac{\mu_{rs}}{\mu_{rav}} \cosh(\beta_v x) \quad (\text{A.6})$$

where  $\mu_{rav}$  is the average relative permeability of the secondary back iron.

Then, the magneto motive force of the secondary back iron for per pole pairs can be expressed as:

$$V_{secv} = \int_{-\tau_v/2}^{\tau_v/2} |H_{mxvav}(x)|dx = \frac{1}{D_{ir}} \frac{2A_{mv}}{\beta_v^2} \frac{1}{|M_v|} \frac{\mu_{rs}}{\mu_{rav}} \quad (\text{A.7})$$

According to the classical theory of electric motors, the saturation factor has an effect on the magnetizing reactance (caused the air-gap is increased).

#### **A4. Equivalent conductivity of the conducting plate**

Due to the closing currents induced in the secondary active zone, secondary conductivity of the conducting plate is corrected by the factor of Russel and Norsworthy factor.

$$k_{RNv} = 1 - \frac{\tanh\left(\beta_v \frac{W}{2}\right)}{\beta_v \frac{W}{2} \left[1 + \tanh\left(\beta_v \frac{W}{2}\right) \tanh(\beta_v h_{ov})\right]} \tanh(\beta_v h_{ov}) \quad (\text{A.8})$$

This coefficient takes account of the the currents which are closed again in the active part of the conducting plate and actually apparent conductivity of the secondary conducting plate reduces. In general, the thickness of the active part of the conducting plate differs from that being located on the both sides of the secondary back iron ( $t_{ov}$ ). Under this condition, the term  $\tanh(\beta_v h_{ov})$  must be corrected by multiplying by following empirical factor [7]:

$$1 + 1,3 \frac{t_{ov}}{d_{al}} .$$

The equivalent conductivity of the conducting plate is modified as follows:

$$\sigma'_{alv} = (1 - k_{RNv}) \sigma_{al} \quad (\text{A.9})$$

The equivalent impedance of the secondary back iron is also corrected by a factor. This correction is again due to the close current in the active part of the secondary back iron [50].

According to Gibbs:

$$k_z = 1 + \frac{2}{\pi} \frac{\tau}{W} \quad (\text{A.10})$$

According to Panasienkov:

$$k_z = 1 + \frac{1}{2} \frac{\tau}{W} \quad (\text{A.11})$$

According to Yee:



$$k_{zv} = \frac{\beta_v W \left[ 1 + \coth\left(\beta_v \frac{W}{2}\right) \right]}{\beta_v W \left( 1 + \coth\left(\beta_v \frac{W}{2}\right) \right) - 2} \quad (\text{A.12})$$

According to Gears et al.:

$$k_{zv} = 1 - \frac{g}{vL} + \frac{2}{v\pi} \frac{\tau}{W} \left[ 1 - \exp\left(-\frac{\pi W}{2L}\right) \right] \quad (\text{A.13})$$

The equivalent impedance of the secondary back iron is modified by

$$z'_1 = k_{zv} z_1 \quad (\text{A.14})$$

In the calculations, (A.13) is used for secondary back iron impedance calculations.

### A5. Longitudinal end effect factor

The end effect in the linear induction motor is due to the limiting the longitudinal length of the motor. It influences the speed on the nonuniform distribution of the induction in the air gap of the LIM and current induced in the secondary. This effect is taken into account by a factor  $k_e$  given on the basis of a distribution of induction in the air gap of LIM made up of a slipping field.

$$B(x, t) = B_{ms} \sin\left(\omega t - \frac{\pi}{\tau} x\right) + B_{me} e^{-\frac{x}{\tau_e}} \sin\left(\omega t - \frac{\pi}{\tau_e} x + \delta\right) \quad (\text{A.15})$$

The electromotive force induced in primary phase is the superposition of two electromotive forces, one due to the fundamental field and the other is induction due to the end effect and it can be expressed in the form:

$$e_p(t) = e_s(t) + e_e(t) = -E_{ms} \cos(\omega t) - E_{me} \cos(\omega t) = -E_{ms} (1 - ke) \cos(\omega t) \quad (\text{A.16})$$

where

$$k_e = -\frac{k_{we}}{k_w} \frac{\frac{\pi}{\tau_e^2}}{\frac{1}{t_e^2} + \left(\frac{\pi}{\tau_e}\right)^2} f(\delta) e^{\frac{-p\tau_e}{t_e}} \frac{\sinh\left(\frac{p\tau_e}{t_e}\right)}{p \sinh\left(\frac{\tau_e}{t_e}\right)} \quad (\text{A.17})$$

where:

$$f(\delta) = \frac{1}{t_e} \sin \delta + \frac{\pi}{\tau_e} \cos \delta \quad (\text{A.18})$$

$\delta$  is dephasing between the fundamental wave of induction in the air-gap and induction due to the end effect being propagated in the direction of the slipping field, with the entry of the motor. It is approximated in an empirical way by [50]:

$$\delta = \delta_0 + bV_e \quad (\text{A.19})$$

where

$$\delta_0 = \pi - \arctan\left(\pi \frac{t_e}{\tau_e}\right)_{V_r=V_0} ; b = \frac{1}{150} \arctan\left(\pi \frac{t_e}{\tau_e}\right)_{V_r=V_0} \quad (\text{A.20})$$

and

$$V_e = \left\{ \begin{array}{ll} V_e = \frac{V_r - V_0}{V_s - V_0} V_s & \text{if } V_r \geq V_e \\ V_e = 0 & \text{if } V_r < V_e \end{array} \right\} \quad (\text{A.21})$$

where  $V_0$  is the boundary speed and it is expressed as,

$$V_0 = 0.5 \frac{V_s^2}{150} \quad (\text{A.22})$$

$\tau_e$  and  $t_e$  represent the pole pitch of the end wave and attenuation factor respectively. It can be calculated by using the following expressions [4]:

$$\tau_e = \frac{2\pi}{D} \quad (\text{A.23})$$

$$t_e = \frac{2gk_c}{Cgk_c - V_r\mu_0\sigma_{Al}D_{Al}} \quad (\text{A.24})$$

$$C = \frac{1}{\sqrt{2}} \sqrt{\sqrt{X^4 + 16Y^2} + X^2} \quad (\text{A.25})$$

$$D = \frac{1}{\sqrt{2}} \sqrt{\sqrt{X^4 + 16Y^2} - X^2} \quad (\text{A.26})$$

$$X = \frac{\mu_0 V_r \sigma_{Al} d'_R}{k_c (g + D_{Al})} \quad (\text{A.27})$$

$$Y = \frac{\mu_0 \omega \sigma_{Al} d'_R}{k_c (g + D_{Al})} \quad (\text{A.28})$$

Where  $d'_{R}$  is the thickness of a homogeneous layer out of aluminum equivalent to the two layers which constitute the conducting part of the secondary, it can be used to evaluate resistance modeling the eddy currents in the secondary. This thickness is estimated starting from the equivalent impedance of the secondary. Indeed, the conducting layer out of aluminum and that of ferromagnetic of the secondary are equivalent (from electric point of view) to a layer out of aluminum thickness  $d'_{R}$ , which has as impedance (if it is neglected the effect of skin):

$$Z_{\text{sec}} = (a_R + ja_X) \frac{W}{\tau} k_z \frac{1}{s\sigma_{Al}d'_R} \quad (\text{A.29})$$

where  $a_R = 1$  and  $a_X = 1$  for a nonmagnetic material such as aluminum. From where  $d'_{R}$  can be expressed as the equivalent thickness.

The winding factor relating to the wave of induction due to end effect is calculated as below:

$$k_{vwe} = \frac{\sin\left(\frac{\tau}{\tau_e} \frac{\pi v}{2m}\right)}{q \sin\left(\frac{\tau}{\tau_e} \frac{\pi v}{2mq}\right)} \sin\left(\frac{\pi v}{2} \frac{w_c}{\tau_e}\right) \quad (\text{A.30})$$

**Table A.2** Design output in MS Excel format

<b>GENERAL DATA</b>	
Given Rated Thrust(N)	198.7582
Given Rated Speed(m/s)	5
Rated Voltage(V)	219.3931
Winding Connection	Wye
Number of Poles	4
Frequency(Hz)	50
Stray Loss(W)	0
Excitation Type	Constant Voltage
Operating Temperature	75
<b>PRIMARY DATA</b>	
Number of Stator Slots	12
Primary Length(m)	0.2222
Dimension of Stator Slot	
H11(mm)	5
H12(mm)	5
H13(mm)	5
H14(mm)	5
B11(mm)	10
B14(mm)	14
Number of Conductor per Slot	80
Number of Parallel Branches	1
Type of Coils	11
Coil Pitch (m)	0.0556
Wire Diameter(m)	0.0011
<b>REACTION RAIL DATA</b>	
Aluminium Thickness(m)	0.0030
Air Gap(mm)	1
Backiron Thickness (m)	0.0200

Backiron Width(m)	0.1000
Overhang Thickness(m)	0.0030
Overhang Width(m)	0.0100
Conductivity of Iron	4500000
Conductivity of Al	30300000
<b>MATERIAL CONSUMPTION</b>	
Backiron Density(kg/m3)	7900
Conducting Plate Density(kg/m3)	2700
Copper Density(kg/m3)	8900
Winding Copper Weight(kg)	4.1500
Primary Core Weight(kg)	6.4078
Total Primary Core Weight(kg)	10.5578
Secondary Weight(kg)	3.7091
<b>RATED-LOAD OPERATION</b>	
Primary Resistance(ohm)	3.6806
Primary Leakage Reactance(ohm)	2.5310
Secondary Resistance(ohm)	0.6231
Secondary Leakage Reactance(ohm)	1.9119
Magnetizing Reactance(ohm)	
Stator Phase Current(A)	11.8033
Magnetizing Current(A)	4.1178
Secondary Current(A)	7.6855
Iron Core-Loss(W)	
Stray Loss(W)	
Input Power(W)	1104.2
Output Power(W)	993.7910
Efficiency(%)	0.3761
Power Factor	0.3402
Rated Slip	0.1000
<b>NO-LOAD OPERATION</b>	
No-load Stator Resistance(ohm)	3.6806
No-load Stator Leakage Reactance(ohm)	2.5310
No-load Secondary Resistance(ohm)	3.9110
No-load Secondary Leakage Reactance(ohm)	1.6915
No-load Stator Phase Current(A)	9.8752
No-load Slip	0.001

## A6. Simulation Programme (M-File Programming)

```

% MAIN FUNCTION
% Doktora Tezi
% Ali Suat Gerçek
% %
%-----
%-----
function C=ConstantV(GMin, GMax,
Ze,Frated,Vrated,srated,rocu,conFe,conAl,m,Nb,deltaT,Db,f,wc,p1,Z,V1,hp,hov,he
,L,W,tov,Dir,Oe,b11,Dal,NC)

%pole pair ise
p=p1/2;
q=Z/(p1*m);
N=p1*q*NC;
v=v1/((3)^(1/2));
k=0;

% Calculation of Tau and wc
Vs=Vrated/(1-srated);
tau=Vs/(2*f);
if (wc == 1)
    wc = tau;
else
    wc = tau;
end;

%for g=0.001:0.0001:0.005
for g=GMin:0.0001:GMax
    k=k+1;

[Vs, tau, Lp, taud, ld, Lf, kw, Xprime, Rprime, kc, kRNV, conAlprime, ktr, kzv, betav]=IndOf
Sleep(rocu,conFe,conAl,m,Nb,deltaT,Db,f,wc,p1,Z,V, hp,hov,he,L,W,tov,Dir,Oe,b11
,Dal,g,Vrated,srated,q,N);
Vo=(0.5*Vs*Vs/150);
so=(Vs-Vo)/Vs;
Vr=Vs*(1-srated);
n2=1;
KWKWA1=0.2;
KWWWA=1;
while ((abs((KWKWA1-KWWWA)))>0.001)&&(n2<100)
    n2=n2+1;
I=(Frated*Vrated)/(m*v*KWKWA1);
Am=(3*sqrt(2)*kw*N*I)/(p*tau);
H1=Am;
kmuel=1;
[ge,mure,omegi,kv1,kv2,kmueold,H,Vsv,Vdv,Vgv,murs,alfa1,Pen,Ar,Ax,M]=
maxwel(Vs,tau,Lp,taud,ld,Lf,kw,Xprime,Rprime,kc,kRNV,conAlprime,ktr,kzv,betav,
rocu,conFe,conAl,m,Nb,deltaT,Db,f,wc,p1,Z,V, hp,hov,he,L,W,tov,Dir,Oe,b11,Dal,g
,so,kmuel,Am,H1);
[Zv1prime,Zv2,Zvsecprime,Rvsecprime] =
esdeger_devre0(Vs,tau,Lp,taud,ld,Lf,kw,Xprime,Rprime,kc,kRNV,conAlprime,ktr,kz
v,betav,rocu,conFe,conAl,m,Nb,deltaT,Db,f,wc,p1,Z,V, hp,hov,he,L,W,tov,Dir,Oe,b
11,Dal,mure,kv1,kv2,omegi,ge,so,kmueold);%

[del tao,a]=bounded(Vs,tau,Lp,taud,ld,Lf,kw,Xprime,Rprime,kc,kRNV,conAlprime,kt
r,kzv,betav,rocu,conFe,conAl,m,Nb,deltaT,Db,f,wc,p1,Z,V, hp,hov,he,L,W,tov,Dir,
Oe,b11,Dal,omegi,kv1,kv2,mure,ge,so,Zv1prime,Zv2,Zvsecprime);

[ge,mure(n2),omegi,kv1,kv2,kmueold(n2),H(n2),Vsv,Vdv,Vgv,murs(n2),alfa1,Pen(n2
),Ar(n2),Ax(n2),M]=
maxwel(Vs,tau,Lp,taud,ld,Lf,kw,Xprime,Rprime,kc,kRNV,conAlprime,ktr,kzv,betav,
rocu,conFe,conAl,m,Nb,deltaT,Db,f,wc,p1,Z,V, hp,hov,he,L,W,tov,Dir,Oe,b11,Dal,g
,srated,kmuel,Am,H1);

[ke]=endeffect(Vs,tau,Lp,taud,ld,Lf,kw,Xprime,Rprime,kc,kRNV,conAlprime,ktr,kz
v,betav,rocu,conFe,conAl,m,Nb,deltaT,Db,f,wc,p1,Z,V, hp,hov,he,L,W,tov,Dir,Oe,b
11,Dal,omegi,srated,kv1,kv2,mure,ge,deltao,a,q);
murex=mure(n2);

[Fx,eff,Ivsecprime,Rvsecprime,I1,Pem,Pme,Xvsecprime,KWKWA(n2),PF,Fxy,Im,Bmx,Bm
y,Xvo] =
esdeger_devrev(murex,Vs,tau,Lp,taud,ld,Lf,kw,Xprime,Rprime,kc,kRNV,conAlprime,
ktr,kzv,betav,rocu,conFe,conAl,m,Nb,deltaT,Db,f,wc,p1,Z,V, hp,hov,he,L,W,tov,Di
r,Oe,b11,Dal,Ze,mure,kv1,kv2,omegi,ge,Vr,srated,kmueold,I,ke,Am,M,N);%ke
KWWWA=KWKWA(n2);
KWKWA1=(KWKWA1+KWWWA)/2;
end
Bmxx(k)=Bmx;

```

```

Bmyy(k)=Bmy;
Im1(k)=Im;
Ivsecprime1(k)=Ivsecprime;
Rvsecprime1(k)=Rvsecprime;
Xvsecprime1(k)=Xvsecprime;
xx(k)=g;
effr(k)=eff;
I1r(k)=I;
Fxr(k)=Fx;
Pemr(k)=Pem;
Pmer(k)=Pme;
KWKWAr(k)=KWWA;
PFR(k)=PF;
Fxyy(k)=Fxy;
diff(k)=Fxr(k)-Frated;
dmin=min(abs(diff));
end

i=1;
for i=1:1: numel(diff)
    if (dmin ~= abs(diff(i)))
        break;
    end;
end;

Bmxxx=Bmxx(i);
Bmyyy=Bmy(i);
% Im11=Im1(i);
Ivsecprime11=Ivsecprime1(i);
Rvsecprime11=Rvsecprime1(i);
Xvsecprime11=Xvsecprime1(i);
xxr=xx(i)*1e3;
effrr=effr(i);
I11=I1r(i);
Im11=I11-Ivsecprime11;
Fxr=Fxr(i);
Pemr=Pemr(i);
Pmer=Pmer(i);
KWKWAr=KWKWAr(i);
PFR=PFR(i);
Fxyy=Fxyy(i);
roFE=7900;
roAL=2700;
roCU=8900;
Ms=Lp*(roFE*Dir*w+roAL*(w*Da1+hov*tov));
McU=(3*roCU*(2*L+2*Lf)*N*Nb*pi*(Db^2))/4;
MCS=roFE*((p1+1)*wc+2*ld)*(hp-he)*L+(Z+1)*he*ld*L;
Mp=McU+MCS;

%%%%%%%%%%%%%%%%%%%%%%%%%%%%%%%%%%%%%%%%%5

% function ELD=ElectricData();
%
%   ELD.rocu=1.78e-8;   %resistivity of copper
%   %ELD.alfacu=40;   %Alfacu bul bu degeri
%   ELD.conFe=0.450e7;%2*pi;
%   ELD.conA1=0.303e8;
%   %number of phase
%   ELD.m=3;
%   %no of conductor per slot
%   ELD.Nb=120;%105;
%   %Temperature
%   ELD.deltaT=75;
%
%   % diameter choosen
%   ELD.Db=0.0011;
%   ELD.f=50;
%   %coil pitch
%   ELD.wc=0.0501;
%   %pole sayısı
%   ELD.p1=4;
%   %pole pair ise
%   ELD.p=ELD.p1/2;
%
%   %number of fullfilled slot of primary
%   ELD.Z=12;
%   %number of semi filled slot of primary
%   ELD.Ze=4;
%   ELD.q=ELD.Z/(ELD.p1*ELD.m); %kutup
%   ELD.P160=0.65;
%   %no of turn per phase
%   ELD.N=ELD.p1*ELD.q*ELD.Nb;
%   ELD.V1=380;
%   ELD.V=ELD.V1/((3)^(1/2));
%   %%%%%%%%%%%%%%%%%%%%%%%%%%%%%%%%%%%%%%%%%%
% function MD=MagneticData();

```

```

% MD.Bteeth=1.0;
% MD.mu0 = 4*pi*10^-7;
% %%%%%%%%%%%
% function GD=GeometricData();
%
% %primary core heigth
% GD.hp=0.040;
% %overhang thickness
% GD.hov=0.01;
% %slot heigth
% GD.he=0.020;%0.045
% %primary core width
% GD.L=0.1;
% %back iron width
% GD.w=0.10;
% %aluminium cap thickness
% GD.tov=0.003;
% %thickness of AL
% GD.Dir=0.015;
% %slot opening
% GD.Oe=0.0102;
% %slot width
% GD.b11=0.014;
% %air gap
% % GD.g=0.004; % 1cm
% %Aluminium thickness
% GD.Dal=0.003;

k=0;
kemx=[];
for s=0.001:0.01:1.001
    k=k+1;
    Vr(k)=Vs*(1-s); % Rated speed
    gg=xxr*1e-3;
    %primary current
    I=I11;
    Am=(3*sqrt(2)*kw*N*I)/(p*tau);
    H1=Am;
    kmue1=1;
    [ge,mure,omegi,kv1,kv2,kmueold,H,Vsv,vdv,Vgv,murs,alfa1,Pen,Ar,Ax,M]=
maxwel(Vs,tau,Lp,taud,ld,Lf,kw,Xprime,Rprime,kc,kRNV,conAlprime,ktr,kzv,betav,
rocu,conFe,conAl,m,Nb,deltaT,Db,f,wc,p1,Z,V,hp,hov,he,L,W,tov,Dir,Oe,b11,Dal,g
g,so,kmue1,Am,H1);
    [Zv1prime,Zv2,Zvsecprime,Rvsecprime] =
esdeger_devre0(Vs,tau,Lp,taud,ld,Lf,kw,Xprime,Rprime,kc,kRNV,conAlprime,ktr,kz
v,betav,rocu,conFe,conAl,m,Nb,deltaT,Db,f,wc,p1,Z,V,hp,hov,he,L,W,tov,Dir,Oe,b
11,Dal,mure,kv1,kv2,omegi,ge,so,kmueold);%

[del tao,a]=bounded(Vs,tau,Lp,taud,ld,Lf,kw,Xprime,Rprime,kc,kRNV,conAlprime,kt
r,kzv,betav,rocu,conFe,conAl,m,Nb,deltaT,Db,f,wc,p1,Z,V,hp,hov,he,L,W,tov,Dir,
Oe,b11,Dal,omegi,kv1,kv2,mure,ge,so,Zv1prime,Zv2,Zvsecprime);

[ge,mure(k),omegi,kv1,kv2,kmueold(k),H(k),Vsv,vdv,Vgv,murs(k),alfa1,Pen(k),Ar(
k),Ax(k),M]=
maxwel(Vs,tau,Lp,taud,ld,Lf,kw,Xprime,Rprime,kc,kRNV,conAlprime,ktr,kzv,betav,
rocu,conFe,conAl,m,Nb,deltaT,Db,f,wc,p1,Z,V,hp,hov,he,L,W,tov,Dir,Oe,b11,Dal,g
g,s,kmue1,Am,H1);

[ke]=endeffect(Vs,tau,Lp,taud,ld,Lf,kw,Xprime,Rprime,kc,kRNV,conAlprime,ktr,kz
v,betav,rocu,conFe,conAl,m,Nb,deltaT,Db,f,wc,p1,Z,V,hp,hov,he,L,W,tov,Dir,Oe,b
11,Dal,omegi,s,kv1,kv2,mure,ge,deltao,a,q);%(k)
murex=mure(k);

[Fx,eff,Ivsecprime,Rvsecprime,I1,Pem,Pme,xvsecprime,KWKWA,PF,Fxy,Im,Bmx,Bmy,
Xvo] =
esdeger_devreV(murex,Vs,tau,Lp,taud,ld,Lf,kw,Xprime,Rprime,kc,kRNV,conAlprime,
ktr,kzv,betav,rocu,conFe,conAl,m,Nb,deltaT,Db,f,wc,p1,Z,V,hp,hov,he,L,W,tov,Di
r,Oe,b11,Dal,Ze,mure,kv1,kv2,omegi,ge,Vr,s,kmueold,I,ke,Am,M,N);% ,ke

    if (k == 1)
        FirstI1 = I1;
    end;

    Bmxx(k)=Bmx;
    Bmyy(k)=Bmy;
    Im1(k)=Im;
    effr(k)=eff;
    I1r(k)=I1;
    Fxr(k)=Fx;
    Pemr(k)=Pem;
    Pmer(k)=Pme;
    KWKAr(k)=KWKWA;
    PFr(k)=PF;
    Fxyy(k)=Fxy;
    end
Rvsec1=abs(Rvsecprime);
Xvsec1=abs(Xvsecprime);

```



```

I12 = abs(FirstI1);

%
% effr : Efficiency
% Fxr  : Thrust
% Fxy  : Normal force
%
for i=numel(Vr):-1:numel(Vr)/2+1
    tmp = Vr(i);
    Vr(i) = Vr(numel(Vr) -i + 1);
    Vr(numel(Vr) -i + 1) = tmp;
end;

for i=numel(Fxr):-1:numel(Fxr)/2+1
    tmp = Fxr(i);
    Fxr(i) = Fxr(numel(Fxr) -i + 1);
    Fxr(numel(Fxr) -i + 1) = tmp;
end;

for i=numel(effr):-1:numel(effr)/2+1
    tmp = effr(i);
    effr(i) = effr(numel(effr) -i + 1);
    effr(numel(effr) -i + 1) = tmp;
end;

for i=numel(PFr):-1:numel(PFr)/2+1
    tmp = PFr(i);
    PFr(i) = PFr(numel(PFr) -i + 1);
    PFr(numel(PFr) -i + 1) = tmp;
end;

for i=numel(KWKWAR):-1:numel(KWKWAR)/2+1
    tmp = KWKWAR(i);
    KWKWAR(i) = KWKWAR(numel(KWKWAR) -i + 1);
    KWKWAR(numel(KWKWAR) -i + 1) = tmp;
end;

for i=numel(Pmer):-1:numel(Pmer)/2+1
    tmp = Pmer(i);
    Pmer(i) = Pmer(numel(Pmer) -i + 1);
    Pmer(numel(Pmer) -i + 1) = tmp;
end;

for i=numel(I1r):-1:numel(I1r)/2+1
    tmp = I1r(i);
    I1r(i) = I1r(numel(I1r) -i + 1);
    I1r(numel(I1r) -i + 1) = tmp;
end;

for i=numel(Fxyy):-1:numel(Fxyy)/2+1
    tmp = Fxyy(i);
    Fxyy(i) = Fxyy(numel(Fxyy) -i + 1);
    Fxyy(numel(Fxyy) -i + 1) = tmp;
end;

for i=numel(Im1):-1:numel(Im1)/2+1
    tmp = Im1(i);
    Im1(i) = Im1(numel(Im1) -i + 1);
    Im1(numel(Im1) -i + 1) = tmp;
end;

for i=numel(Pemr):-1:numel(Pemr)/2+1
    tmp = Pemr(i);
    Pemr(i) = Pemr(numel(Pemr) -i + 1);
    Pemr(numel(Pemr) -i + 1) = tmp;
end;

csvwrite('vr.lim', Vr);
csvwrite('fxr.lim', Fxr);
csvwrite('effr.lim', effr);
csvwrite('pfr.lim', PFr);
csvwrite('kwkwar.lim', KWKWAR);
csvwrite('pmer.lim', Pmer);
csvwrite('i1r.lim', I1r);
csvwrite('fxyy.lim', Fxyy);
csvwrite('im1.lim', Im1);
csvwrite('pemr.lim', Pemr);

Dizi(1) = Rvsec1;
Dizi(2) = Xvsec1;
Dizi(3) = Bmxxx;
Dizi(4) = Bmyyy;
Dizi(5) = Im11;
Dizi(6) = Vs;
Dizi(7) = tau;
Dizi(8) = Lp;
Dizi(9) = taud;

```

```

Dizi(10) = Id;
Dizi(11) = Lf;
Dizi(12) = kw;
Dizi(13) = xprime;
Dizi(14) = Rprime;
Dizi(15) = kc;
Dizi(16) = kRNv;
Dizi(17) = conAlprime;
Dizi(18) = ktr;
Dizi(19) = kzv;
Dizi(20) = betav;
Dizi(21) = q;
Dizi(22) = V;
Dizi(23) = N;
Dizi(24) = roFE;
Dizi(25) = roAL;
Dizi(26) = roCU;
Dizi(27) = xxr;
Dizi(28) = effrr;
Dizi(29) = I11;
Dizi(30) = Fxrr;
Dizi(31) = Pemrr;
Dizi(32) = Pmerr;
Dizi(33) = KwKWArr;
Dizi(34) = PFrr;
Dizi(35) = Fxyyy;
Dizi(36) = Ms;
Dizi(37) = Mcu;
Dizi(38) = Mcs;
Dizi(39) = Mp;
Dizi(40) = Ivsecprime11;
Dizi(41) = abs(Rvsecprime11);
Dizi(42) = abs(xvsecprime11);
Dizi(43) = Vrated;
Dizi(44) = srated;
Dizi(45) = rocu;
Dizi(46) = conFe;
Dizi(47) = conAl;
Dizi(48) = m;
Dizi(49) = Nb;
Dizi(50) = deltaT;
Dizi(51) = Db;
Dizi(52) = f;
Dizi(53) = wc;
Dizi(54) = p1;
Dizi(55) = Z;
Dizi(56) = hp;
Dizi(57) = hov;
Dizi(58) = he;
Dizi(59) = L;
Dizi(60) = w;
Dizi(61) = tov;
Dizi(62) = Dir;
Dizi(63) = Oe;
Dizi(64) = b11;
Dizi(65) = Da1;
Dizi(66) = Xvo;
Dizi(67) = I12;

%for i=1:1:numel(Dizi)
%   Dizi(i) = Dizi(i) * 10.0^4;
%end;

C = Dizi;

```

```

%%%%%%%%%%%%%%%%%%%%%%%%%%%%%%%%%%%%%%%%%%%%%%%%%%%%%%%%%%%%%%%%%%%%%%%%
%%% Maxwell Function %%%
%%%%%%%%%%%%%%%%%%%%%%%%%%%%%%%%%%%%%%%%%%%%%%%%%%%%%%%%%%%%%%%%%%%%%%%%

```

```

function [ge,mure,omegi,kv1,kv2,kmueold,H2,Vsv,Vdv,Vgv,murs,alfa1,Pen,Ar,Ax,M]
=
maxwel(Vs,tau,Lp,taud,ld,Lf,kw,Xprime,Rprime,kc,kRNV,conAlprime,ktr,kzv,betav,
rocu,conFe,conAl,m,Nb,deltaT,Db,f,wc,p1,Z,V1,hp,hov,he,L,W,tov,Dir,Oe,b11,Dal,
g,s,kmue1,Am,H1)
mu0 = 4*pi*10^-7;
n1=0;
H2=-1;
kmueold=kmue1;
%input radial frequency
omegi=2*pi*f*s;
while ((abs((H2-H1)))>0.001)&&(n1<100)
n1=n1+1;
if H2>0
H1=H2;
end
[B,Ar,Ax]=interpolasyon_BH(H1);

murs=(B/(mu0*H1));
muprime=Ar*Ax;
mudouble=0.5*((Ar^2)-(Ax^2));
mure=abs(murs*(muprime-1i*mudouble));
alfa1=sqrt(1i*omegi*mu0*mure*conFe);
alfa2=sqrt(1i*omegi*mu0*conAlprime);

kv1=sqrt((alfa1^2)+betav^2);
kv2=sqrt((alfa2^2)+betav^2);

%effective gap
ge=kc*kmueold*g;
coh=cosh(kv2*Dal);
soh=sinh(kv2*Dal);
M=(kv2/betav)*((kv1/kv2)*coh+mure*soh)*cosh(betav*ge)+...
(mure*coh+(kv1/kv2)*soh)*sinh(betav*ge);

%penetration depth
Pen=(sqrt(pi*s*f*mu0*murs*conFe))^(-1);
tt=0.5*Dir;
if Pen < tt
dav=Pen;
else
dav=tt;
end

%HmxFe the de farklı Gier da farklı kontrol et
y4=g+Dal+dav;
Hmx=(-1*kv1*Am)/(M*betav) * exp(-1*kv1*(y4-Dal-ge));
Hmy=(1i*Am)/M * exp(-kv1*(y4-Dal-ge));
HFeav=sqrt((abs(Hmx))^2+(abs(Hmy))^2);

muravg=(B/(mu0*HFeav));

%saturasyon faktörünü hesapla
t19=(1i*Am)/M;
t20=((mure*coh+(kv1/kv2)*soh)*sinh(betav*ge))/betav;
t23=(kv2/betav) * ((kv1/kv2)*coh+mure*soh);
t26=(1-cosh(betav*ge))/betav;
Vgv=abs(t19*(t20-t23*t26));

t27=(mure*soh)/kv2;
t28=(kv1/kv2)*((1-coh)/kv2);
Vdv=abs(((1i*Am)/M)*(t27-t28));

Vsv=abs((1/Dir)*((2*Am)/(betav^2))*(1/abs(M))*(murs/muravg));
kmueeff=1+(Vsv/(2*(Vdv+Vgv)));
kmueold=kmueeff; % saturasyon faktörü

% yüzeydeki HmsFe hesaplandı yukarıya dönderip
y8=g+Dal;
Hsx=(-1*kv1*Am)/(M*betav) * exp(-1*kv1*(y8-Dal-ge));
Hsy=(1i*Am)/M * exp(-kv1*(y8-Dal-ge));
H2=sqrt((abs(Hsx))^2+(abs(Hsy))^2);

end

```

```

%%%%%%%%%%%%%%%%%%%%%%%%%%%%%%%%%%%%%%%%%%%%%%%%%%%%%%%%%%%%%%%%%%%%%%%%
%%% End Effect Function %%%%
%%%%%%%%%%%%%%%%%%%%%%%%%%%%%%%%%%%%%%%%%%%%%%%%%%%%%%%%%%%%%%%%%%%%%%%%

```

```

function
[ke]=endeffect(Vs,tau,Lp,taud,ld,Lf,kw,Xprime,Rprime,kc,kRnv,conAlprime,ktr,kz
v,betav,rocu,conFe,conAl,m,Nb,deltaT,Db,f,wc,p1,Z,V,hp,hov,he,L,W,tov,Dir,Oe,
b11,Dal,omegi,s,kv1,kv2,mure,ge,deltao,a,q)
mu0 = 4*pi*10^-7;
Vr=Vs*(1-s);
Zv1prime=-1*((1i*omegi*mu0*mure*kzv)/(kv1*tanh(kv1*Dir)));
Zv2=(-1i*omegi*mu0)/(kv2*tanh(kv2*Dal));
Zvsecprime=(Zv1prime*Zv2*ktr*L)/((Zv1prime+Zv2)*tau);
Z2=(Zv2*Zv1prime)/(s*(Zv2+Zv1prime));
drprime=kzv*L/(conAl*real(tau*Zvsecprime));
%Vo ve V nin initial hizını degilmi bak Vs senkron hız
Vo=(0.5*Vs*Vs/150);%*IOS.Vs/150
if(Vr<=Vo)
    Ve=0;ke=0;
else
    Ve=((Vr-Vo)/(Vs-Vo))*Vs;

    E=(Vr*mu0*conAl*drprime)/(kc*(ge+drprime));%IELD.conAl
    F=(omegi*mu0*conAl*drprime)/(kc*(ge+drprime));% g
    U=sqrt((E)^4+16*(F)^2);
    V=(E)^2;
    D=sqrt(U+V)/sqrt(2);
    C=sqrt(U-V)/sqrt(2);

    %taue aynı zamanda taue=(1-s)*taue diyede hesaplanıyor
    taue=(2*pi)/D;
    Te=2*ge*kc/(C*ge*kc-Vr*mu0*conAl*drprime);%g
    %Lon. end effectli winding factor
    te5=(tau/taue)*(pi/(2*m));
    te6=(tau/taue)*(pi/(2*m*q));
    te7=(pi*wc)/(2*taue);
    kwe=(sin(te5)/(q*sin(te6)))*sin(te7);
    delta=deltao+a*Ve;
    fofdelta=(1/Te)*sin(delta)+(pi/taue)*cos(delta);
    te8=-1*kwe/kw;
    te9=pi*taue/(tau^2);%????????????% (pi*taue/(IOS.tau))^2
    te10=exp(-1*(p1/2)*taue/Te);
    te11=sinh((p1/2)*taue/Te);
    te12=(p1/2)*sinh(taue/Te);
    te13=(1/(Te^2))+((pi/taue)^2);
    ke=abs((te8*te9*fofdelta*te10*te11)/(te12*te13));
end

```

```

%%%%%%%%%%%%%%%%%%%%%%%%%%%%%%%%%%%%%%%%%%%%%%%%%%%%%%%%%%%%%%%%%%%%%%%%
%%%Equivalentcircuit Function %%%%
%%%%%%%%%%%%%%%%%%%%%%%%%%%%%%%%%%%%%%%%%%%%%%%%%%%%%%%%%%%%%%%%%%%%%%%%

```

```

function
[Fx,eff,Ivsecprime,Rvsecprime,I1,Pem,Pme,Xvsecprime,KWKWA,PF,Fxy,Im,Bmx,Bmy] =
esdeger_devre(murex,Vs,tau,Lp,taud,ld,Lf,kw,Xprime,Rprime,kc,kRnv,conAlprime,k
tr,kzv,betav,rocu,conFe,conAl,m,Nb,deltaT,Db,f,wc,p1,Z,V,hp,hov,he,L,W,tov,Dir
,Oe,b11,Dal,Ze,mure,kv1,kv2,omegi,ge,Vr,s,kmueold,I,ke,Am,M)
mu0 = 4*pi*10^-7;
Zv1prime=-1*((1i*omegi*mu0*mure*kzv)/(kv1*tanh(kv1*Dir)));%));
Zv2=(-1i*omegi*mu0)/(kv2*tanh(kv2*Dal));%tanh(kv2*GD.Dal)
Zvsecprime=(Zv1prime*Zv2*ktr*L)/((Zv1prime+Zv2)*tau);%*s
Rvsecprime=real(Zvsecprime);
Xvsecprime=imag(Zvsecprime);
Xvo=(omegi*mu0*ktr*L)/(betav*betav*ge*tau);
Zvo=-1i*Xvo;
Ztot=(Zvsecprime*Zvo)/(Zvsecprime+Zvo);
E=abs(I*Ztot);
Ccf=100;
Ch=25;
Bteeth=1;
deltapfe=(Ccf+Ch*ELD.f)*ELD.f*Bteeth^2;
Rvo=ELD.m*(E^2)/deltapfe;
Ivsecprime=abs((ELD.I*Zvo)/(Zvsecprime+Zvo));
R11=Xvo^2*Rvo/(Xvo^2+Rvo^2);
X11=Xvo*Rvo^2/(Xvo^2+Rvo^2);
Zver=R11+1i*X11;
Ztot1=Zvsecprime*Zver/(Zvsecprime+Zver);
E1=abs(I*Ztot1);
Ivsecprime=abs(E*(1-ke)/(Zvsecprime));%*(1-ke)

Pem=abs((m*(Ivsecprime)^2)*Rvsecprime)/s);
Pme=abs(Pem*(1-s));
Poprime=m*Rprime*I^2;
eff=abs(Pme/(Pem+Poprime));

```

```

Fx=abs((m*((Ivsecprime)^2)*Rvsecprime)/(s*Vs));
Zprime=Rprime+1i*Xprime;
Zall=((Zvo*Zvsecprime)/(Zvo+Zvsecprime))+Zprime;
Sa=m*I*V;
KWKWA=Pme/Sa;
PF=KWKWA/eff;
I1=V/abs(Zall);
Im=I1-Ivsecprime;
Bmy=(E*(1-ke))/(2*sqrt(2)*f*N*kw*tau*L);%2*sqrt(2)
Hmx=(-1*Am/(betav*M))*(kv1*cosh(kv2*Da1)+kv2*murex*sinh(kv2*Da1));
Bmx=mu0*abs(Hmx);
deltax=Ze*(Oe+1d);
Fza=(1/2*mu0)*(Bmy^2)*p*(tau*deltax)*L;
Fzr=Fx*Bmx/Bmy;
Fxy=abs(Fza-Fzr);
xx=0.0;

```

```

%%%%%%%%%%%%%%%%%%%%%%%%%%%%%%%%%%%%%%%%%%%%%%%%%%%%%%%%%%%%%%%%%%%%%%%%
%%%%%%%% Bounded Function %%%%%%%%%
%%%%%%%%%%%%%%%%%%%%%%%%%%%%%%%%%%%%%%%%%%%%%%%%%%%%%%%%%%%%%%%%%%%%%%%%
function
[del tao, a]=bounded(Vs, tau, Lp, tau d, l d, Lf, kw, Xprime, Rprime, kc, kRNV, conAlprime, kt
r, kzv, betav, rocu, conFe, conAl, m, Nb, del taT, Db, f, wc, p1, Z, V1, hp, hov, he, L, W, tov, Di r
, Oe, b11, Da1, omegi, kv1, kv2, mure, ge, so, Zv1prime, Zv2, Zvsecprime)
mu0 = 4*pi*10^-7;
Vo=(0.5*Vs*Vs/150);
Z2=(Zv2*Zv1prime)/(so*(Zv2+Zv1prime));
drprime=kzv*L/(conAl*real(tau*Zvsecprime));
E=(vo*mu0*conAl*drprime)/(kc*(ge+drprime));%IELD.conAl
F=(omegi*mu0*conAl*drprime)/(kc*(ge+drprime));% g g+GD.Da1
U=sqrt(((E)^4)+16*((F)^2));
V=(E)^2;
D=sqrt(U+V)/sqrt(2);
C=sqrt(U-V)/sqrt(2);

%taue aynı zamanda taue=(1-s)*taue diyede hesaplanıtor
taue=(2*pi)/D;
Te=2*ge*kc/(C*ge*kc-Vo*mu0*conAl*drprime);%g GD.Da1
del tao=(pi-atan(pi*Te/taue));%pi (180/pi)*
a=(1/150)*atan(pi*Te/taue);%pi
xxxxxx=0.0;

```

```

%%%%%%%%%%%%%%%%%%%%%%%%%%%%%%%%%%%%%%%%%%%%%%%%%%%%%%%%%%%%%%%%%%%%%%%%
%%%%%%%% B-H Interpolation Function %%%%%%%%%
%%%%%%%%%%%%%%%%%%%%%%%%%%%%%%%%%%%%%%%%%%%%%%%%%%%%%%%%%%%%%%%%%%%%%%%%

```

```

function [B,A1,A2]=interpolasyon_BH(H)

A=[...
1 0.0001 0.1 0.4
25 0.009 0.70 0.8
100 0.014 0.84 0.94
350 0.75 0.9 0.9
1000 1.15 1.61 0.93
2000 1.35 1.72 0.8
4000 1.475 1.61 0.78
6000 1.51 1.56 0.8
1e4 1.53 1.52 0.82
1.6e4 1.55 1.49 0.85
1e5 1.81 1.45 0.94
1e6 1.9 1.38 0.98 ];

if nargin==0
disp('Hata: giriş yok');
B=[];
return;
end

%giriş değerlerinin kontrolü
if (min(H)< min(A(:,1))) || (max(H) > max(A(:,1)))
disp('Hata: giriş değerleri aralık dışında');
B=[];

```

```

        H
    return;
end

x=log10(A(:,1)');
y3=A(:,2)';
y1=A(:,3)';
y2=A(:,4)';

B=(interp1(x,(y3),log10(H),'spline'));%

n1=7;
B1=polyfit(y3,sqrt(y1),n1);
A1=polyval(B1,B).^2;

n2=7;
B2=polyfit(y3,sqrt(y2),n2);
A2=polyval(B2,B).^2;

return

```

## **CURRICULUM VITAE**

### **PERSONAL INFORMATION**

Surname, Name: GERÇEK, Ali Suat

Nationality: Turkish (T.C.)

Date and Place of Birth: 22 March 1968, Yavuzeli

Marital status: Married

Phone: 90 342 3171703

Fax: 90 342 360 11 70

e-mail: [gercek@gantep.edu.tr](mailto:gercek@gantep.edu.tr)

### **EDUCATION**

<b>Degree</b>	<b>Institution</b>	<b>Year of Graduation</b>
MS	Gaziantep Univ.-Elec.- Electr. Engineering	2001
BS	METU	1993
High school	Gaziantep High school	1984

### **WORK EXPERIENCE**

<b>Year</b>	<b>Place</b>	<b>Enrollment</b>
1994-Present	GAZÜ- Gaziantep Vocational high school	Instructor

### **FOREIGN LANGUAGE**

English

### **PUBLICATION**

Gerçek A.S., Karşlı V.M., (2009), Performance prediction of the single-sided linear induction motors for transportation considers longitudinal end effect by using analytic method, Contemporary Engineering Science (ISSN 1313-6569), 2, 95-104